University of Oxford

Mechanistic studies on 2-oxoglutarate dependent oxygenases

A thesis submitted to the board of the Faculty of Physical Sciences at the University of Oxford in partial fulfilment of the requirements for the degree of Master of Science by Research

Andrea Szöllössi

St Peter's College, Oxford

Trinity Term 2012

Abstract

Mechanistic studies on 2-oxoglutarate dependent oxygenases

Andrea Szöllössi **MSc (by Research) in Chemical Biology**

St Peter's College **Trinity Term, 2012**

The first identified 2-oxoglutarate (2OG) dependent oxygenase was a collagen modifying enzyme in the work by Hutton *et al.*in 1967. Subsequent work has revealed that 2OG dependent oxygenases are a large family with diverse biological roles. With small molecule substrates, these enzymes catalyse a wide range of oxidative reactions, including those that form part of antibiotic biosynthetic pathways. The currently accepted consensus mechanism for catalysis by 2OG-dependent oxygenases is based on crystallographic data, kinetics and on quantum chemical calculations. The consensus mechanism involves oxidative decarboxylation of 2OG by reaction with an oxygen molecule producing CO_2, succinate and a reactive oxidising species that reacts with the 'prime' substrate.

Deacetoxycephalosporin C synthase (DAOCS) is a 2OG-dependent oxygenase involved in cephalosporin biosynthesis (Figure 1). The mechanism of DAOCS is of particular interest because it has recently been proposed to be different from the consensus mechanism [1]. The new mechanism proposal from Valegård *et al.* is primarily based on high-resolution crystallographic data with support from steady-state kinetic experiments and quantum-chemical calculations.

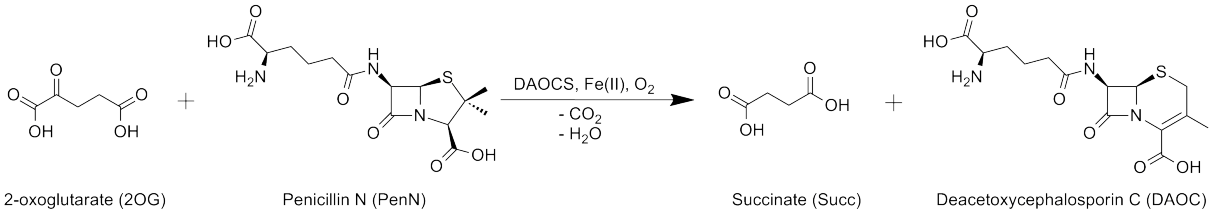

Figure 1: *The reaction catalysed by deacetoxycephalosporin C synthase (DAOCS).*

The work in discussed in this thesis aimed to test the proposal of Valegård *et al.* by using a combination of spectroscopic and spectrometric methods analysing enzyme-substrate interactions. Substrate binding was investigated using both protein-observe (Chapter 3) and ligand-observe (Chapter 4.1 and 4.2) methods. Preliminary UV-visible data on enzyme-substrates complex formation was also obtained. The strength of substrate and cosubstrate binding was characterised through dissociation constant measurement. An activity assay (Chapter 2) that allows for direct and simultaneous monitoring of 2OG decarboxylation and penicillin ring expansion was optimised.

Both the ligand-observe and protein-observe binding experiments as well as the preliminary UV-visible data indicate that the formation of a ternary complex between DAOCS, 2OG and the penicillin substrate is viable. The activity assay conclusively showed that in the presence of unnatural substrates, such as penicillin G, 2OG oxidation is significantly uncoupled from penicillin oxidation. Uncoupled turnover does not occur in the presence of the natural substrate, penicillin N, which is an aspect that should be considered in the analysis of the steady-state kinetic data.

Overall, the results provide evidence that, the consensus mechanism for 2OG-dependent oxygenases is viable for DAOCS, at least in the presence of the natural substrate, penicillin N. It is possible that in the presence of an unnatural substrate, the catalytic process undergoes a more complex mechanism, possibly with the direct involvement of reducing agents in the system.

Acknowledgements

I am incredibly grateful to my supervisor, Professor Christopher J. Schofield, for the opportunity to work in his laboratory on a project involving such a range of different techniques, for the freedom and for the support he offered me in pursuing my own ideas. Of course, all of this would never have happened had I not been receiving funding from the Dinu Patriciu Foundation as part of the "Open Horizons" program.

A great big thank you to Dr. Aman Iqbal for introducing me to the world of molecular biology, microbiology and protein purification. The NMR part, that is over half of this dissertation, owes its existence to the endless hours spent in the CRL basement with Ivanhoe K.H. Leung. Few things in this world are as beautiful as a clean non-denaturing ESI-MS protein spectrum – here I thank Marina Demetriades for helping me with this. It is also here that I thank Luc Henry and Jacob T. Bush for making the magic happen in the synthesis lab - you guys are awesome! I thank Dr. Emily Flashman for her input on the kinetics part, as well as the UV-Vis studies. However, equally if not more, I thank you, Emily, for introducing me to Systems Biology and for supporting me as I was doing my DPhil application. And for the "little" things, like a working computer or a nicely packed Superdex®75 ready to use, I thank Dr. Adam Hardy and Wendy Sobey – thank you for putting up with my questions, complaints and requests.

It is very hard to acknowledge everyone properly when you have spent two years working in a 50-people research group. Nevertheless, it has been a pleasure to work in the CJS group and I thank you for being there whenever I needed it, be it a column cleaning protocol, NMR tubes, chocolate or a piece of advice. Thus I shall take one deep breath and write down the names, for posterity, for the person reading the acknowledgements of this dissertation: Anna R, Anna B, Rubén, Inga, Rok, Richard, Rashed, Mike, Alex, Matthias, Dante, Tom B, Anders, Tristan, Alex D, Hanna, Naomi, Sophie, Marcus, Wei Shen, Monica, David, Cyrille, Elena, Jose, Lukas, Louise, Akane, Nathan, Christoph, Refaat, Tobias, Lars, Ollie, Clarisse, Zhihong, Nikita, Eleanor, Maggie, Armin, Ian, Esther, Ming, Wei, and... Manso!

In my period of writing up, I have had a great deal of support coming from different places and for this I would like to thank Christopher J. Schofield, my supervisor; Elspeth Garman, my DTC programme director; Dr. Mark Moloney, my college advisor; Mr. Mark Damazer, the Master of St Peter's College; the proofreading squad – thank you Ivan, Tim, Rubén, Marina, Emily, Adam and Hanna; last but not

least, thanks to all those who have annoyed me by enquiring about the dissertation (way too many to be named here).

I would also like to thank the people from world outside the lab: the friends I have made in college and the friends from back home who don't mind my lack of keeping in touch skills. It is friends outside the lab as well as friends that I have made in the lab that have kept me sane all this time with short tea breaks in the basement, dinners, noodles, gigs, guest nights, football, Friday drinks at the Uni Club, travelling far and wide and last but not least, company during late nights in the lab – and here I should mention Anna R, Marina, Ivan, Inga, Rubén, Richard and Anna B.

The last paragraph is always reserved for the family, for the people I owe my life to. Thank you for raising me to be able to become what I am today, thank you for your love and support, thank you for sunshine on a rainy day.

Contents

List of Figures

List of Tables

Abbreviations

2OG	2-oxoglutarate
ACV	L-δ-(α-aminoadipoyl)-L-cysteinyl-D-valine
APS	ammonium peroxydisulfate
Asc	ascorbate
CAS	clavaminate synthase
DAOCS	deacetoxycephalosporin C synthase
DAOC	deacetoxycephalosporin C
DAOC/DACS	deacetoxy/deacetylcephalosporin C synthase
DSBH	double-stranded β-helix
EDTA	ethylenediaminotetraacetic acid
ESI-MS	electrospray ionisation mass spectrometry
FPLC	fast protein liquid chromatography
HIF	hypoxia inducible factor
IPNS	isopenicillin N synthase
IPTG	isopropyl-β-D-thiogalactoside
K_d	dissociation constant
kDa	kilodalton
M	concentration in mol per litre
m/z	mass to charge ratio
MW	molecular weight
nd	not determined
NMR	nuclear magnetic resonance
NOE	nuclear Overhauser effect
NOG	N-oxalyl glycine
OD_{600}	optical density at 600 nm (in absorption units)
P4H	prolyl-4-hydroxylase
PenG	penicillin G
PenN	penicillin N

PHD2	prolyl hydroxylase domain 2
ppm	parts per million
rpm	rotations per minute
Q-ToF	quadrupole time-of-flight
SDS-PAGE	sodium dodecyl sulphate polyacrylamide gel electrophoresis
Succ	succinate
T_1	longitudinal spin relaxation rate constant
$T_{1(0)}$	initial longitudinal spin relaxation rate constant
TauD	taurine dioxygenase
TEMED	N, N, N', N'-tetramethylethylene diamine
Tris	trishydroxymethylaminomethane
UV-Vis	ultraviolet-visible
WT	wild type

Collaborations

Nuclear Magnetic Resonance (NMR) spectroscopy experiments were performed in collaboration with Ivanhoe K.H. Leung and Dr. Timothy D.W. Claridge. The synthesis of penicillin N was performed by Jacob T. Bush as part of a 10-week rotation project in our laboratory. ^{13}C -labelled penicillin G and *N*-oxalyl glycine were synthesized by Luc Henry.

Chapter 1

Introduction

2-Oxoglutarate (2OG) and ferrous ion dependent oxygenases are the largest known family of non-heme oxygenases. They catalyse a wide range of reactions [2] and are ubiquitously present in living organisms. 2OG oxygenases catalyse reactions involved in many important processes, including steps in antibiotic [3] and collagen [4] biosynthesis, oxygen sensing [5], DNA repair [6, 7] and transcriptional regulation by histone demethylation [8].

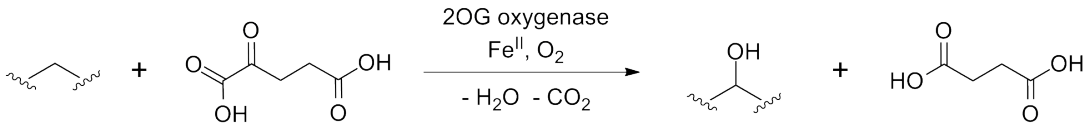

Figure 1.1: *Hydroxylation is the most common type of reaction catalysed by 2OG oxygenases.*

While the hydroxylation of alkyl groups is the most common identified reaction type catalysed by 2OG oxygenases (Figure 1.1), in plants and microorganisms, they catalyse a much wider range of oxidative reactions (Figure 1.2). Many of the reactions catalysed by 2OG oxygenases cannot be reproduced by current organic synthesis methods, a fact that makes the mechanism of 2OG oxygenases of chemical interest.

Reactions catalysed by 2OG oxygenases proceed via two stages that are coupled to each other. 2OG is decarboxylated in the presence of oxygen with the concomitant generation of succinate, carbon dioxide and a reactive oxidising species. In the second stage, the reactive oxidising species mediates the two-electron oxidation of the prime substrate.

Regarding the role of 2OG oxygenases in biosynthesis, an interesting feature is the ability of some of them to catalyse several sequential or closely related steps. For example, two consecutive steps of the cephalosporin biosynthesis in eukaryotes, penicillin ring expansion followed by cephem hydroxylation, are catalysed by the same 2OG oxygenase, deacetoxycephalosporin/deacetylcephalosporin C synthase (DAOC/DACS) [10]. In prokaryotes however, the two transformations are largely catalysed by separate

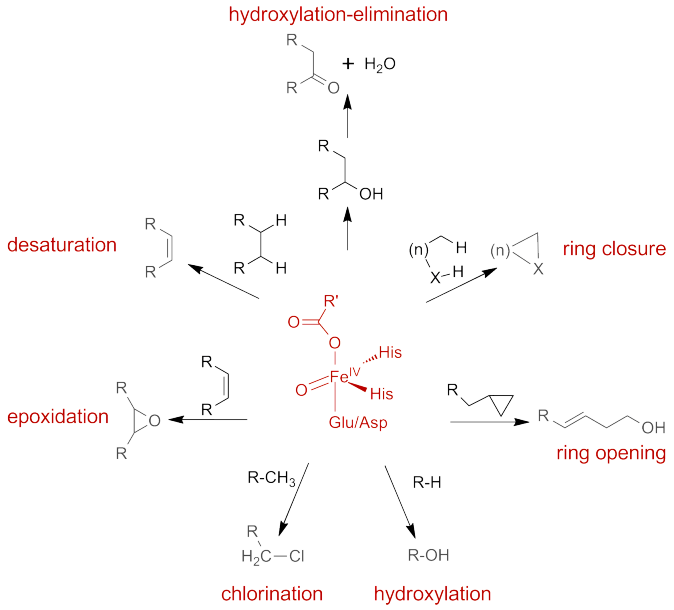

Figure 1.2: *An overview of reactions catalysed by bacterial 2OG oxygenases, as shown in a review by Clifton et al. [9]. The reactive ferryl intermediate postulated in the consensus mechanism (Section 1.2.2) can perform a wide range of oxidation reactions; other types of reactions include ring expansion, epimerisation and C-C bond fragmentation.*

enzymes [11].

1.1 The 2OG oxygenase structural family

2OG oxygenases require Fe(II), 2OG and oxygen in order to perform catalysis. However, there are Fe(II) and oxygen dependent enzymes that are structurally and mechanistically related to 2OG oxygenases but that do not employ a 2OG co-substrate. The most studied enzyme of this category is ispoenicillin N synthase (IPNS) which catalyzes the oxygen-dependent four electron oxidation of a tripeptide to give the bicyclic penicillin nucleus [12, 13] (Figure 1.3).

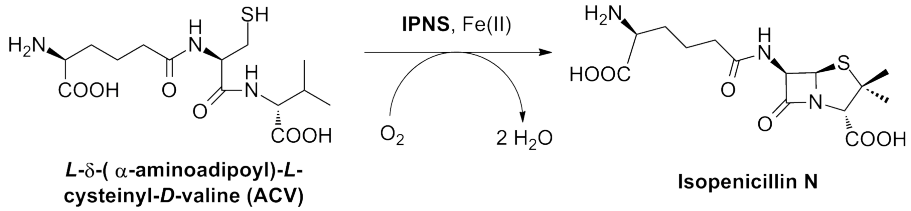

Figure 1.3: *The reaction catalysed by isopenicillin synthase. IPNS catalyses the oxidation of the tripeptide* L-*δ-(α-aminoadipoyl)-*L-*cysteinyl-*D-*valine (ACV) to yield the penicillin nucleus.*

A crystal structure of IPNS was the first one of a member of the 2OG oxygenase structural family to be solved [13]. The IPNS crystal structure revealed a double-stranded β-helix (DSBH) motif, also known as a jelly roll fold or double Greek key motif. All members of the 2OG oxygenase structural family contain the DSBH motif (Figure 1.4). One role of the DSBH is to provide a rigid scaffold for the ferrous cofactor. The

metal is normally coordinated by three amino acid residues, two histidines and an aspartate/glutamate that are part of an HXD/E...H motif.

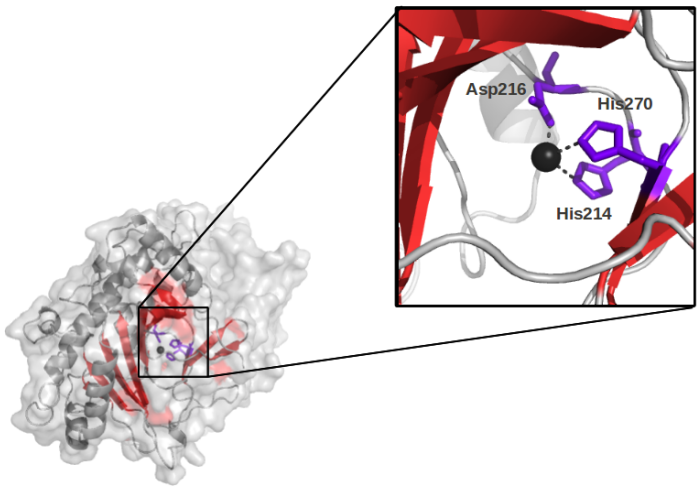

Figure 1.4: *Features of the 2OG oxygenase structural family illustrated by IPNS (1IPS): The characteristic DSBH motif (coloured in red) and the three amino acid residues of the HXD/E..H motif in the active site that coordinate the metal cofactor (coloured in purple).*

High resolution structures of 2OG oxygenases show that in the absence of 2OG, the three 'open' coordinations of Fe(II) can be occupied by water molecules [9]. When 2OG is present, Fe(II) is octahedrically coordinated. 2OG coordinates to Fe(II) in a bidentate manner via the 2-oxo group and one of the 1-carboxylate oxygens [14]. The 2-oxo group of 2OG coordinates *trans* to the Asp/Glu residue fo the HXD/E...H motif but the 1-carboxylate has been observed to coordinate *trans* to either of the histidines of the triad [2].

Evidence for an induced fit upon substrate binding had first been provided by crystallographic work on IPNS: the Arg279 residue moves to bind to the substrate valine carboxylate [15] . In the case of 2OG oxygenases with peptide substrates, significant conformational changes seem to occur in both the enzyme and the substrate [9]. Induced fit models have been proposed to enable optimum substrate orientation in the active site in order for it to undergo oxidation.

1.2 Mechanistic studies on 2OG oxygenases

1.2.1 Binding of Fe(II) and substrates

Kinetic [16], spectroscopic [17] and crystallographic data [14, 2, 9, 18] have revealed that the Fe(II) cofactor binds to 2OG oxygenases prior to binding of cosubstrates/substrates The ferrous ion is generally tightly bound but it can be removed using metal chelators, dialysis or by competition with other metals. As shown by structural studies, a binary enzyme.Fe(II).2OG complex is formed by the bidentate chelation of 2OG to the ferrous metal centre.

Spectroscopic and crystallographic studies on 2OG oxygenases employing small molecule substrates suggest that substrate binding to the enzyme.Fe(II).2OG complex occurs close to but not at the metal centre [17]. This binding event is proposed to displace one of the water molecules coordinated to Fe(II), thereby activating the complex [19]. Crystallographic studies on 2OG oxygenases with polymeric substrates indicate that it is possible to form a ternary enzyme.Fe(II).2OG.substrate complex, consistent with kinetic studies on 2OG oxygenases with small molecules. Studies on clavaminate synthase (CAS) indicate that such a complex can react to produce an enzyme.Fe(II).succinate.product complex [19].

1.2.2 Consensus mechanism of 2OG oxygenases

Almost 30 years ago, a chemical mechanism for 2OG oxygenases was proposed by Hanauske-Abel and Günzler for prolyl-4-hydroxylase (P4H) [20]. Since then, variations of this model have been shown to be applicable to other members of the 2OG oxygenase family, leading to it being adopted as a consensus mechanism (Figure 1.5).

Catalysis by 2OG oxygenases involves coupling of 2OG oxidative decarboxylation with substrate oxidation. These transformations are carried out at the mononuclear non-heme Fe(II) centre which is facially coordinated by a HXD/E...H motif. Kinetic, crystallographic and spectroscopic studies suggest that 2OG oxygenases employ an ordered sequential mechanism, with the binding of 2OG generally followed by that of the prime substrate and then oxygen [21, 22, 23, 24, 16, 2] (Section 1.2.1).

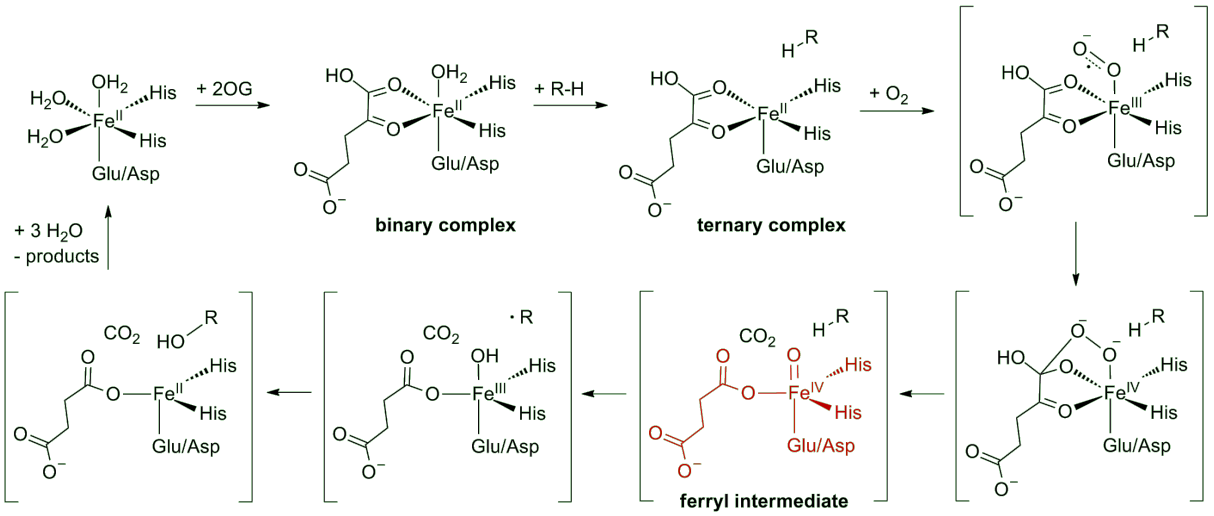

Figure 1.5: *The consensus mechanism proposed for the catalysis by 2OG oxygenases, adapted for a generic hydroxylation reaction. The proposed ferryl intermediate [23] is shown in red.*

2OG oxygenases are thought to adopt a conserved mechanism for dioxygen activation and formation of an Fe(IV)-oxo intermediate that attacks the substrate performing a two-electron oxidation. In the first step of the mechanism, 2OG chelates to the ferrous centre as described previously (Section 1.2.1). The iron site of the enzyme.Fe(II).2OG complex is six coordinate and in high-spin configuration [19]. In the second step, the substrate binds in the vicinity of, but not directly to the Fe(II) centre [21]. At least

in some cases, during this binding event, the water molecule is displaced from the metal centre which becomes five-coordinate square pyramidal [19].

Next, addition of dioxygen to the coordinatively unsaturated Fe(II) centre initiates the oxidative decarboxylation of 2OG that goes through several computationally predicted intermediates (Figure 1.5) to finally yield the Fe(IV)-oxo (ferryl) intermediate [23] (Figure 1.5, in red). Experimental evidence for the ferryl intermediate comes from spectroscopic studies on taurine dioxygenase (TauD) and P4H. There is considerable variation after this point due to the very broad range of reactions catalysed by this family of enzymes [2]. Considering the number of different reactions catalysed by 2OG oxygenases, it is also possible that the reactive oxidizing species is not always a ferryl intermediate.

After substrate oxidation, the iron centre returns to the ferrous form, releasing the products and rebinding water to complete the cycle (Figure 1.5).

1.2.3 Uncoupled turnover

It has been reported that in the presence of an unnatural substrate, the enzyme.Fe(II).2OG complex can undergo substrate uncoupled turnover reaction with oxygen [25, 26]. The reactive oxygen species thus generated has been proposed to be neutralised by reducing agents present in the system [27]. Such reducing agents could be amino acid residues in the active site or small molecule reducing agents present in the intracellular environment, such as ascorbate or glutathione [28]. A nearby protein residue could be easily oxidized in absence of substrate, resulting in enzyme deactivation. Ascorbate was found to stimulate the activity of some but not all 2OG oxygenases [27]; extensive studies on P4H have shown that in the absence of its collagen substrate, 2OG turnover is stoichiometric with that of ascorbate oxidation [25]. It has been suggested that uncoupled turnover could be an editing process contributing to the attainment of substrate selectivity in the case of 2-oxoglutarate dependent enzymes [29].

1.3 DAOCS - a 2OG oxygenase

Penicillins and cephalosporins share the first two steps in their biosynthesis (Figure 1.3). In the first step, three amino acids undergo a condensation reaction to yield L-δ-(α-aminoadipoyl)-L-cysteinyl-*textscd*-valine (ACV), while in the second step, ACV takes part in the four electron oxidation catalysed by isopenicillin N synthase (IPNS) to give isopenicillin N [30].

Cephalosporins are characterised by the six-membered dihydrothiazine nucleus. This six-membered ring is formed by the expansion of the five-membered thiazolidine penicillin nucleus. In prokaryotic cephalosporin producers, this ring-expansion reaction is catalysed by deacetoxycephalosporin C synthase (DAOCS) [31, 32, 29]. However, in the case of eukaryotic cephalosporin producers, a bifunc-

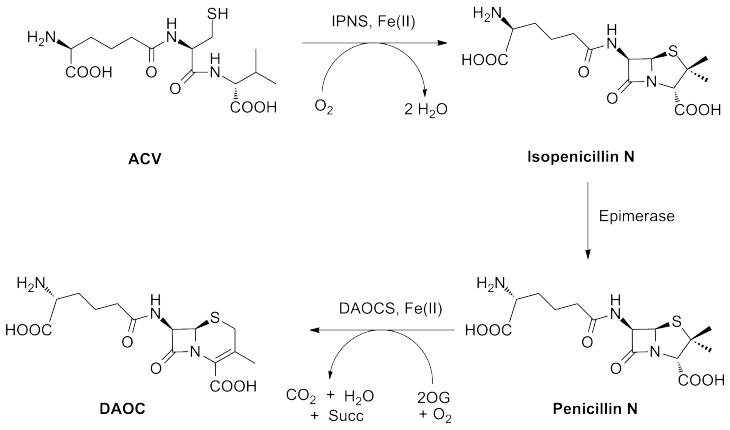

Figure 1.6: *The key steps of penicillin and cephalosporin biosynthesis.*

tional enzyme (DAOC/DACS) performs both the ring-expansion as well as the subsequent hydroxylation [10, 33, 34].

1.3.1 Structural features of DAOCS

The first crystal structures of a 2OG dependent oxygenase to be obtained was for prokaryotic DAOCS by Valegård *et al.* in 1998 [35]. They reported the structures of the apoenzyme (1DCS), the enzyme complexed with Fe(II) (1RXF), and the structure of the complex with Fe(II) and 2OG (1RXG). Within the family of 2-oxoacid dependent enzymes, DAOCS belongs to a subfamily with high structural motif similarity to IPNS (Figure 1.3.1).

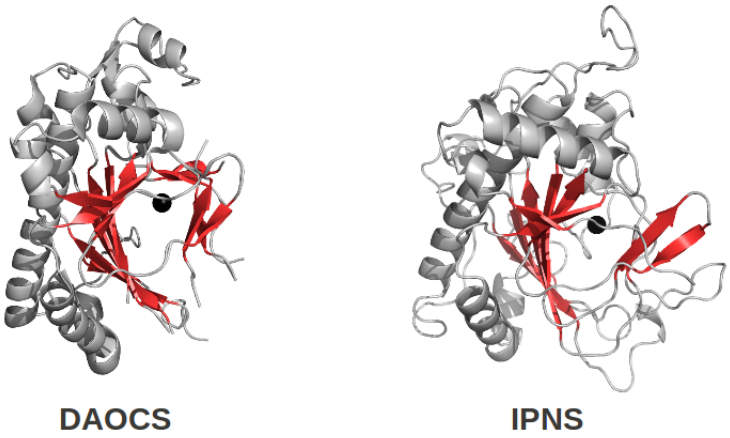

Figure 1.7: *Structures of DAOCS (1UOB) and IPNS (1IPS) emphasizing the double-stranded β helix fold characteristic to the 2OG structural family, in red. The metal ion in the active site is in black.*

The DAOCS protein chain folds into the 2OG oxygenase characteristic DSBH motif. The apo-enzyme was revealed to be a crystallographic trimer with the C-terminal arm (residues 308-311) penetrating the active site of the neighbouring subunit in a cyclic manner.

Addition of Fe(II) and 2OG to DAOCS favours dissociation into monomers. The DAOCS.Fe(II) complex

was obtained by soaking the apo-enzyme crystals into a Fe(II) solution. As a result of Fe(II) binding, the *C*-terminal arm moves away from the active site, loosening intermolecular contacts. Similarly to other members of the 2OG oxygenase structural family, the ferrous iron is coordinated by His 183, His 243, Asp 185 and three water molecules in octahedral geometry. The 2OG binds in a bidentate manner by replacing two of the water molecules around the metal centre. The 1-carboxylate of 2-oxoglutarate binds *trans* to His 243, and the 2-carbonyl group binds *trans* to Asp 185. The only accessible site around the iron in the DAOCS.Fe(II).2OG complex is located in a hydrophobic pocket. This site is occupied by a solvent molecule and it was proposed that this is where dioxygen binds.

Subsequently, in 2003, Valegård *et al.* reported high-resolution structures for ferrous DAOCS in complex with penicillins, the cephalosporin product, the cosubstrate and the coproduct [1]. These structures revealed intriguing modes of binding for substrates and products, which led to the proposal of an alternative mechanism for DAOCS (see Section 1.3.3).

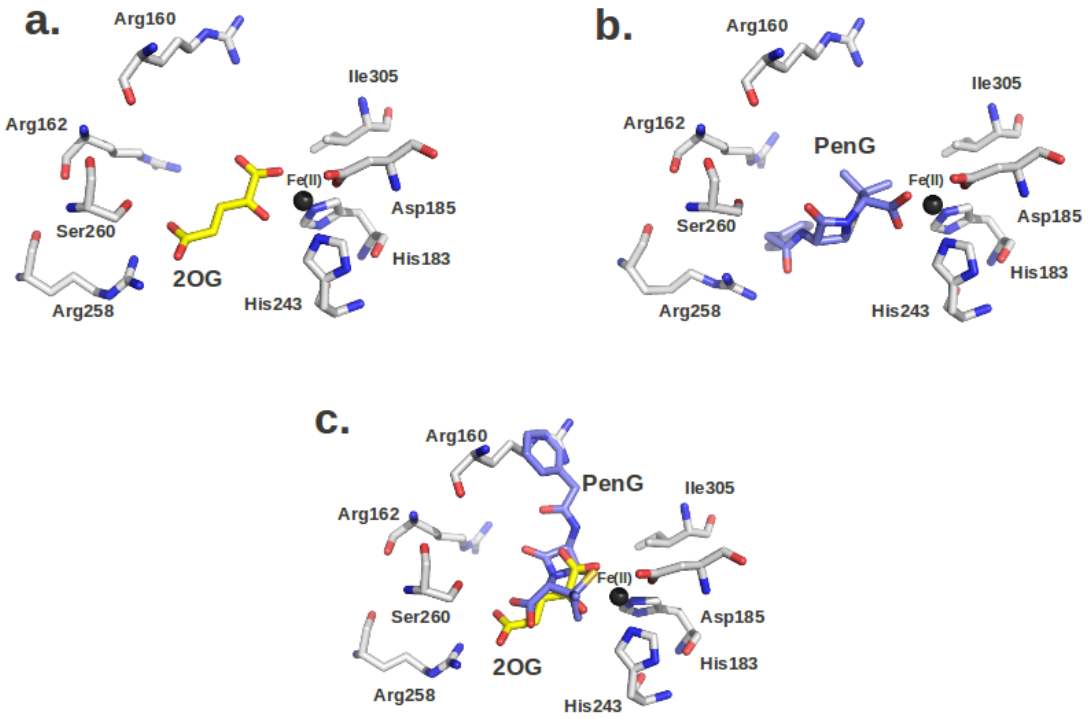

Figure 1.8: *View of the active site as shown by crystal structures a) DAOCS complexed with Fe(II) and 2OG (1E5I) ; b) DAOCS complexed with Fe(II) and penicillin G, PenG, (1UOF); c) overlapping of 2OG and penicillin G in the active site (1UOB).*

1.3.2 Uncoupled turnover

Like other 2OG-dependent oxygenases, DAOCS can catalyse the uncoupled decarboxylation of 2OG. Lloyd *et al.* proposed uncoupled turnover to be an "editing" mechanism used by DAOCS to select the correctly bound penicillin substrate [29]. Subsequent studies revealed that mutations of the DAOCS C

terminus have a strong negative influence on the coupling of 2OG oxidation to penicillin ring expansion [36]. Investigations regarding the substrate selectivity of DAOC/DACS, the eukaryotic homologue of DAOCS, have also been carried out using various penicillins as substrates [37]. Results have shown varying levels of ring expansion and some cases indicated a high level of uncoupling between 2OG decarboxylation and penicillin oxidation [38, 29, 37].

Thus, uncoupled turnover seems to be favoured if substrates cannot bind in the catalytically active conformation. This situation could occur either due to an unnatural structure of the substrate or due to enzyme mutations in the substrate binding site(s) [38, 39, 40, 29, 37].

1.3.3 An alternative mechanism proposed for DAOCS

The crystallographic work of Valegård *et al.* on DAOCS substrate binding apparently shows overlapping binding sites for 2OG and penicillin substrate, as well as for product (Figure 1.3.1c) and coproduct [1]. Based on these results, it was inferred that both substrates could not simultaneously exist in the active site. As a consequence, an alternative mechanism for catalysis by DAOCS was proposed.

With arguments based primarily on the aforementioned crystallographic studies, but supported by some solution kinetics and quantum mechanical calculations, Valegård *et al.* propose an alternative mechanism; a very reactive oxidizing species stored in a tamed form, but ready to react when the other substrate enters the active site, was proposed to answer the questions about the creation, storage and usage of the proposed iron intermediate. This intermediate was modelled to be a less reactive planar peroxo species (potentially in some equilibrium with the ferryl form).

The alternative mechanism proposes that the binding of 2OG activates Fe(II) for oxygen binding. The decarboxylation of 2OG forms the oxidising iron intermediate, as well as succinate and carbon dioxide. Since carbon dioxide is a weak ligand, it was proposed to leave the acive site easily, while succinate remains bound to stabilise the iron intermediate. The entrance of the penicillin substrate into the active site is proposed to displace succinate and triggers the oxidative attack the penicillin [1]. It was proposed that the oxidative ring expansion would then occur via a radical mechanism involving the β-methyl group of the penicillin nucleus [1].

Steady-state kinetic measurements performed by Valegård *et al.* involve the concentration of one substrate being varied while the concentration of the other one was kept constant. A significant decrease in steady-state rate at fixed penicillin G and ampicillin concentrations was observed when the concentration of 2OG was increased. A less pronounced but similar behaviour was observed at fixed 2OG concentrations when the concentration of PenG (or ampicillin) was increased [1].

Valegård *et al.* used uncoupled turnover to explain the inhibition observed at increasing 2OG concentrations, proposing that excess 2OG would drive the reaction toward uncoupled turnover with a second

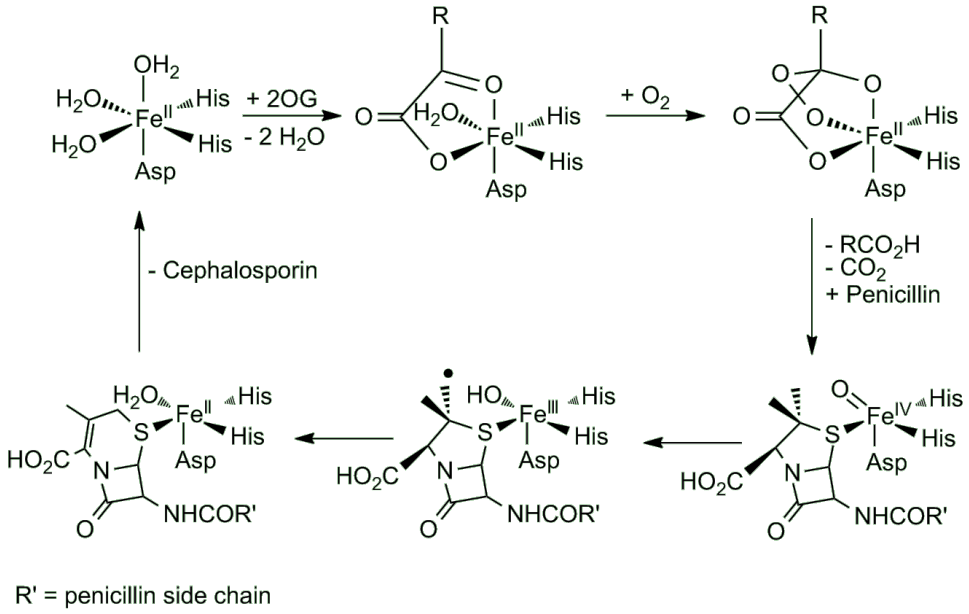

Figure 1.9: *Alternative mechanism for DAOCS, as proposed by Valegård et al. [1].*

molecule of 2-oxoglutarate reacting with the activated ferryl species during a coproduct-cosubstrate exchange [1]. Such substrate inhibition kinetic data alone is not sufficient to draw definite conclusions regarding the mechanism of DAOCS, but the results obtained are consistent with the crystallographic studies.

1.4 Motivation

Combined kinetic, spectroscopic and crystallographic studies over the last three decades have led to the proposal of a common mechanism for 2OG oxygenases. However, high-resolution crystal structures for ferrous DAOCS in complex with penicillins, the cephalosporin product, 2OG and succinate obtained by Valegård *et al.* were interpreted as suggesting an alternative mechanism. These crystal structures in combination with steady-state kinetic data and quantum-chemical calculations were put forward to support a ping-pong mechanism, in contrast to the consensus ternary complex mechanism for 2OG oxygenases [1].

An important question is how well the high-resolution structures obtained by Valegård *et al.* reflect the catalytic intermediates. If indeed, as suggested by Lee *et al.*, there is cooperativity between the 2-oxoacid and the prime substrate binding sites [39], it could be that the soaking procedure used to obtain the crystals did not allow for the substrates and/or the protein to adopt the catalytically relevant binding configuration. The catalytic relevance of the structures containing the products is perhaps more questionable given the way in which they were formed, *i.e.* the complexes are not products of the catalytic cycle. Further, refinement of the structure with mixed occupancy was not trivial.

The kinetic data that accompanies the crystal structures consists of inhibition studies with penicillin G, a relatively poor substrate. This type of kinetic experiments might not be enough to support the ping-pong mechanism on their own. However, as argued by Valegård *et al.*, in the context of the crystal structures they have obtained, the substrate inhibition that was observed can be explained by means of a ping-pong mechanism [1].

An important aspect to be mentioned is that the work of Valegård *et al.* used unnatural penicillin substrates [1]. While it has been shown that unnatural penicillin substrates can be turned over by DAOCS [38, 29, 37], it has also been suggested that there is a proportion of uncoupled turnover in these cases, due to lower specificity of unnatural substrates. Uncoupled turnover was not accounted for in the substrate inhibition kinetic studies carried out by Valegård *et al.* [1] but it is likely that uncoupled turnover might have influenced the inhibition studies. Moreover, the reduced specificity of unnatural substrates can easily lead to incorrect binding, *i.e.* binding in a non-optimal conformation, which would affect the turnover rates as well as the binding conformation observed in the crystal structures.

Additional studies in solution would help build a more complete image of the DAOCS substrate binding mechanism. Experiments involving the natural substrate, penicillin N, could help in gaining a more relevant perspective on the binding events. Further, alternative assay methods that allow distinction between these two reaction stages would be useful for kinetic data interpretation.

1.5 Objectives

The main objective of the described work was to provide further insight into the mechanism of DAOCS. The approach taken involved a combination of spectroscopic and spectrometric methods aimed at enzyme-substrate binding. Specific aims of this work were:

1. To investigate the binding of substrates using both protein-observe and ligand-observe approaches.
2. To quantify the strength of substrate and co-substrate binding by ligand dissociation constant measurements.
3. To optimise an assay that enables direct and simultaneous monitoring of both 2OG oxidation and penicillin ring expansion.
4. To perform initial studies for UV-Vis detection of reaction intermediates.
5. To carry out the above-mentioned studies using both penicillin G (the substrate used by Valegård *et al.* and penicillin N (the natural substrate).

Chapter 2

NMR-based activity assay for DAOCS

2.1 Reported assays for DAOCS

An extensive set of assays has been developed with the purpose of measuring the activity of various 2OG oxygenases [41]. Some of these assays could, in principle, be applied to all members of the family in order to quantify 2OG turnover while others are specifically designed to monitor prime substrate turnover. For DAOCS, the commonly used assays reported in literature are summarised in Table 2.1.

Most of these methods enables monitoring of turnover for only one of the substrates. Three different methods have been developed to measure the ring-expansion activity of DAOCS by exploiting various properties of the cephem [10, 29, 32, 38, 42] and/or penicillin [29, 32] molecule. The general [1-^{14}C]-2OG radioactive assay [43] as well as the succinyl-coenzyme A synthetase, pyruvate kinase, and lactate dehydrogenase coupled spectrophotometric assay [42] have been optimised for 2OG decarboxylation by DAOCS.

Simultaneous observation of 2OG and the penicillin substrate could provide valuable insight into the coupling mechanism. The values obtained from any of the reported ring-expansion assays cannot be accurately correlated with the values obtained from any of the 2OG turnover assays due to the very different

Table 2.1: *Assays used for DAOCS activity measurements*

Method of analysis	**Detecting**	**Analytical method**	**Ref.**
Hole plate bioassay	Cephalosporin	measurement of antibiotic activity (diameter of inhibition zone)	[10]
HPLC	Penicillin and cephalosporin	Separation by anion exchange or RP-HPLC	[32, 29]
Continous direct spectrophotometric	Cephalosporin	Absorbance at 260 nm characteristic of the dihydrothiazine moiety	[42] [38]
Coupled spectrophotometric	Succinate	Absorbance at 340 nm characteristic of NADH	[42]
NMR	Penicillin	Integration of characteristic resonance at 5.6 ppm against TSP	[29]
Decarboxylation of [1-^{14}C]-2OG	2OG	Radioisotope measurement of [^{14}C]-CO_2	[43]

experimental conditions in each case (Table 2.1). Thus, information regarding the coupling between 2OG oxidation and penicillin ring expansion in the same assay sample has not yet been reported.

2.1.1 NMR assays used for 2OG oxygenases

In the work of Flashman *et al.* [44], ^{1}H -NMR spectroscopy (700 MHz) was used to quantify the turnover catalysed by prolyl hydroxylase domain 2 (PHD2), a member of the 2OG oxygenase family. Integration of relevant peaks offered insight into the coupling between 2OG decarboxylation, succinate formation and substrate hydroxylation. Similarly, the activity of 2OG-dependent histone demethylases has been monitored using NMR in the work of Hopkinson *et al.* [45]. Using this as a starting point, together with conditions reported for previous assays (Table 2.1), a reaction mixture suitable for DAOCS turnover monitoring by NMR was established.

In one report NMR was used to analyse quenched reaction mixtures for DAOCS with PenG as a substrate [29]. Unlike the studies carried out by Flashman and Hopkinson, the analysis of the reaction catalysed by DAOCS was not performed continuously nor did it quantify coupling or 2OG turnover.

The focus of the next section was to optimise the NMR assay for the study of the reaction catalysed by prokaryotic DAOCS. It was hoped that insights into the catalytic mechanism would be gained by analysis of data on the coupling between 2OG decarboxylation and penicillin ring expansion.

2.2 Optimisation of an NMR-based assay

A final volume of 500 μL assay mixture (90% H_2O, 10% D_2O) was analysed in a 5 mm CORTECNET glass tube using a 500 MHz Bruker AVB machine. An initial delay of 4 min was inevitable due to the time taken to place the tube into the machine, and the time taken to set up the experiment: solvent locking (lock was performed on 90% H_2O, 10% D_2O and a water suppression scheme was used), frequency tuning, magnetic field shimming and pulse calibration. Turnover was then monitored in real time at room temperature by acquiring spectra every 93 s (8 scans per spectrum) for 15 min (total of 10 spectra). Control experiments were run by acquiring a spectrum of a sample containing buffer instead of DAOCS.

Deuterated NMR buffer was used in the assays in order to avoid signal suppression at the high buffer concentrations used (50 mM). It was decided against using HEPES buffer due to the more cost-efficient commercial availability of deuterated Tris buffer. Phosphate buffer was avoided in the assay as it substantially increases the rate of Fe(II) oxidation(Lambeth 1982 and Miller 1990) to Fe(III). It has been suggested that β-lactams, especially penicillins, may be hydrolysed by Tris or other cationic buffers [38]. However, it was hoped that any degradation occurring in the assay mixture would be visible in the ^{1}H -NMR spectrum (Figures S2 and S4).

2.2.1 Fe(II) concentration

A DAOCS concentration of 5-10 μM was used throughout. As shown by Dubus *et al.* [38], the variation of the Fe(II) concentration on reaction rate is negligible. A five fold excess of Fe(II) was used, which is the amount used in previous assays (Table 2.1). A higher amount of Fe(II) could also mean that in the absence of an appropriate reducing environment, the paramagnetic Fe(III) species would be formed causing peak broadening. This is undesirable in the context of an assay that relies on accurate peak integrations. It has been reported in the literature that certain bivalent metals, especially Zn [46] and Cd [47], catalyse penicillin G degradation through hydrolysis of the β-lactam ring. Control experiments were performed overnight, to assess the extent of degradation in the presence of Fe(II). Figure S2 shows how the presence of 50 μM Fe(II) leads to significant penicillin degradation after 4 hours. In order to avoid this undesired process as much as possible, the Fe(II) concentration used was a maximum of five-fold excess relative to DAOCS, while time courses for initial rate determination were kept around 20 minutes to further minimise degradation. 2OG and penicillin substrate concentrations varied according to the purpose of the experiment, but were close to the values previously reported (Table 2.1, typically 0.5 mM for 2OG, 2 mM for penicillin G and an equimolar ratio between 2OG and penicillin when penicillin N was used as a substrate).

2.2.2 Reducing agents

The activity of most 2OG oxygenases, including DAOCS, has been found to increase if reducing agents are present in the assay buffer. There are seven cysteinyl residues in DAOCS, but no intramolecular disulphide bridges, and no sulphydryl group involved in the binding of the active-site iron or the substrate [35]. Fe(II) can be easily oxidised by molecular oxygen at neutral pH. Therefore the reducing agents in the assay mixture could be fulfilling several roles: keeping the iron in a reduced state, deactivating reactive oxygen species (enzyme-bound or in solution) and reducing potentially faulty disulphide bridges.

Ascorbate was used as the only reducing agent. DTT was not used in the assay mixture as it has been reported [38] that its removal increases DAOCS activity. Ascorbate appears to be devoid of the negative effects of DTT [38]. It is possible that ascorbate keeps DAOCS active by maintaining the iron in the ferrous state. Ascorbate has also been proposed to reduce the ferryl species during uncoupled turnover, *e.g.* as in prolyl-4-hydroxylase catalysis [25], though other mechanisms are also possible.

2.2.3 Turnover observation

Simultaneous turnover of both 2OG and penicillin substrate was measured by quantifying the increase/decrease of relevant peak areas. The peaks chosen for integration correspond to more than 2 protons in order to increase signal-to-noise ratio and thus reduce integration errors. Penicillin turnover was measured by

integration of the penicillin (1.5 ppm region) and deacetoxycephalosporin (1.8 ppm region) methyl protons (Figures 2.1 and 2.2). 2OG turnover was quantified by integration of the 2OG (2.35 ppm and 2.91 ppm) and succinate (2.32 ppm) methylene protons, as previously described [44, 45]. The variations in peak areas for substrates/products were plotted against time and initial rates were calculated by linear fitting.

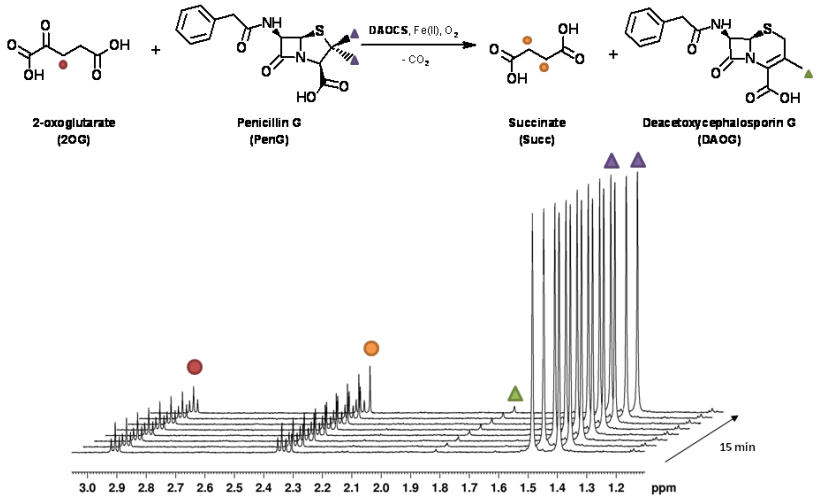

Figure 2.1: *Overview of the PenG ring expansion reaction catalysed by DAOCS (top), along with the main changes occurring in the high field region of* ^1H *-NMR spectrum (bottom). The stacked spectra were acquired every 93 s.*

As can be seen in Figure 2.1, in the experiments using penicillin G, the peaks chosen to monitor turnover do not overlap with other signals. However, in the case of penicillin N, the methylene signals of the side chain are in the same chemical shift region as the deacetoxycephalosporin methyl singlet. Similarly, there is another methylene group from the penicillin N side chain whose signal overlaps with signals for both 2OG and succinate in the region of 2.3 - 2.4 ppm.

Therefore, it is for the reason of signal overlapping that we chose not to calculate rates from absolute concentrations. As described above, the increase in peak area relative to the first acquired spectrum was used instead for initial rate determinations.

In performing their catalytic function, 2OG oxygenases couple the decarboxylation of 2OG with substrate oxidation *i.e.* oxidative ring expansion in the case of DAOCS (Section 1.2.2). If these two reactions are fully coupled (coupling is approximately 100%), then for every molecule of 2OG that is decarboxylated, there is one molecule of penicillin that undergoes the ring expansion reaction. The coupling of the two transformations (Equation 2.1) is thus defined as being the ratio between the amounts of turnover quantified in each case and it can be calculated using substrate/product concentrations or initial rates:

$$coupling(\%) = \frac{[Pen]_0 - [Pen]}{[2OG]_0 - [2OG]}100 = \frac{[DAC]}{[Succ]}100\frac{v_{0(Pen)}}{v_{0(2OG)}}100 = \frac{v_{0(DAC)}}{v_{0(Succ)}}100 \tag{2.1}$$

Where:

$[2OG]_0$ and $[Pen]_0$ are the initial concentrations of 2OG and the penicillin substrate.

$[Succ]$ and $[DAC]$ are the succinate and deacetoxycephalosporin concentrations determined for a particular time point.

$v_{0(2OG)}, v_{0(Pen)}, v_{0(Succ)}$ and $v_{0(DAC)}$ are the initial rates determined for 2OG, penicillin substrate, succinate and deacetoxycephalosporin product.

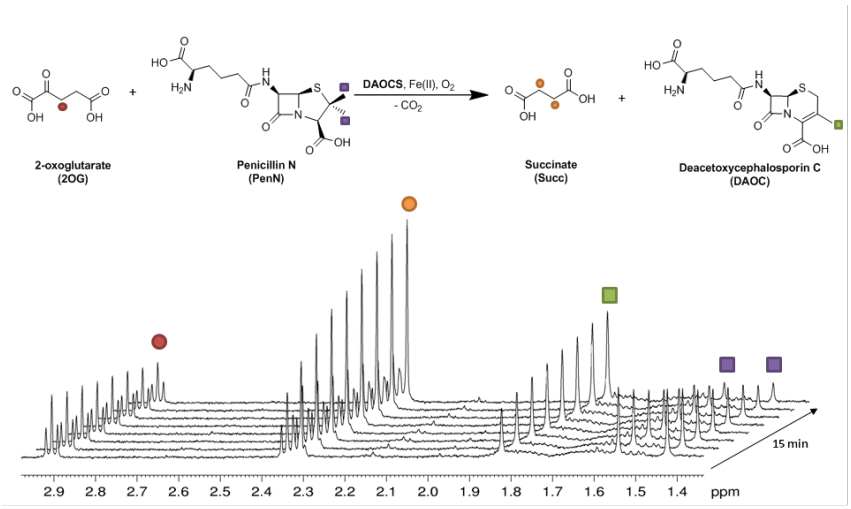

Figure 2.2: *Overview of the PenN ring expansion reaction catalysed by DAOCS (top), along with the main changes occurring in the* ^1H *-NMR spectrum (bottom). The stack spectra were acquired every 93 s.*

A graphical approach of analysing coupling between 2OG and penicillin oxidation is by plotting the concentrations of the products of the two reactions against each other. If the reactions are coupled, the data points will describe a line passing through origin. Moreover, the gradient provides an indication of the coupling ratio. In the present experimental context where the reaction stoichiometry is 1:1, a gradient of 1 describes 100% coupling between the two reactions. A slope smaller than one is due to more succinate being present and would thus be indicative of either uncoupled turnover or of cephalosporin product degradation. Control experiments have confirmed that the latter does not occur, at least to the limit of detection by NMR (Figure S3).

2.3 Results

2.3.1 Coupling ratios

Figure 2.3(left) shows turnover data for penicillin N ring expansion. By plotting the concentrations of succinate on the x axis and the ring expansion product concentrations on the y axis, as shown in Figure 2.3 (right), average coupling values can be obtained for the catalytic process. The amount of coupling was determined by calculating the slope of the linear fit.

When using penicillin N as the prime substrate, coupling of approximately 100% was observed. However, when using penicillin G, a decrease in coupling under the same reaction conditions was observed, with the average coupling being reduced to approx. 20%, *i.e.* the initial rate for penicillin G oxidation is lower than penicillin N oxidation.

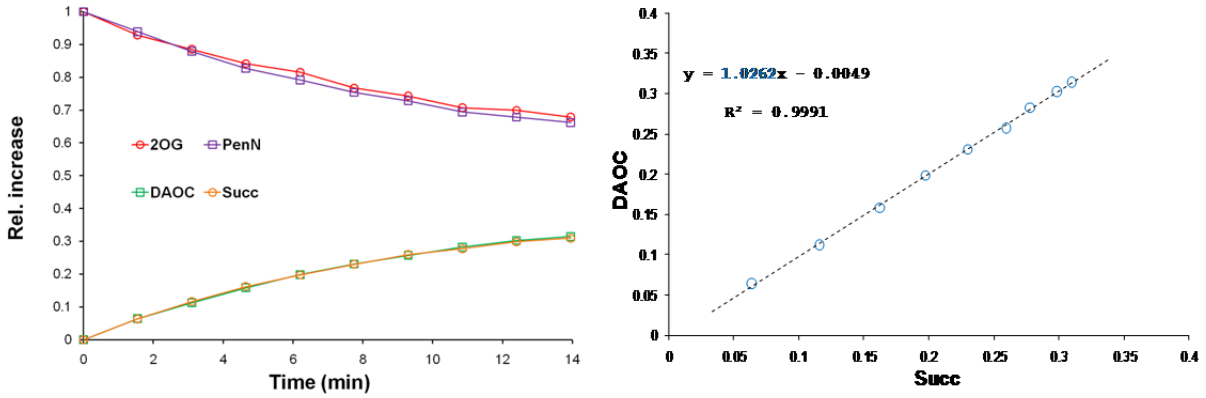

Figure 2.3: *General plot showing the turnover of 2OG and penicillin N at 93 s time intervals. The relative increase in peak area was plotted against time (left); the line connecting the data points was added for ease of interpretation. The coupling between 2OG oxidation and penicillin N ring expansion was assessed by plotting the concentrations of the products against each other (right). The slope of the linear fit describes the coupling between the two reactions.*

Experimental data shows that 2OG decarboxylation remains approximately 100 % coupled to penicillin oxidation when the natural substrate is used, regardless of the ratio between substrates. However, when PenG is used as a substrate, the ratio between 2OG and PenG strongly influences the coupling between the two oxidative reactions. As shown in Figure 2.4, an increase in PenG concentration from 0.25 mM to 10 mM, leads to a very slight decrease in the initial rate of PenG turnover, but more importantly, to an increase in coupling from 35 % to 70 %. The dramatic increase in coupling is determined by the decrease of initial rate for 2OG decarboxylation at increasing PenG concentrations.

Upon performing the same experiment but monitoring only penicillin G turnover, Valegård *et al.* have concluded that an increase in penicillin G concentration determines a decrease in DAOCS turnover rate, thereby proposing substrate inhibition. The small decrease in penicillin G initial rate at high concentrations was also visually augmented by the choice of Valegård *et al.* to present their results using a double reciprocal plot. In the light of the new insight obtained by the NMR-based assay, the result could be attributed to a mechanism that is not substrate inhibition due to binding at overlapping sites. Considering the fact that penicillin G is not the natural substrate and has lower affinity for DAOCS (Section 4.1.4.2.3), increasing its concentration could contribute to the increase in coupling by not allowing the reactive oxidising species to be reduced by other species present in the system; the negative effect on the 2OG turnover rate could be explained by penicillin G being a weaker reducing agent than other species present.

Substrate concentrations were varied as described by Valegård *et al.* in the context of using the natural

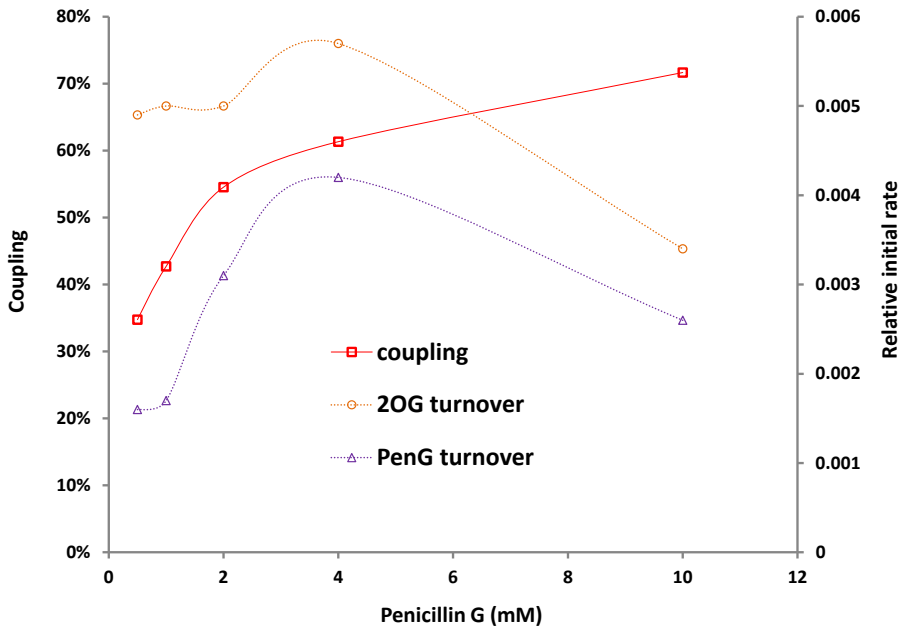

Figure 2.4: *The influence of penicillin G concentration on coupling. The natural substrate, penicillin N, was used in experiments where 2OG concentration was varied (PenN was kept at 0.5 mM, red circles) as well as in experiments where penicillin N concentration was varied (2OG was kept at 0.5 mM, blue triangles). The lines connecting the data points have been inserted for ease of interpretation.*

substrate, penicillin N (Figure 2.5). It was found that penicillin N concentrations above 1 mM cause a substantial decrease in the rate of turnover. A much smaller effect was observed with increasing 2OG concentrations. A possible explanation for this phenomenon could be the Fe(II) cofactor being chelated by penicillin N when high amounts are available in the system. This observation is consistent with the discussions in Section 3.2.3.

2.3.1.1 The influence of ascorbate on coupling

As described earlier in Section 2.2.2, the reducing agent chosen for the assays is ascorbate. The low concentration of Asc recommended in literature (0.1 mM) [38] is rather counter-intuitive considering the very high ascorbate (4 mM) concentrations used in assays for many but not all other 2OG oxygenases [4, 25, 27].

DAOCS catalysis is low in the absence of ascorbate (Figure 2.6). However, addition of ascorbate in the reaction mixture increases the catalytic activity of DAOCS. It is interesting to note that the addition of ascorbate changes the coupling between 2OG and penicillin G oxidation. While in the absence of ascorbate coupling of around 70% is achieved, the addition of ascorbate leads to a decrease in coupling down to about 40% (Figure 2.6).

Previous literature data, particularly work from Dubus *et al.* [38], indicate that a relatively low concentration of ascorbate (approx. 100 μM) is preferred in DAOCS assays. These conclusions however, have

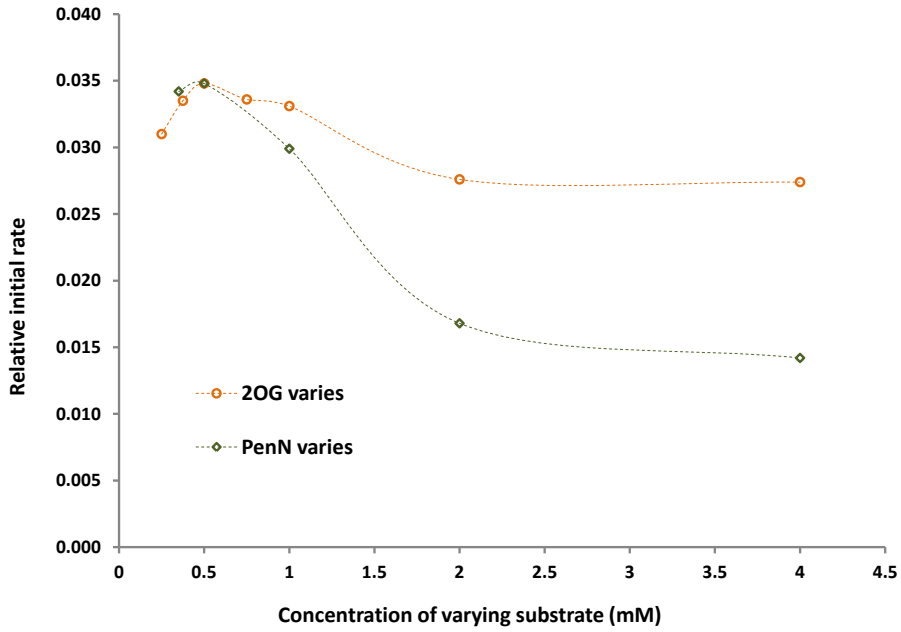

Figure 2.5: *Basic substrate inhibition experiments in which the concentration of one substrate was varied while the concentration of the other remained constant. The natural substrate, penicillin N, was used in experiments where the 2OG concentration was varied (PenN was kept at 0.5 mM, red circles) as well as in experiments where penicillin N concentration was varied (2OG was kept at 0.5 mM, blue triangles). The lines connecting the data points have been inserted for ease of interpretation.*

been drawn from experimental data that only quantifies penicillin G turnover. Assays carried out in the presence of increasing amounts of ascorbate by NMR (Figure 2.7) reveal that indeed, ascorbate concentrations above 0.1 mM are inhibitory for penicillin G ring expansion. Nevertheless, a crucial observation to be made is that 2OG turnover in the same samples was only slightly inhibited by concentrations of reducing agent above 0.75 mM. It is a consequence of this discrepancy that the coupling between 2OG decarboxylation and penicillin G ring expansion decreases with increasing ascorbate concentrations. If the assay is carried out using penicillin N, results show that, turnover is inhibited at ascorbate concentrations lower than 0.1 mM. The 2OG decarboxylation remained coupled 1:1 to penicillin N ring expansion at all ascorbate concentrations (Figure S10).

2.3.2 Substrate inhibition

As described in Section 1.3.3, Valegård *et al.* have performed simple substrate inhibition experiments in which the concentration of one substrate was varied while the concentration of the other remained constant [1]. The assay they used quantifies ring expansion turnover. Their results show a major decrease in reaction rate when 2OG concentration was increased while PenG concentration was maintained constant. Analogous behaviour, but less pronounced was observed when penicillin G concentration was increased and the 2OG concentration was kept the same [1].

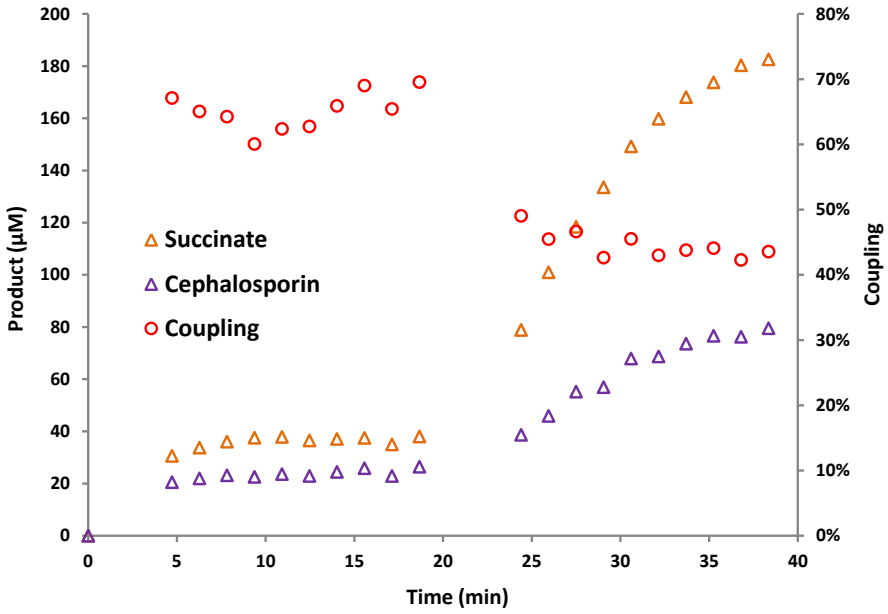

Figure 2.6: *The presence of ascorbate in the reaction mixture has a significant influence on the degree of coupling of 2OG to penicillin G turnover. For the first 20 minutes, the reaction was allowed to proceed in the absence of ascorbate. The reducing agent was then added (0.25 mM) and a dramatic increase of turnover. However, the ratio between decarboxylation (succinate formation, orange triangles) and ring expansion (cephalosporin G formation, purple triangles) was not preserved after the addition of ascorbate, as described by the decrease in coupling values calculated for each time point (red circles). The reaction is likely to occur in the first 4 minutes, prior to NMR analysis.*

The results of analogous experiments performed by NMR as described here are in agreement with the results obtained by Valegård *et al.* in terms of PenG turnover. However, increasing the 2OG concentration would lead to an increase the rate of uncoupled 2OG decarboxylation, the consequence of which would be a decrease in PenG ring expansion. Increasing PenG concentration while 2OG concentration is kept constant (Figure 2.4) leads to more efficient coupling despite a relatively small decrease in turnover rate at concentrations higher than 4 mM.

2.4 Discussion

As shown in Figure 2.4, the coupling ratio is strongly influenced by the relative amount of penicillin G but not penicillin N present. The very pronounced decrease in initial rate for 2OG decarboxylation at increasing PenG concentrations could be interpreted as substrate inhibition. However, it is known that DAOCS is capable of sustaining uncoupled 2OG decarboxylation, both in the absence of any penicillin substrate as well as in the presence unnatural substrates [29]. The lower binding affinity of unnatural substrates could 'promote' uncoupled turnover, but increasing the concentration of the unnatural substrate will allow more molecules of unnatural substrate to be bound, leading to coupled catalysis, which, in the case of penicillin G, occurs at a slower rate than uncoupled. This will reduce the amount of uncoupled

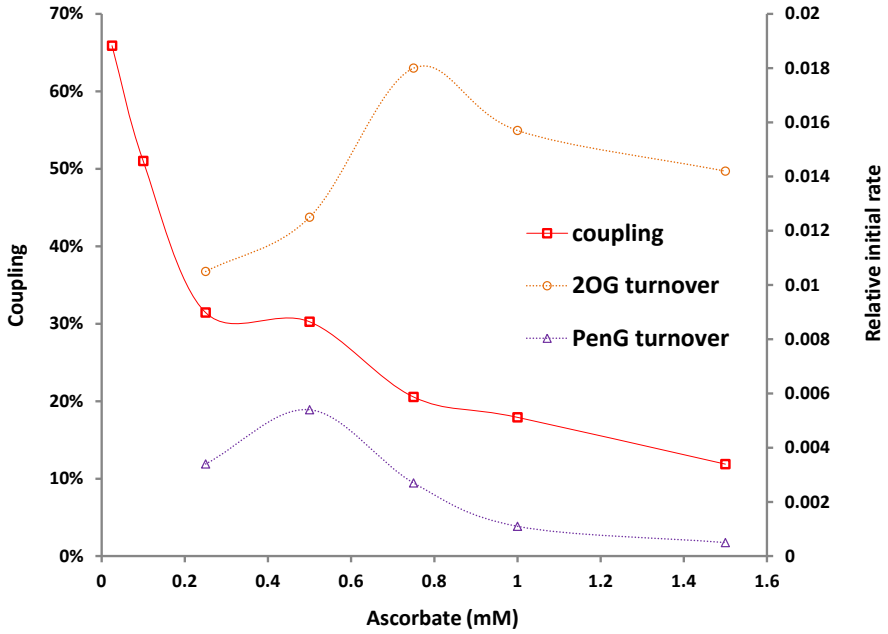

Figure 2.7: *The influence of ascorbate concentration on the coupling between the penicillin G ring expansion and 2OG decarboxylation reactions. Initial rates for 2OG decarboxylation (orange circles) and penicillin G ring expansion (purple triangles) as well as the coupling between the two (red squares) were plotted against increasing concentrations of ascorbate. The lines connecting the data points have been inserted for ease of interpretation.*

turnover.

Valegård *et al.* argue that the rate of uncoupled turnover increasing with increasing concentrations 2OG, supports their proposed ping-pong mechanism [1]. However, in light of the coupling information obtained in this study, this may not be the case. The results obtained here indicate that in the presence of penicillin G, there is a high proportion of uncoupled turnover occurring. Increasing 2OG concentration should naturally increase the rate of uncoupled turnover, by allowing the enzyme to follow a different catalytic pathway. It thus follows that while uncoupled turnover can be observed with unnatural substrates, it does not support or reject the consensus mechanism.

It is interesting to note that the concentration of ascorbate has an influence on the coupling between 2OG oxidation and PenG ring expansion. When PenN was used as a substrate, ascorbate was not found to have any influence on coupling; DAOCS sustains it catalytic activity at a very low (barely detectable) rate in the absence of ascorbate. It was found that increasing concentrations of ascorbate has a detrimental effect on penicillin G ring expansion. However, the increase in ascorbate concentration did not affect the rate of 2OG decarboxylation. It is thus possible that in the presence of an unnatural substrate displaying poorer binding affinity, such as penicillin G, ascorbate may enter the active site more easily and thus gets oxidised by the reactive oxidising species instead of the penicillin substrate.

2.5 Conclusions

The coupling between 2OG decarboxylation and penicillin ring expansion was found to be dependent on the type of penicillin substrate used. It was observed that the two reactions were fully coupled in the presence of the natural substrate, penicillin N, while in the presence of an unnatural substrate, penicillin G, a high degree of uncoupled turnover was observed.

For penicillin G (but not penicillin N) it was also observed that the amount of ascorbate present in the system also has an influence on coupling. In the presence of penicillin G substrate, ascorbate was found to have a strong influence on the coupling between the two reactions. The increase in uncoupled turnover at high ascorbate concentrations led to the proposal that under such conditions ascorbate may be preferentially oxidised over penicillin G.

High ascorbate concentrations do not disrupt the 1:1 coupling between 2OG oxidation and penicillin N ring expansion. This fact is consistent with penicillin N having a higher binding affinity that penicillin G, as indicated by the dissociation constants determined in Section 4.1.4.2.2 (Table 4.1).

Chapter 3

Binding studies by mass spectrometry

The characterisation of molecular interactions between recombinant proteins and ligands of interest can be achieved using various biophysical affinity-based technologies [48]. However, the relatively recent development of 'non-destructive' ionisation methods for mass spectrometry has enabled, at least in some cases, the study of folded proteins without disrupting their tertiary structure [49, 50]. This technique is referred to as non-denaturing or native mass spectrometry.

Non-denaturing mass spectrometry can be used as a 'protein-observe' technique towards the study of non-covalent protein-ligand interactions under near physiological conditions [51, 52]. Accurate determination of mass and stoichiometry can be achieved while using relatively small amounts of protein and in a short experiment time [48].

3.1 Electrospray ionisation mass spectrometry (ESI-MS)

The scientific importance of electrospray ionisation mass spectrometry (ESI-MS) was recognised by the 2001 Chemistry Nobel Prize being awarded to John B. Fenn and Koichi Tanaka *for their development of soft desorption ionisation methods for mass spectrometric analyses of biological macromolecules*. Electrospray ionisation uses a strong magnetic field (approx. 3 kV) to produce a charged spray of droplets under atmospheric pressure. The droplets are then passed through a drying gas (typically nitrogen) at high a temperature (100-200 ℃) which causes the solvent to evaporate from the droplets and thereby reducing their size. It is proposed that the increased charge per size ratio causes Coulombic repulsion that overcomes the surface tension if the droplets. The subsequent "explosion" of droplets leads to the formation of desolvated/partially desolvated ions that are then passed into a vacuum where they are focused and accelerated.

One of the most common analysers used for the ions produced by ESI is the time-of-flight (TOF) analyser

Table 3.1: *Comparison between non-denaturing and denaturing ESI-MS conditions.*

	Non-denaturing ESI-MS	**Denaturing ESI-MS**
Solvent	Ammonium acetate or ammonium bicarbonate	0.1 % formic acid, 50 % acetonitrile or 10 % methanol in water (% v/v)
Pressure	High	Lower
Protein	Predominantly folded	Predominantly unfolded

where they are separated based on their mass-to-charge ratio. The time-of-flight analyzer uses an electric field to accelerate all the ions through the same potential, and then measures the time they take to reach the detector. If the particles all have the same charge, the kinetic energies will be identical, and their velocities will depend only on their masses. Lighter ions will reach the detector first whereas the heavier take longer. [53]

3.1.1 ESI-MS studies on protein-ligand interactions

The ability of ESI to transmit multiple charges on a protein molecule as well as to desolvate the resulting ion with minimal energy transfer, opened up the perspective of studying biomolecular interactions by mass spectrometry. The general conditions for detecting such weak interactions by ESI-MS include spraying the protein from a near-neutral volatile aqueous buffer solution, with a low desolvation temperature (typically lower than 50 ℃), and a reduced cone voltage setting (typically 20 - 50 V, but dependent on instrument type). The use of collisional cooling can also be effective in reducing the internal energy of non-covalent ion complexes, thus preventing dissociation [54].

Volatile buffers are used in non-denaturing conditions (Table 3.1) as other common buffers (HEPES, MES or Tris) can form adducts with the protein of interest. The protein sample thus has to be desalted prior to use in the ESI-MS experiment. Organic or acidic media are not normally suitable for non-denaturing (native) analysis by ESI-MS because protein folding is disrupted under these conditions. However, some proteins do not ionise easily or give poor spectra. In these cases non-denaturing ESI-MS is not an appropriate method of analysis.

Partially denaturing conditions (Table 3.1) can be used to analyse the mass of a protein. The fact that the protein is partially unfolded under these conditions, makes the amino acid residues more accessible to protonation leading to highly charged species being observed in the spectrum. ESI-MS spectra collected under denaturing conditions do not contain information about oligomerisation and non-covalent interactions.

Under non-denaturing conditions protein oligomerisation can be distinguished from monomeric species, with the molecular weight of the species present being calculated from the series of m/z values. The stoichiometry of interaction and strength of binding can also be assessed by this method. ESI-MS has been used for the investigation of metalloenzyme inhibition [55, 56] and enzyme-metal ion interactions

[57]. It is important to note that even though certain types of interactions are influenced differently by the solution to gas phase transition [58], it has been shown that for metalloenzymes, at least in some cases, there is good agreement between non-denaturing ESI-MS and solution-to-gas-phase analyses [55, 56, 57, 59, 60].

3.2 DAOCS substrate binding studies by ESI-MS under non-denaturing conditions

3.2.1 Studies on 2OG oxygenases by ESI-MS under native conditions

Non-denaturing ESI-MS has successfully been applied to the study of enzyme-metal, enzyme-substrate and enzyme-inhibitor interactions for members of the 2OG oxygenase family. For example, Rose *et al.* have used non-denaturing ESI-MS for screening of inhibitor scaffolds for the human 2OG-dependent JMJD2 subfamily of histone demethylases [61] and subsequently for gaining insight into the binding potential of inhibitor probes [62]. Various potential iron-chelating groups of PHD2 inhibitors have been screened using non-denaturing ESI-MS [59]. A combined library/residue substitution/ESI-MS approach was used for analyzing residue reactivity in the work of Mecinovic *et al.* [63]

In terms of enzyme-metal interactions, studies on PHD2 revealed an unanticipated second metal binding site using non-denaturing ESI-MS in combination with mutagenesis analyses [57]. Loenarz *et al.* used non-denaturing ESI-MS for the characterisation of the *Trichoplax adhaerens* prolyl hydroxylase domain in terms of iron and substrate binding [64]. Non-dentaturing ESI-MS has thus proven to be a useful tool in assessing the binding of metals, substrates and ligands to 2OG-dependent oxygenases. This method was therefore used in my work to gain insights into enzyme-substrate complex formation for DAOCS.

3.2.2 Studies on DAOCS by ESI-MS under native conditions

3.2.2.1 DAOCS

DAOCS was found to be suitable for ESI-MS analyses under non-denaturing conditions: samples containing 5 μM DAOCS, yielded a clean spectrum with sharp peaks (Figure 3.1). Dominant ions could be observed at m/z 2879, 3141 and 3455, corresponding to the M+12, M+11 and M+10 charge states, respectively. These are the charge states used for deconvolution of mass spectra throughout the work in this chapter.

Deconvolution of the mass spectrum reveals a molecular weight of 34543.5 Da (Figure 3.1, insert), a value which is similar to the one predicted by using the amino acid sequence (34555.7 Da). The ProtParam

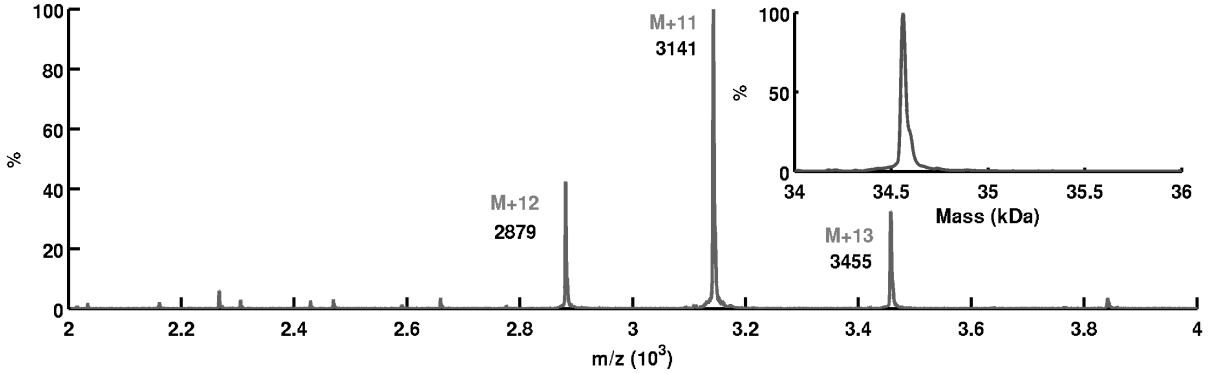

Figure 3.1: *The mass spectrum for DAOCS contains dominant ions that correspond to the M+12, M+11 and M+10 charge states. The insert contains a deconvoluted spectrum for DAOCS. The spectrum was obtained at 50 V cone voltage.*

tool provided by ExPASy was used to calculate the molecular weight of DAOCS from its amino acid sequence [31].

The purification protocol uses EDTA in the ion exchange chromatography buffers which has most likely removed any Fe(II) or other metals DAOCS may co-purify with. Additional ETDA treatment followed by ESI-MS analysis did not reveal any change in the spectrum. Thus, it was concluded that DAOCS is purified in apo form and the batch used in the experimental work of this chapter was not further treated to remove metals.

3.2.2.2 Binding of metals

Samples containing increasing amounts of metal were run under non-denaturing conditions in order to establish the ratios required to form complete ezyme-metal complexes. The metals used in this study were Fe(II), Mn(II) and Zn(II). Being the natural cofactor and considering how it binds to most other studied 2OG oxygenases [9], Fe(II) was expected to bind to DAOCS in an 1:1 enzyme:metal ratio, it became apparent that a five fold excess of Fe(II) is required in order to achieve complete formation of the DAOCS.Fe(II) complex at least as observed by ESI-MS (Figure 3.2, complex B).

Mn(II) and Zn(II) binding to DAOCS was then analysed because these metals are used as substitutes for the natural cofactor in the experiments in Sections 4.1 and 4.2. The results showed that Mn(II) binds similarly to Fe(II) to the *apo* form of DAOCS. At a five fold excess of Mn(II), the DAOCS.Mn(II) complex is dominant (*apo*-DAOCS:DAOCS.Mn(II) = 1:2), as observed by ESI-MS (Figure 3.2, complexes A and B"). However, complete formation of the DAOCS.Mn(II) complex could not be observed by this method due to the fact that at higher than five fold excess Mn(II), the quality of the mass spectrum deteriorates significantly.

In order to form a saturated DAOCS.Zn(II) complex, a lower Zn(II):DAOCS ratio is required than in the cases of Fe(II) and Mn(II). A two-fold excess of Zn(II) was found to be the minimum amount of metal

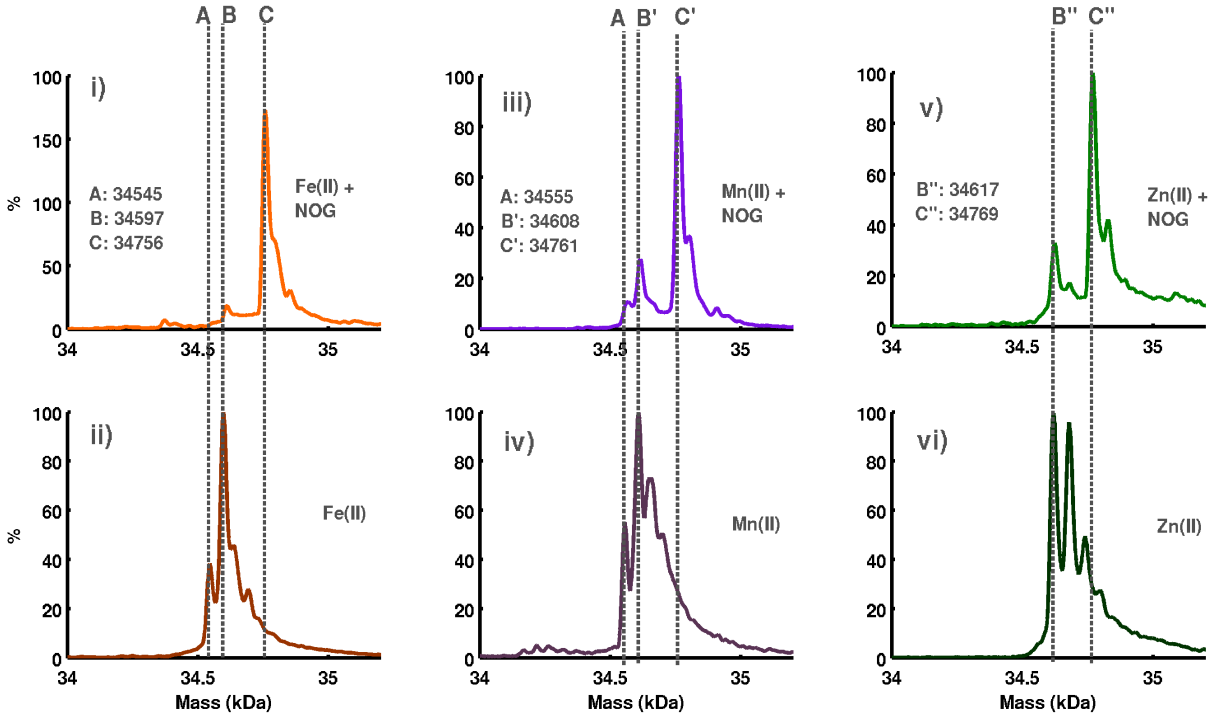

Figure 3.2: *Complexes of DAOCS with various metals and with N-oxalyl glycine (NOG) as observed by non-denaturing ESI-MS at a 50 V cone voltage. The peaks in the spectrum correspond to the masses of (A)* apo-*DAOCS, (B) DAOCS.Fe(II) complex, (C) DAOCS.Fe(II).NOG complex, (B') DAOCS.Mn(II) complex, (C') DAOCS.Mn(II).NOG, (B") DAOCS.Zn(II) complex, (C") DAOCS.Zn(II).NOG complex. In the case of Fe(II) a five-fold excess was used while in the case of Zn(II) and Mn(II), a two-fold and a four-fold excess were used, respectively. For NOG, five, five, and two equivalents were used in the presence of Fe(II), Mn(II) and Zn(II), respectively.*

that leads to complete DAOCS.Zn(II) complex formation (Figure 3.2, complex B'). However, the excess of Zn(II) in the system leads to the formation of complexes containing more than one Zn(II) per molecule of DAOCS.

The DAOCS.Fe(II) complex can be clearly seen at 50 V cone voltage. Increasing the cone voltage to 200 V leaves the mass spectrum virtually unchanged. If a higher than five-fold Fe(II) excess is used, additional peaks corresponding to DAOCS complexes with more than one Fe(II) ion are observed at a 50 V cone voltage. Increasing the cone voltage in this case leads to the disappearance of the additional peaks, leaving the DAOCS.Fe(II) peak as the dominant one. This result indicates that one Fe(II) ion binds to DAOCS significantly more strongly than the others and the site where this occurs is probably the catalytic pocket.

The DAOCS.Mn(II) complex observed at 5-fold Mn(II) excess displays similar stability. Increasing the cone voltage up to 200 V does not have a significant influence on the spectrum that is obtained.

In the case of zinc, complexes with more than one Zn(II) were found to have reduced stability; increasing the cone voltage to 100 V leaves only the DAOCS.Zn(II) complex visible in the mass spectrum. This complex remains stable, even at higher voltages, like the previously discussed Fe(II) and Mn(II) ones.

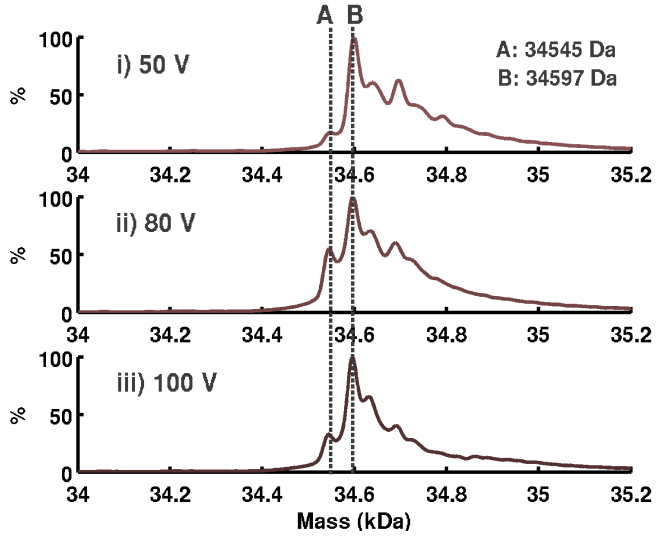

Figure 3.3: *Complexes of DAOCS with ten-fold excess Fe(II) at increasing cone voltages: i) 50V; ii) 80V; iii) 200V. Though several Fe(II) ions are observed to bind to DAOCS, these complexes are unstable in the mass spectrometer at high cone voltages. A: DAOCS; B: DAOCS.Fe(II)*

Non-denaturing mass spectrometric studies do not provide direct information about the binding site of ligands. Therefore, in order to establish whether Fe(II), Zn(II) and Mn(II) bind at the same site, competition experiments with a mixture of all three metals were carried out. DAOCS was incubated with all three metals at saturating concentrations relative to the amount of enzyme present. The resulting spectrum, acquired at a 50 V cone voltage, did not reveal evidence for binding of more than one metal. The mass spectrum contained just one peak corresponding to the DAOCS.metal complexes.

3.2.2.3 Binding of 2OG and 2OG analogues

Binding of 2OG to the *apo*-DAOCS and DAOCS.metal complexes was then investigated. No binding of 2OG to DAOCS was observed in the absence of a metal cofactor at a five- and ten-fold excess of 2OG. In the presence of Fe(II), a DAOCS.Fe(II).2OG complex can be observed at a five fold excess 2OG (relative to DAOCS). The intensity of the peak corresponding to this complex decreases over time (Figure 3.4), which would be indicative of 2OG being turned over to succinate and carbon dioxide. A distinct peak corresponding to the DAOCS.Fe(II).Succ complex was not observed. Other peaks present correspond to the masses of *apo*-DAOCS and the DAOCS.Fe(II) complex.

When using Mn(II) as the metal cofactor, a clear spectrum could not be obtained for a mixture containing 2OG. In the case of zinc, a small peak (50% intensity) corresponding to the DAOCS.Zn(II).2OG complex could be observed when mixing the DAOCS.Zn(II) complex with a five-fold excess of 2OG at 50 V. Increasing the cone voltage up to 80 V led to the disappearance of the DAOCS.Zn(II).2OG complex from the mass spectrum, with the DAOCS.Zn(II) complex being the only one that is stable at high cone voltages.

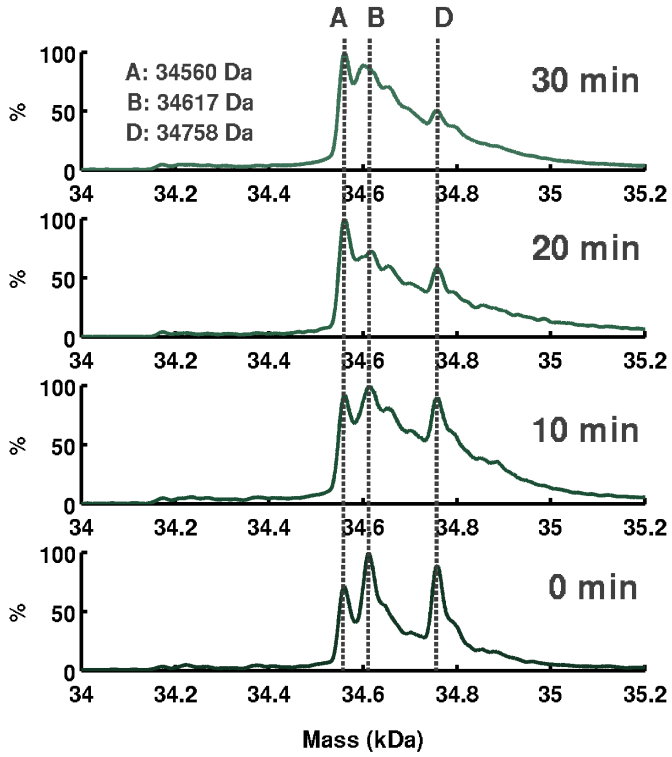

Figure 3.4: *Time course analysis of the DAOCS.Fe(II).2OG complex by non-denaturing ESI-MS. The notations correspond to (A)* apo-*DAOCS, (B) DAOCS.Fe(II) and (D) DAOCS.Fe(II).2OG. Peak height for complex D decreases in time, indicating that 2OG is being consumed during uncoupled turnover. The spectra were acquired at a 50 V cone voltage.*

The binding of *N*-oxalyl glycine (NOG), an analogue of 2OG, was also studied. NOG does not react because it has an amide group instead of a ketone, however, it binds similarly to 2OG. Non-denaturing mass spectrometric binding studies using NOG have shown that only a two fold excess of inhibitor is necessary to form the DAOCS.Fe(II).NOG complex (Figure 3.2, complex C). The complex is stable both in time and at higher voltages.

With a Mn(II) cofactor, NOG forms a DAOCS.Mn(II).NOG complex that is unstable at voltages higher than 50 V (Figure 3.2, complex C'). Increasing the cone voltage to values above 50 V led to the observation of *apo*-DAOCS and DAOCS.Mn(II) peaks.

When using Zn(II) as the metal cofactor, a stable DAOCS.Zn(II).NOG complex is observed at 50 V (Figure 3.2, complex C"). In this case, similar to the case of Mn(II), increasing the cone voltage above 80 V leads to the observation of the DAOCS.Zn(II) complex without the DAOCS.Zn(II).NOG complex (Figure 3.2, complex B').

3.2.2.4 Binding of penicillin substrates

Unlike the binding of 2OG and NOG, penicillin G (PenG) binds to *apo*-DAOCS, when a ten-fold excess of penicillin G is used (30% intensity relative to the *apo*-DAOCS peak). However, increasing the cone

voltage decreases the peak intesity of this DAOCS.PenG complex, finally leading to its disappearance above 80 V cone voltage. In contrast to PenG, binding of penicillin N (PenN) is not observed in the absence of a metal cofactor.

In the presence of Fe(II), the formation of a strong DAOCS.Fe(II).PenG complex is observed. However, use of higher cone voltages (above 80 V) leads to the disappearance of the signal for this complex, with only the *apo*-DAOCS and DAOCS.Fe(II) being visible in the mass spectrum. In contrast, when penicillin N is used, no peak corresponding to a DAOCS.Fe(II).PenN complex is observed. However, prolonged incubation of PenN with the DAOCS.Fe(II) complex leads to an increase in the *apo*-DAOCS peak over time (Figure 3.5). This is possibly due to metal chelation by penN or its degradation products. The same phenomenon is only mildly detectable in the case of penicillin G. Similar behaviour was observed in the presence of Zn(II), but with Mn(II) clear spectra could not be obtained.

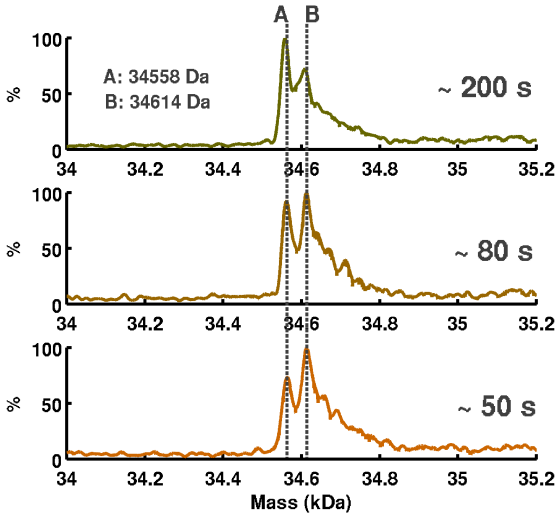

Figure 3.5: *Time course analysis of the DAOCS.Fe(II) complex in the presence of PenN. Incubation of the DAOCS.Fe(II) complex with PenN shows that over the course of 200 seconds, the intensity for the DAOCS.Fe(II) peak (B) decreases relative to the* apo-*DAOCS peak (A).*

When PenG is added into a mixture containing DAOCS, Fe(II) and 2OG, the mass spectrum that is obtained displays a series of peaks. The quality of the spectrum is poor due to the large number of compounds present as salts and most likely due to turnover probably occurring. The experiment was thus repeated using NOG instead of 2OG. The resulting spectrum (Figure 3.6, left spectrum) clearly displays a dominant peak corresponding to the DAOCS.Fe(II).NOG complex (C), as well as a smaller peak (50% relative intensity) corresponding to a ternary DAOCS.Fe(II).NOG.PenG complex (V). A very small peak corresponding to a DAOCS.Fe(II).NOG.2PenG complex is also visible.

Using penicillin N instead of penicillin G in an equivalent experiment, produces a spectrum containing a dominant peak corresponding to the ternary DAOCS.Fe(II).NOG.PenN complex (Figure 3.6A).

The lack of a DAOCS.NOG.PenG peak in Figure 3.6B confirms the previous results which indicate that NOG does not bind to DAOCS if a metal cofactor is not already bound.

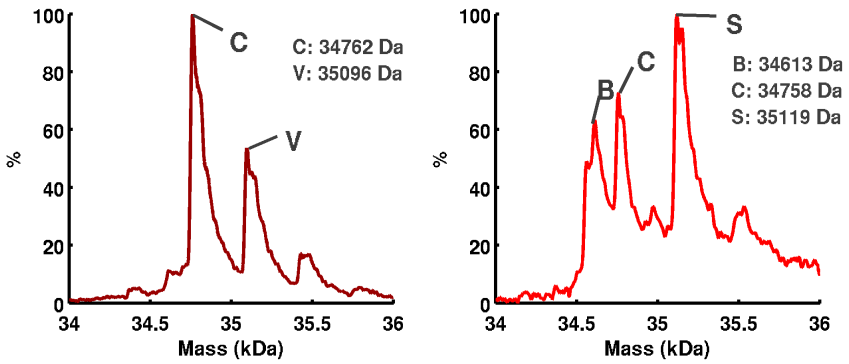

Figure 3.6: *The formation of a ternary complex between DAOCS, NOG and its penicillin substrate was detected using non-denaturing mass spectrometry (50 V cone voltage). The penicillin substrates used were penicillin N (the natural substrate, right) and penicillin G (used by Valegård et al. in their studies, left). The complexes present in the spectrum correspond to (B) DAOCS.Fe(II), (C) DAOCS.Fe(II).NOG, (V) DAOCS.Fe(II).NOG.PenG, and (S) DAOCS.Fe(II).NOG.PenN.*

Analogous experiments could not be carried out with Zn(II) as the metal centre because complexes containing several Zn(II) ions are formed at the cone voltage (50 V) used in this experiment (Figure 3.2). Whilst increasing the cone voltage will remove additional Zn(II) ions bound (probably) to the surface of DAOCS, it also appears remove (some of) the bound penicillin G.

3.2.3 Discussion

Non-denaturing mass spectrometry was found to be a suitable method for the analysis of substrates binding to DAOCS. They show that DAOCS is purified in *apo* form and it is able to bind metals such as Fe(II), Zn(II) and Mn(II). In all cases the DAOCS.metal complex could be observed as a predominant peak. Competition experiments imply that in the case of the DAOCS.metal complexes, Fe(II), Zn(II) and Mn(II) bind at the same site.

2OG and NOG bind to DAOCS.metal complexes but not to *apo*-DAOCS. This result is consistent with the order of substrate binding proposed in the consensus 2OG oxygenase mechanism, whereby the ferrous cofactor binds to the enzyme, followed by 2OG which binds to the Fe(II) centre. When Fe(II) was used as a cofactor, uncoupled turnover could be observed through the disappearance of the DAOCS.Fe(II).2OG peak over a 30 minute time course. Use of the non-reactive substrate analogue, NOG, gave a stable complex over the 30 minute time course analysis.

Complete formation of the DAOCS.Fe(II).2OG complex was not observed using non-denaturing mass spectrometry. Replacing the Fe(II) with other metal cofactors (*i.e.* Mn(II) or Zn(II)) that do not enable DAOCS to sustain the catalytical function also did not lead to complete formation of a DAOCS.metal.2OG complex. It is possible that DAOCS.metal.2OG complexes are not very stable under the ESI-MS conditions.

Importantly, penicillin G was observed to bind to DAOCS even in the absence of a metal cofactor or

2OG. Increasing the cone voltage leads to the dissociation of DAOCS.PenG and DAOCS.metal.PenG complexes. It is therefore possible that PenG can bind to DAOCS, away from the active site, possibly via hydrophobic interactions of its benzylic side chain. The presence of 2OG or NOG leads to the formation of a ternary enzyme-substrate complex that is stable at higher voltages. An explanation for the increased binding strength of PenG in the presence of 2OG could be that 2OG binding induces conformational changes that create a more specific binding site for the penicillin substrate, as reported for other 2OG oxygenases. Nevertheless, the fact that PenG also binds (though very weakly) in the absence of 2OG and even in the absence of Fe(II), makes it difficult to assess the affinity of PenG for ternary complex formation.

In contrast, the natural substrate, PenN, does not behave in the same manner as PenG. PenN was only observed to bind to DAOCS.metal complexes in the presence of 2OG/NOG. This result further supports the hypothesis that 2OG/NOG binding induces conformational changes that help accommodate the penicillin substrate. The PenN side chain is not hydrophobic, which could explain why PenN does not "stick" to DAOCS in the way PenG does.

An interesting aspect to be noted is that when PenN is incubated with the DAOCS.Fe(II) complex, there is an increase in the *apo*-DAOCS peak relative to the iron complex peak. This observation suggests that the presence of PenN in the system can lead to the disruption of the DAOCS.Fe(II) complex. This could occur via Fe(II) chelation by PenN, possibly followed by penicillin degradation, as previously observed for penicillins in the presence of bivalent metal ions [65, 66, 47, 46].

The relative intensity of the DAOCS.Fe(II).NOG.PenN peak (A) is greater than the relative intensity of the DAOCS.Fe(II).NOG.PenG peak (B), as shown by the mass spectra in Figure 3.6. This is indicative of the fact that the ternary complex with PenN is more stable than the one with PenG.

The weaker and less specific binding of PenG could be an explanation for the high level of uncoupled 2OG decarboxylation (Section 2.3.1) recorded in the presence of this non-natural penicillin substrate. The natural penicillin substrate, PenN, displays stronger binding, as revealed by both mass spectrometry and K_d measurement (Section 4.1.4.2), and also lack of uncoupled turnover (Section 2.3.1).

3.3 Conclusions

The results of binding studies carried out by non-denaturing ESI-MS suggest that it is possible to have both 2OG and penicillin substrate simultaneously bound to DAOCS. Non-denaturing ESI-MS experiments do not provide details about the binding site. The binding sites for 2OG and penicillin N is very likely the active site, but other more direct experiments are needed to conclusively validate this proposal.

An order for substrate binding can be inferred from these binding experiments. Based primarily on

the results obtained using the natural substrate, penicillin N, it appears that after the formation of the DAOCS.Fe(II) complex, 2OG/NOG binds and causes changes that enable penicillin N binding. These observations support the proposal that DAOCS catalysis proceeds via the consensus 2OG oxygenase mechanism, rather than the ping-pong mechanism proposed by Valegård *et al.* [1]. The results also suggest that penicillin G can bind away from the active site.

Chapter 4

Binding studies using spectroscopic methods

NMR spectroscopy can provide detailed information on molecular structure as well as information about atomic level molecular interactions. Changes in NMR parameters, such as chemical shift, are sensitive to the exact environment of the atom and can thus be used to gain information about biomolecular interactions. NMR-based methods are valuable tools for mechanistic studies through the depth in information they can provide on biomolecular interactions [67, 68, 69, 70, 71]. Proteins can be subjected to ligand binding studies by NMR provided that sufficient quantities of expressed protein can be obtained [72, 48, 73]. The fact that ligand signals are observed directly makes this approach to biomolecular interactions a robust one, that generates few false negatives or false positives.

In the particular context of DAOCS being a metallo-enzyme, it was considered that enzyme-substrate complex formation could be validated by observing the various enzyme-metal-substrate complexes using UV-Vis spectroscopy. Previous studies on 2OG oxygenases suggest that enzyme-substrate complexes display characteristic spectral features [74, 23].

Thus far, the described ESI-MS binding experiments provided protein-observe data in support of ternary complex formation (Chapter 3). In this chapter, two different NMR binding methods are applied in order to gain more insight on substrate binding. In the first part, water relaxation experiments are described that provide information on binding events occurring close to the metal centre, with the possibility of binding constant determination. The second part takes a ligand-observe approach to the study of substrate displacement experiments. The third and last part of this chapter shows preliminary results regarding the applicability of UV-Vis spectroscopy for the study of enzyme-substrate complexes involved in DAOCS catalysis.

4.1 NMR solvent-water relaxation studies

4.1.1 Dissociation constant measurement

The dissociation constant, K_d, is the parameter used to characterise the interactions between a protein and a ligand in thermodynamic equilibrium. In the simplest case, which is the one of a single molecule of protein receptor (P) binding a single molecule of ligand (L), K_d is defined as

$$P + L \rightleftharpoons PL \tag{4.1}$$

$$K_d = \frac{[P][L]}{[PL]} \tag{4.2}$$

where [P], [L] and [PL] are the equilibrium concentrations of the protein, ligand and protein-ligand complex respectively. K_d has the units of concentration in the situation described by Equation 4.1. Thus a dissociation constant in the micromolar range for example, describes a much more stable protein-ligand complex than a K_d value in the millimolar range.

In order to determine the K_d of a protein-ligand complex, the equilibrium concentrations of free and bound species must be measured. This can be achieved using NMR by employing techniques that allow quantitative observation and that enable us to distinguish between the free and bound states of the protein and/or ligand.

Graphical methods and non-linear regression methods are the two main types of data treatment for K_d determination [75]. The advantage of non-linear regression methods is that no approximations are being made with the method being based on the comparison of experimental data with a calculated binding isotherm that characterises the binding event(s). The observed NMR parameter and K_d are separate variables and the correct values are those that produce the best fit of calculated to observed data. For a 1:1 binding model, the general 2 parameter fit equation below is the one proposed by Fielding [75]:

$$\Delta_{obs} = \Delta_{max}\frac{1}{2[PL]_{sat}}(K_d + [L] + [PL]_{sat} - \sqrt{(K_d + [L] + [PL]_{sat})^2 - 4[L][PL]_{sat}} \tag{4.3}$$

where

[L] is the concentration of ligand present in the system

Δ_{obs} is the observed NMR parameter corresponding to a ligand concentration of [L]

Δ_{max} is the value of the observed NMR parameter when the protein is saturated with ligand

K_d is the value of the dissociation constant

$[PL]_{sat}$ is the concentration of the saturated protein-ligand complex. In most cases, this is equal to the

protein concentration.

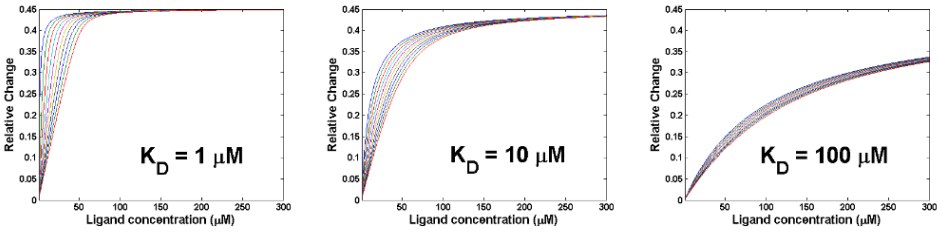

Figure 4.1: *Binding curve simulation for different K_d values. Other parameters are Δ_{max}=0.45, $[PL]_{sat}$=1, 5...50 μM and [L]=1,2,...300 μM .*

Binding curves have been simulated in MATLAB using equation 4.3 for different parameter values. Graphic representations obtained for ligands with affinities ranging from 1μM to 100 μM are reproduced in Figure 4.1. It is apparent that graphical fitting by this method is most suitable for distinguishing ligands that bind strongly. The binding curve of a strong ligand is characterised by a steep slope and rapid plateauing close to a 1:1 protein-ligand ratio whilst the curve for a weak ligand has a far less steep gradient and the plateau is only reached at a very large ligand excess. Weak binding (higher μM and mM region) is difficult to be characterised accurately due to errors arising from the inability to know the exact concentration of the saturated complex which in turn leads to poor fitting. Weak binders also raise the problem of ligand availability, solubility and aggregation at high concentration [72]. From an experimental point of view, when working with strong ligands, it is important that the concentration of the saturated protein-ligand complex be known with as much accuracy as possible.

4.1.2 The longitudinal spin-lattice relaxation time

By applying a radio frequency (RF) pulse on a sample at thermal equilibrium in a magnetic field, the nuclear spins are perturbed from their alignment with the field. The amount of time it takes the nuclear spins to re-align with the magnetic field is known as spin relaxation time. The fact that this amount of time ranges from a few seconds to minutes for nuclear spins (as opposed to under a picosecond in the case of electrons) is what makes NMR spectroscopy a successful analytical tool [76].

As a result of pulse excitation of the nuclear spins, the bulk magnetisation vector is moved from its equilibrium position along the z axis. The recovery of magnetisation along the z axis is termed longitudinal relaxation [76]. To characterise the longitudinal relaxation of nuclear spins, it has been found that exponential recovery is an accurate model for most -1/2 spin nuclei. Starting from equilibrium (M_0), the longitudinal magnetisation (M_z) at time t will be described by

$$M_z = M_0(1 - e^{-t/T_1}) \tag{4.4}$$

T_1 is usually referred to as the longitudinal relaxation time whereas it is in fact a time constant rather than a measure of the time needed for recovery [76].

For spins to relax fully after a $\pi/2$ RF pulse, an interval of time of approximately $5T_1$ is necessary (magnetisation is 99.33% recovered at this point). It is for this reason that the delay between scans must be at least $5T_1$ for an accurate determination of the relaxation time.

There are different experimental methods designed to measure T_1, with the most common one being inversion recovery [77]. The pulse sequence for this method consists of a π and a $\pi/2$ pulse, separated by a varying interval of time, τ. Thus, as described in Figure 4.2, the spins are first inverted along the z axis after which they are allowed to relax for an interval of time, τ. The following rotation of the spins into the x-y plane allows for a spectrum to be recorded [77].

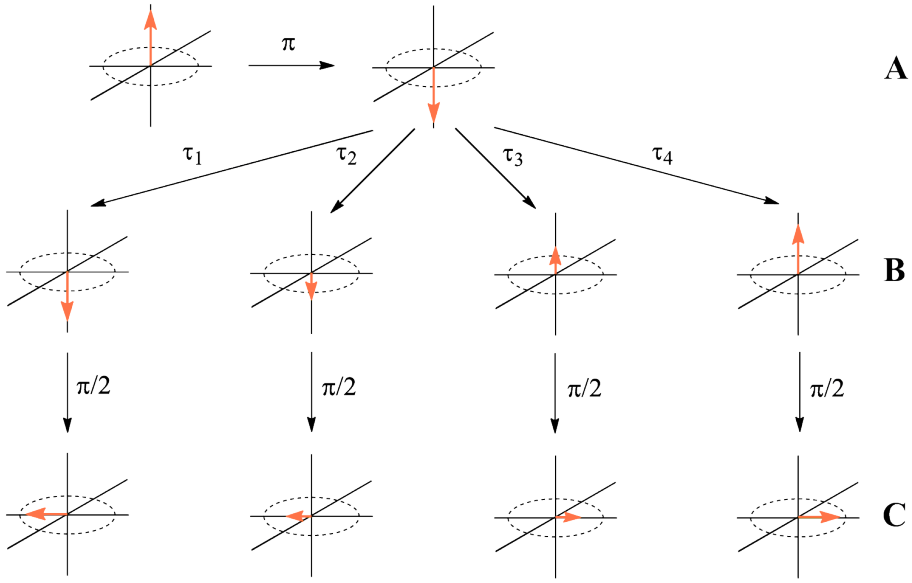

Figure 4.2: *Inversion recovery method for measuring T_1. The spins are inverted by a π pulse, A; The spins relax for an interval of time, τ, B; The spins are rotated into the x-y plane by a $\pi/2$ pulse, C, where the spectrum is acquired.*

The intervals of time for which the spins are allowed to relax along the z axis, τ, are defined by a variable delay list. A typical set of spectra recorded during the inversion recovery method is represented in Figure 4.3A. The insert describes the T_1 curve obtained by plotting the peak area versus time. The value of T_1 itself is obtained by fitting a form of equation 4.4 corrected for imperfect inversion [76]. This method is time-consuming, especially for samples with long T_1 values [76]. This is because the system must be allowed to reach equilibrium and the method requires 8 scans to complete a phase cycle (using a Bruker system).

A different method for measuring T_1, which is the one that has been used throughout the work described in this section, is saturation recovery, shown in Figure 4.4. This method relies on the use of a field gradient which produces the saturation of the spins. To begin with, the spins are rotated into the x-y plane after they have been dephased using a field gradient. At this point the sample has no net magnetisation. After

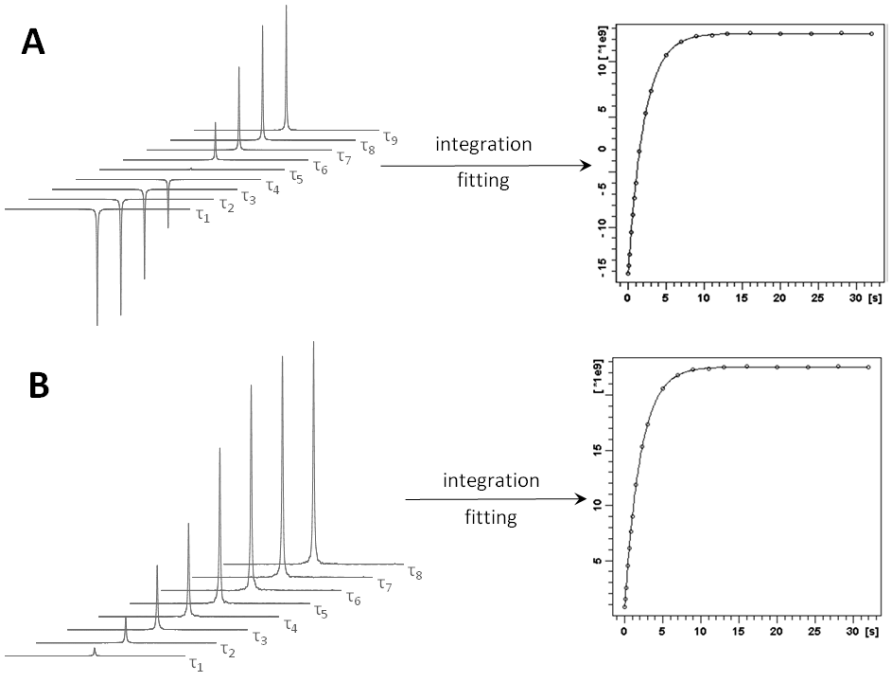

Figure 4.3: *Inversion recovery (A) and saturation recovery (B) methods for measuring* T_1.

a delay time, τ, partially recovered magnetisation results along the z axis. A second $\pi/2$ pulse rotates the spins back into the x-y plane which allows for a spectrum to be recorded [77].

By plotting peak area versus time, the T_1 curve can be obtained (Figure 4.3B). This curve is similar to the one obtained from the inversion recovery experiment (Figure 4.3A), with the exception that it starts at 0 without reaching negative values on the y axis. The value of T_1 is obtained by fitting a form of equation 4.4 which is corrected for incomplete saturation at τ=0 s [76].

The duration of the saturation recovery experiment is considerably shorter because the spins are saturated at the beginning of every measurement, thus removing all magnetisation, so the system does not need the 8 scans to complete a phase cycle. In this experimental setup, one scan is enough due to the use of a gradient pulse. However, in order to achieve accurate measurements, the pulse calibration must be accurate. Saturation recovery is the method of choice for T_1 measurement described throughout this section due to the significantly shorter experiment time [77].

4.1.3 Solvent water relaxation rate measurement applied to dissociation constant determination

It is most often the case in ligand-protein binding experiments that water molecules are being displaced upon ligand binding to the protein. Water would potentially be an excellent reporter ligand for binding studies, considering the 110 M concentration of water protons in contrast to that of a reporter ligand whose concentration is in any case submolar. However, if one were to attempt to use water as a reporter

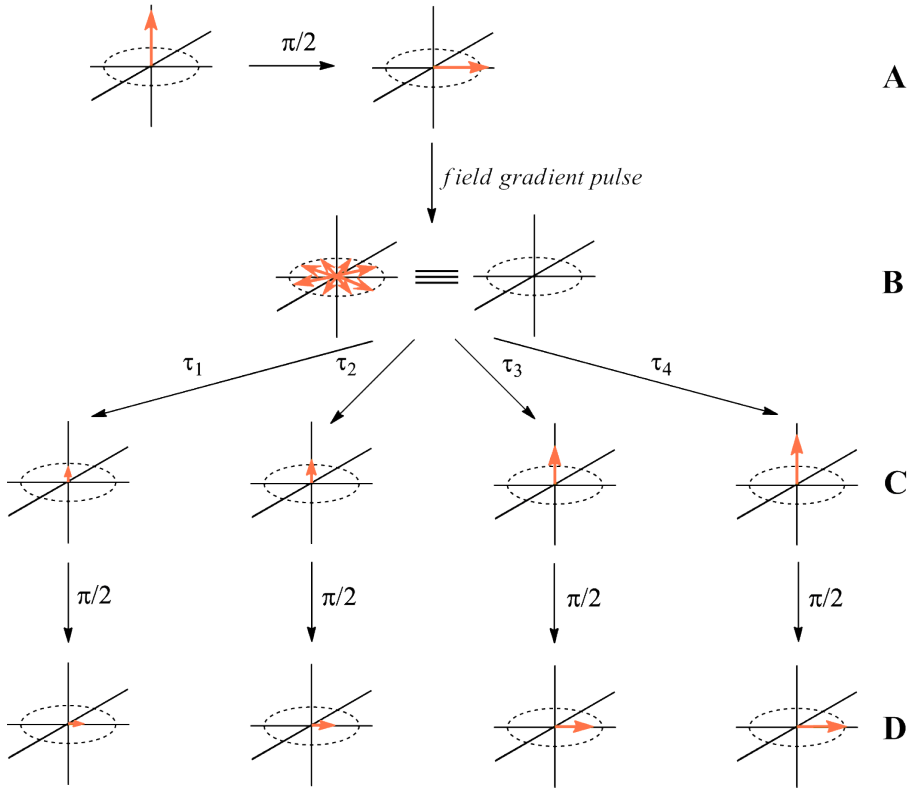

Figure 4.4: *Saturation recovery method for measuring T_1. The spins are rotated into the x-y plane by a $\pi/2$ pulse, A; The spins are being dephased by using a field gradient pulse, B; New magnetisation resulting along the z axis after varying intervals of time, τ, C; The spins are rotated into the x-y plane by a second $\pi/2$ pulse, D, where the spectrum is acquired.*

ligand, the measurable differences would be negligibly small because there are very few protein-bound water molecules being displaced when compared to the free unbound water molecules.

However, Bertini *et al.* [68] have shown that these drawbacks can be overcome for a system which has the water molecules that are to be displaced by the ligand bound to a paramagnetic metal ion. Due to the close proximity of bound water protons to the paramagnetic metal, the relaxation rate of the former is increased by several orders of magnitude. When compared to other ligand-based NMR methods, the water-based method can be applied to both small and large proteins, does not require isotopic labelling and is less restricted by the upper and lower affinity limits imposed by ligand exchange kinetics. Because the paramagnetic effect is most pronounced at low field (lower than 50 MHz), enzyme concentrations as low as 15 μM can be used for experiments performed in such machines [68].

The general applicability of this method (Figure 4.5) was demonstrated by Leung *et al.*, who applied it to prolyl hydroxylase domain containing enzyme isoform 2 (PHD2), a human enzyme involved in hypoxic sensing [78]. PHD2 is a non-heme Fe(II) and 2OG dependent oxygenase. Because Mn(II) is paramagnetic and PHD2 is unable to sustain its catalytic activity in the presence of Mn(II), the ferrous ion from the active site was substituted by Mn(II).

A potential applicability for mechanistic studies of enzyme mechanisms had been suggested for the water-

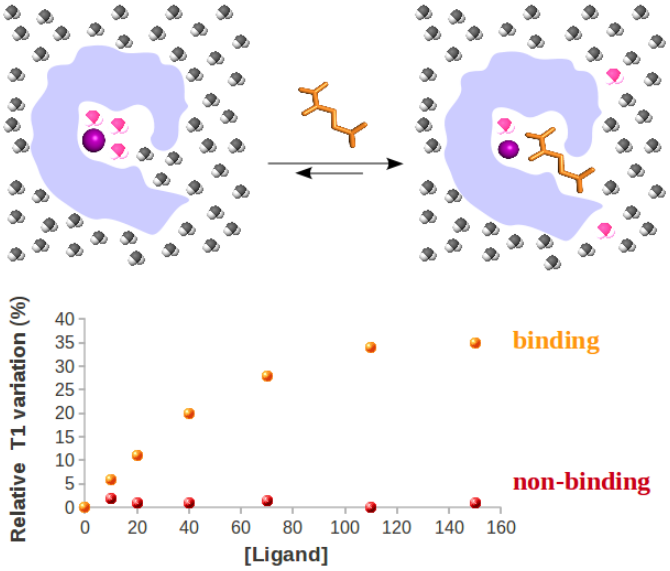

Figure 4.5: *The principle of T_1 binding assays. This type of assay is applicable to a metalloprotein containing a paramagnetic metal centre to which ligands coordinate. In the absence of any ligand, water molecules are coordinated to the paramagnetic metal (purple). The binding of a ligand to the paramagnetic metal centre will occur with displacement of one or more water molecules. These water molecules will then be transferred to the bulk water, thereby increasing the T_1 of the sample (orange). If however, a non-binder is added to the sample, no increase in T_1 will be recorded (red). One can monitor the change in T_1 upon ligand titration intro a paramagnetic metalloprotein sample and thus determine binding affinity (K_d).*

relaxation method due to its ability to detect multiple binding events such as the formation of ternary protein-substrate complexes [68, 78]. The method is highly sensitive towards detecting the binding of ligands directly at the paramagnetic metal or in its vicinity. The method enables the distinction between ligand binding affinities through the possibility of K_d determination.

4.1.4 Dissociation constant determination for DAOCS substrates

Non-denaturing mass spectrometric experiments have shown that DAOCS appears to bind metals and ligands more weakly than PHD2 (Chapter 3). Using the work of Leung *et al.* as a starting point, the water relaxation method was optimised in the context of weaker lingand binding for DAOCS. The method was then further applied in order to gain insight on the mechanism of DAOCS substrate turnover.

4.1.4.1 Method optimisation

4.1.4.1.1 Optimisation of Mn(II) concentration Non-denaturing mass spectrometric studies on DAOCS provided indications towards the strength with which DAOCS binds various metals. A five fold-excess of Fe(II) is needed in order to completely saturate DAOCS as opposed to PHD2 which forms a saturated complex at an equimolar protein-to-metal ratio. Similar results were obtained for Mn(II).

In light of the five fold Mn(II) excess required for complete formation of DAOCS.Mn(II) complex, two

approaches can be taken for the experimental determination of K_d values for substrates. When choosing the relative amounts of protein and ligand, there is a trade-off between the amount of protein used, total experiment time and the sensitivity of the assay.

One approach would be to use an excess of Mn(II). In this context, the parameter c from equation 4.3 will take the value of the protein concentration used (limiting factor). The concentration of protein in this context should ideally be in the region of 30 to 50 μM as seen from such studies on this family of enzymes [78]. However, using an excess of Mn(II) in the system may lead to the titrated ligand binding to free metal, which will also be reflected in the T_1 values obtained. Simple T_1 measurements make it impossible to distinguish between the two simultaneous binding events and therefore the values obtained in this context could not be used for K_d determination. Moreover, this protein concentration would imply a Mn(II) concentration above 150 μM which brings the values obtained for T_1 in the millisecond region. Having such short T_1 values leads to inaccurate measurements because the change in T_1 will be proportionally smaller. Taking the protein concentration lower in order to increase the absolute value for T_1 will lead to a decrease in the value for parameters c and a (equation 4.3) which in turn leads to loss of sensitivity, as previously noted by Leung *et al.* [78].

Another approach is to use an excess of DAOCS. This is not an attractive alternative from the point of view of the cost involved. Also, the amount of Mn(II) in the sample should not be too low as this will lead to very long periods of time required for T_1 measurement. Thus, in this experimental context, protein concentrations used have to be of at least 150 μM in order to reach a compromise between experiment time, the amount of protein used and the sensitivity of the assay.

Of the two available options, a system with excess protein was selected. Even though this system is not the most cost-efficient, it was considered the system least prone to provide erroneous T_1 values. The two main assumptions made here are that the ligands will have negligible binding to the apo-enzyme and that the effective DAOCS.Mn(II) concentration will be similar to the Mn(II) concentration.

4.1.4.1.2 Addition of salt An important aspect to be considered is the amount of Mn(II) present in the sample solution when dissolving 2.75 μg/mL Mn(II) (50 μM). An increase in T_1 values for a 50 μM Mn(II) solution was observed. The increase in T_1 indicates a longer time required for the spins in the sample to relax which, in the context of the method, points in the direction of a decrease in concentration of the paramagnetic source, which is Mn(II) in our case.

One explanation for the increase in the observed T1 could be due to trace metal adsorption onto the glass surface of the NMR tube, as proposed by Smith 1973. For samples containing 5 mg/mL Mn(II), atomic absorption spectrophotometric measurements showed that a pH of 5 or less would be required to maintain all of the Mn(II) in solution, the glass needs to be thoroughly cleaned and preferably aged before use [79] and that the presence of 0.5% NaCl (w/v) in the solution does not lead to any significant

change in the amount of Mn(II) detected.

The pH of the environment could not be modified due to protein stability reasons. For each titration a new high-throughput 3 mm Bruker MATCH tube was used and therefore the glass was clean but not aged. 125 mM NaCl was added to the sample in order to stabilise the Mn(II) concentration over time and reduce what appears to be glass adsorption of Mn(II). Trace metal adsorption by borosilicate glass may be a problem in the experimental context of the present work because DAOCS is a relatively weak metal binder. Also, metal adsorption on glass surface is not reproducible across samples. Since metal glass adsorption is a phenomenon that develops in time, it introduces errors by decreasing the Mn(II) concentration available in solution. Thus the value obtained for T_1 is constantly higher and increasing ever so slightly, making it hard to see where the binding curve flattens out and also making the ligand seem to be a weaker binder than it actually is.

4.1.4.1.3 Other sources of errors An important alternative source of errors comes from extra paramagnetic metal species being introduced into the system during titration. If all ligands used are properly purified and all compounds used to make up the assay mixture are of high grade purity, this should not be a problem. However, since the titration is carried out using a 5 μL wired syringe, there is a high risk of rust being formed inside the syringe. In this way, Fe(III) which is a paramagnetic species, can be introduced into the sample, which leads to an artificial decrease in T_1 value. Thus, ligand binding affinities will appear reduced and the shape of the curve will no longer be levelling of as saturating concentrations are reached, it will be decreasing instead. For the experiments described herein, the 5 μL syringes used were carefully inspected and replaced at any indication of rust formation.

4.1.4.1.4 Experimental approach Substrate and substrate analogue binding to DAOCS was first screened by conducting an endpoint titration *i.e.* a 2-point assay with and without a high concentration (2-10 mM) ligand. A significant change in T_1 was correlated with ligand binding.

The absolute values obtained for T_1 are strongly influenced by variations in concentration for the protein and paramagnetic metal ion. Such small differences from separate sample preparations therefore has a great influence on the ability to distinguish binding affinities when comparing across samples. Therefore, as suggested by Leung *et al.*, relative changes in T_1 are plotted as (1-($T_1/T_{1(0)}$)) against the titrated ligand concentration [78]. By carrying out data analysis in this way it is readily possible to distinguish between strong and weak binders. A binding curve described by equation 4.3 with corresponding parameters is then fitted to the plot and provides a value of the dissociation constant.

The T_1 ratio at which a saturated complex is formed is dependent upon the kinetics of complex formation, the accessibility of water molecules and the number of water molecules that are being displaced. As shown by Leung *et al.* [78], the position of the plateau (parameter Δ_{max} in equation 4.3) is also dependent upon the amount of saturated complex being formed (parameter $[PL]_{sat}$ in equation 4.3) which is difficult to

determine due to difficulties in accurate protein concentration measurement and the slight variation in paramagnetic metal on concentration between samples. It is for this reason that titrations for each ligand were performed in triplicates and the fittings were performed individually for each data set.

4.1.4.2 Results

In the case of PHD2, its peptide substrate (CODD) binds in a well-defined cleft, whilst 2OG binds directly to the metal centre in a bidentate manner [80]. By performing sequential substrate titrations in a sample containing the PHD2.Mn(II) complex, a clear additive affect was observed by Leung *et al.* [78]. This effect is the same regardless of the order the substrates are being titrated. This sequential binding profile is consistent with existing data in the literature on PHD2 [81] which reports the formation of a ternary complex between the enzyme and its two substrates. Therefore, using the work on PHD2 as a starting point, the mode of binding of the DAOCS substrates was studied using the T_1 relaxation method.

4.1.4.2.1 Binding of Mn(II) Initially, Mn(II) binding to DAOCS was investigated. Non-denaturing mass spectrometric data already had suggested a five fold excess of metal is necessary to obtain a saturated enzyme-metal complex. In order to quantify the affinity of DAOCS for Mn(II) by K_d measurement, small amounts (1 to 3 μL) of DAOCS were titrated into a 50 μM Mn(II) solution. It was chosen to titrate DAOCS into the metal solution rather than the other way around because T_1 values are very sensitive to Mn(II) concentration and therefore titrating Mn(II) into an enzyme solution may lead to errors due to pipetting inaccuracy of small volumes.

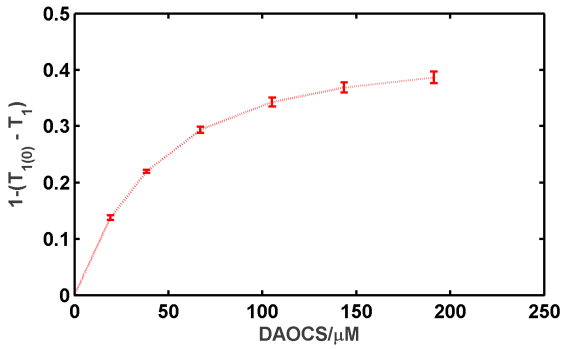

Figure 4.6: *Titration of DAOCS into 50 μM Mn(II). This figure displays one of the data sets obtained for this titration. Similar curves have been obtained for the other two data sets. DAOCS affinity for Mn(II) was determined as K_d= 16±4 μM .*

The value obtained for the DAOCS affinity to Mn(II), K_d=16±4 μM , was consistent with the non-denaturing ESI-MS data and the observed necessity for at least a five-fold excess of enzyme in order to saturate Mn(II).

4.1.4.2.2 Binding of 2OG and NOG to DAOCS.Mn(II) The non-denaturing mass spectrometric data indicates weak binding of 2OG and much stronger binding of NOG. Endpoint titrations of 2OG and

Table 4.1: *K_d values determined for DAOCS substrates and substrate analogues. Plots of relative T_1 variation, as well as the curve fitting plots are presented in the supplementary material (Figure 6.7.5).*

Compound	**Determined K_d(μM)**	**Comments**
Mn(II)	16±4	DAOCS was titrated into 50 μM Mn(II);
2OG	29±8	binding to DAOCS.Mn(II)
NOG	6±3	bindng to DAOCS.Mn(II)
PenG	nd	binding to DAOCS.Mn(II); decrease in T_1
	nd	binding to DAOCS.Mn(II).2OG; slow T_1 increase over time
PenN	nd	binding to DAOCS.Mn(II); decrease in T_1
	24±6	binding to DAOCS.Mn(II).2OG

NOG into 50 μM DAOCS.Mn(II) complex resulted in a 0.31±0.01 and, respectively, 0.45±0.03 relative increase in T_1, thus showing that binding occurs and it can be detected by this method.

Dissociation constants were then determined as being K_d=29±8 μM for 2OG and K_d=6±3 μM for NOG. This data is in qualitative accordance with the results of the ESI-MS experiments (Section 3).

4.1.4.2.3 Binding of penicillin G and penicillin N to DAOCS.Mn(II) As discussed in the Introduction, PenG is not the natural substrate for DAOCS, but it was the substrate used in the work Valegård *et al.*, which serves as a basis for the alternative mechanistic proposal [1]. Endpoint titrations for PenG showed no increase in T_1.

PenN is the natural substrate for DAOCS. To date, no crystal structures have been obtained with this substrate (in complex with DAOCS or otherwise), most likely due to its relative instability. There was no increase in T_1 detected upon addition of a large excess of PenN (2 mM) to DAOCS.Mn(II) either.

However, a slight decrease in the T_1 value was observed for both PenG and PenN after which the T_1 value increased again to approximately the initial value. This trend was reproducible but it was not further quantified. Thus, K_d values could not determined for the binding of PenG and PenN to DAOCS.Mn(II) due to this unusual behaviour of the system. A possible explanation however, is that the penicillin molecule could remove some of the Mn(II) from the active site, thus allowing more water molecules to coordinate to these Mn(II) ions. This would result in a higher relaxation rate for the water protons and a lower T_1.

4.1.4.2.4 Binding of PenG and PenN to DAOCS.Mn(II).2OG Because no increase in the T_1 value was detected when the binding of penicillin substrates to the DAOCS.Mn(II) complex was investigated, binding to the DAOCS.Mn(II).2OG complex was then studied.

In the case of PenG, the value for T_1 was observed to increase in time (measurements were made over an interval of 5 hours), indicating that the system has not reached equilibrium. The increase observed meant that performing titrations in order to determine the K_d for PenG binding to DAOCS.Mn(II) was not possible.

In contrast to the results with PenG, when a saturating amount of PenN was added to 50 μM of the

DAOCS.Mn(II).2OG complex, a clear increase in T_1 was observed (from 4.632±0.021 s to 7.224±0.010 s). Even though no increase in T_1 was observed for PenN titration into DAOCS.Mn(II), the addition of a saturating amount of 2OG led to the same increase in T_1 (of up to 7.224±0.010 s), as when 2OG was added before PenN. The binding curve obtained for PenN binding to DAOCS.Mn(II).2OG defines a K_d=24±6 μM . This value is qualitatively consistent with the ESI-MS data.

4.1.5 Discussion

Overall, the results of the relaxation experiments are in qualitative accordance with the information obtained form non-denaturing mass spectrometry. Mn(II) indeed binds more weakly to DAOCS than PHD2, as quantified by K_d measurement (Table 4.1, K_d= 2 for PHD2 binding to Mn(II) [78]), and this binding event leads to a 0.314±0.006 relative increase in T_1. It was confirmed that 2OG and NOG also bind to the DAOCS.Mn(II) complex with moderate strengths (overall relative variation in T_1 increased to 0.562±0.002 and 0.607±0.001, respectively). There was no significant further increase in T_1 upon addition of either penicillin N or penicillin G substrates to DAOCS.Mn(II) complex which was associated with a lack of binding to this complex. However, the addition of penicillin N to the DAOCS.Mn(II).2OG complex induces an ovarall relative increase in T_1 of 0.717±0.001). Moreover, the addition of a saturating amount of 2OG into a mixture containing the DAOCS.Mn(II) complex and penicillin N (saturating) will induce the same overall variation in T_1. Thus, the 0.717±0.001 overall increase in T_1 (corresponding to a T_1 value of 7.224±0.010 s) was associated with ternary complex formation between DAOCS, 2OG and penicillin N.

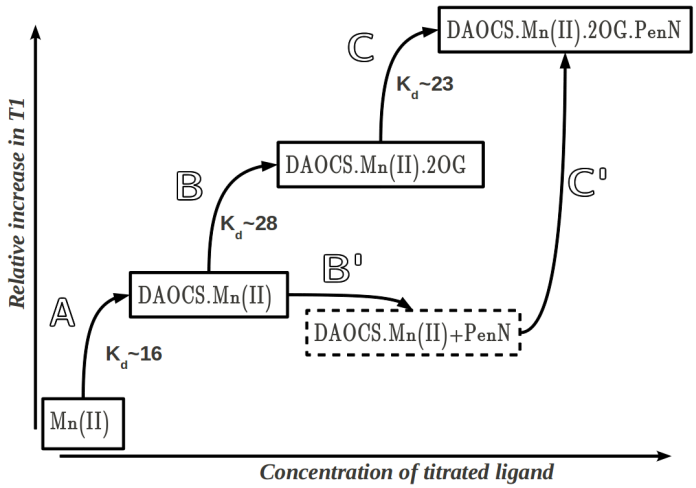

Figure 4.7: *Overview of DAOCS substrate binding as revealed by T_1 relaxation measurements.* ***A****: DAOCS binds free Mn(II) from solution to form a saturated complex with a0.314±0.006 relative increase in T_1;* ***B****: a saturated DAOCS.Mn(II).2OG complex can be formed by addition of 2OG, which corresponds to an overall 0.562±0.002 relative increase in T_1;* ***B'****: adding PenN to the DAOCS.Mn(II) complex does not lead to the formation of a DAOCS.Mn(II).PenN complex, as concluded from T_1 measurements; However, addition of PenN to the DAOCS.Mn(II).2OG complex (****C****), as well as the addition of 2OG to the mixture of DAOCS.Mn(II) complex and PenN* ***C'*** *leads to the same overall increase in T_1 of 0.717±0.001.*

Moreover, the K_d values obtained for PenN (24±6 μM) corelates well with the K_m value reported for in literature (33±16 μM [82]). In the case of PenG, the 30-fold higher K_m values reported in the literature [40] are in accordance with the very weak binding observed by MS and NMR.

The additive effect observed by Leung *et al.* for PHD2 T_1 increase upon binding of substrates, can also be noted in the case of DAOCS with PenN as a substrate. The difference is that there is no prime substrate binding to DAOCS.Mn(II) in the absence of 2OG; once 2OG is added in the mixture containing the DAOCS.Mn(II) complex and PenN, binding is observed. A potential explanation for this phenomenon is that the binding of 2OG to the DAOCS.Mn(II) complex induces conformational changes of the active site that promotes subsequent binding of the prime substrate.

The T_1 value for the DAOCS.Mn(II) complex dropped upon addition of a large excess of PenN or PenG. While an increase in the T_1 value is indicative of ligand binding close to the paramagnetic metal centre, a decrease of the T_1 value could be associated with the paramagnetic metal being removed from its binding site. By being removed from its binding site, the paramagnetic metal would become more exposed to water molecules which would lead to an increase in the water relaxation rate and thus a decrease in T_1. Certain ligands could promote this through mechanisms like metal chelation or reaction with metal.

Chelation of Mn(II) by PenN would be in accordance with the ESI-MS data that shows an increase of the apo-DAOCS peak relative to the DAOCS.Mn(II) peak in the presence of PenN (Figure 3.5). Moreover, NMR turnover data shows inhibition of DAOCS activity at increasing concentrations of penicillin substrate (Figure 2.5). As discussed earlier (Sections 3.2.3 and 4.1.5), substrate inhibition in this context could be explained by the chelation and removal of the metal ion by the penicillin. β-Lactam antibiotics have been shown to form complexes with transitional metals via coordination of carbonyl groups and, in some cases, side chain nitrogen atoms too [65, 66, 83, 84]. Considering that metal coordination involves the β-lactam carbonyl a significant increase in the lability of the β-lactam ring could be anticipated [85]. Binding of 2OG to the DAOCS.Mn(II) complex is then proposed to be stronger than the affinity of penicillin substrates for the metal ion, thus making it possible to keep Mn(II) in the active site in the presence of 2OG.

The very slow increase in T_1 value in the case of PenG could be indicative of weak binding to the DAOCS.Mn(II) complex or of weak non-specific interactions (such as hydrophobic interactions between the PenG aromatic side chain and hydrophobic amino acid residues in the active site) that occur close to the paramagnetic metal centre. Binding of PenG was expected to be weak considering the ESI-MS data and the uncoupled turnover in the presence of PenG.

The similar K_d values obtained for 2OG and PenN binding are reflected in the 1:1 coupling ratio between 2OG decarboxylation and PenN ring expansion. The very weak binding of PenG, poorly detected through the water T_1 relaxation method, is also reflected in the high amount of uncoupled 2OG turnover that occurs when PenG is used as a substrates.

4.1.6 Conclusions

Dissociation constant determination via solvent water relaxation rate measurement was successfully applied to determine the strength of binding of substrates to DAOCS (Table 4.1). While 2OG and PenN were found to have similar K_d values (Sections 4.1.4.2.2 and 4.1.4.2.3) display high coupling between decarboxylation and ring expansion (Section 2.3.1), the very low affinity of PenG could be regarded as an explanation for uncoupled turnover.

The T_1 value was observed to increase for PenN (indicating binding) only in the presence of 2OG, regardless of the order in which the two were added. This fact further supports the hypothesis that 2OG binding may induce some conformational changes upon binding, thereby enabling subsequent prime substrate binding.

4.2 Ligand displacement by 1D-HSQC

4.2.1 Experimental approach

The main experimental evidence brought forward by Valegård *et al.* [1] in support of the alternative ping-pong mechanism is the crystal structure showing that 2OG and the penicillin substrate bind at overlapping sites. The obvious approach towards probing the existence of overlapping binding sites is performing competition experiments. In the context of overlapping binding sites, addition of an equimolar mixture of the two substrates to a sample containing the protein-metal complex will lead to the formation of two types of protein-metal-substrate complexes. However, if the binding sites do not overlap, a ternary complex containing the protein and both substrates should be formed. Moreover, in a binding experiment, a large excess of one of the substrates should displace the other one if the binding sites overlap.

Such experiments were performed by non-denaturing MS. The results (Section 3) showed that formation of a ternary complex between DAOCS, 2OG and the penicillin substrate is possible under the non-denaturing mass spectrometric conditions. The non-denaturing ESI-MS binding studies fall within the protein-observe category, which means complex formation was being observed from the perspective of the protein. NMR offers the possibility to perform in solution ligand-observe binding experiments that would complement the protein-observe MS studies. The ligand-observe NMR approaches can be used to either observe the complexes directly, by experiments such as inter ligand NOE (IL-NOE) [67],[70] or indirectly via ligand displacement experiments [71]. In the case of penicillin G, IL-NOE experiments were unfortunately not an option due to the very different binding affinities of 2OG and penicillin G (as shown by water relaxation experiments (Section 4.1.4.2)) and the necessity to obtain deuterated protein. It was considered that ligand displacement experiments however would be most suitable in this context as they enable detection of a larger ligand affinity range [86, 87].

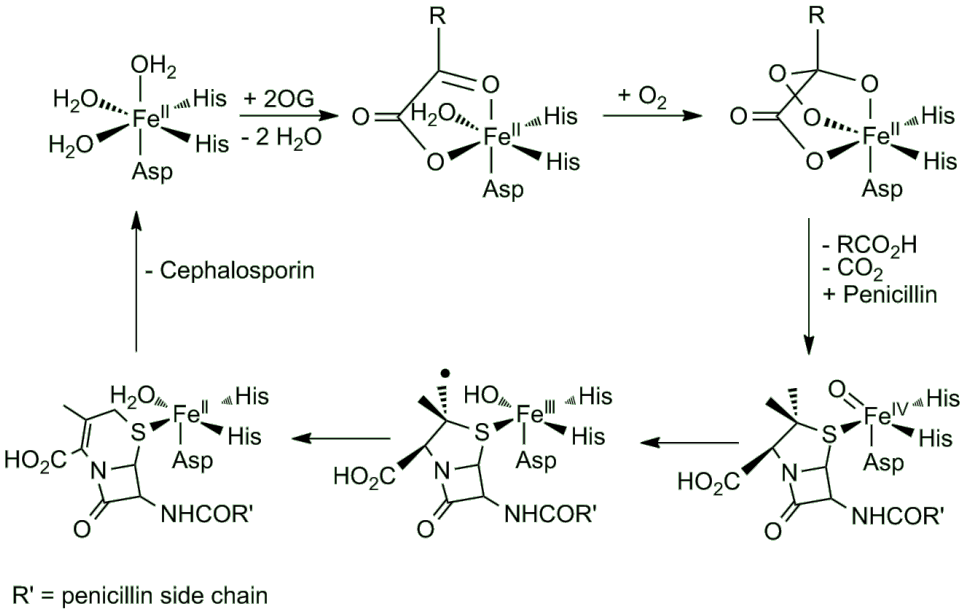

Figure 4.8: *Alternative mechanism proposed for DAOCS by Valegård et al.[1]*

4.2.2 Method development

Line exchange broadening has been used to study the binding of ligands to proteins [73, 86, 87]. The majority of such NMR binding experiments require an excess of ligand. If, however, the experiment does not use an excess of ligand, it is possible to observe binding directly: the signals of an unbound ligand will be visible while the signals of a bound ligand may disappear due to exchange broadening (Figure 4.9).

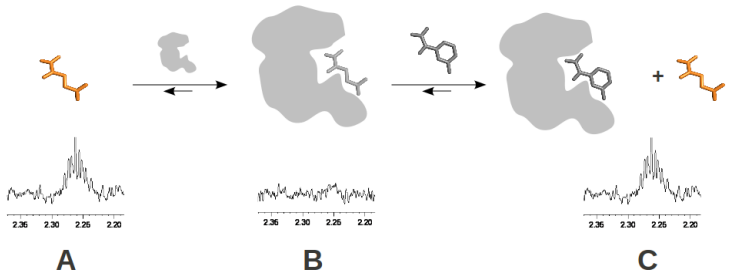

Figure 4.9: *The principle of displacement experiments using 1D-HSQC. A) When the ^{13}C -ligand (orange) is free in solution, its signal appears in the 1D-HSQC spectrum; B) The presence of a macromolecular receptor that binds the ligand will cause the signal to disappear due to exchange broadening (the ligand is now coloured in grey because it is bound to the receptor and its signal is no longer visible in the 1D-HSQC spectrum); C) Adding a stronger competitive ligand into the system will displace the ^{13}C -labelled ligand (orange) which is now again free in solution and thus its signal can be seen in the 1D-HSQC spectrum.*

Without the use of an excess of ligand, usually it is not possible to distinguish ligand signals from the protein background in an standard ^{1}H -NMR experiment. It has been shown that a one-dimensional Heteronuclear Single Quantum Coherence (1D-HSQC) experiments can provide sensitivity as well as selectivity for proton observation [45]. A 1D-HSQC experiment allows selective irradiation of a carbon resonance of interest which will produce a ^{1}H spectrum that retains only responses from protons bound

directly to that specific carbon atom. This type of experiment is time consuming due to the low level of natural ^{13}C abundance (1.1 %). However, using a ^{13}C -labelled ligand would speed up the experiment as well as provide selectivity down to the level of natural ^{13}C abundance. However, selectivity achieved in this way is unsatisfactory in the experimental context of ligand displacement where millimolar range concentrations are often used to displace ligands. Selectivity in the pulse sequence is still needed so that the resulting spectrum would selectively display only signals of protons bound to the ^{13}C label. Each resonance displays the characteristic doublet structure of a coupled spectrum, arising from one-bond ^{1}H -^{13}C coupling.

It is important that there be no turnover happening in the sample prepared for this experiment because this phenomenon could easily lead to false positives or false negatives. One way of achieving this is the substitution of the natural metal cofactor with a different one that renders the enzyme catalytically inactive without affecting the enzyme structurally.

Known bicyclic competitive 2OG oxygenase inhibitors that bind in the 2OG site were used as negative controls for binding of 1,2,3,4-^{13}C -2OG and 2-^{13}C -NOG.

4.2.2.1 Proof of principle using PHD2

The ligand displacement method was developed using prolyl hydroxylase domain containing enzyme 2 (PHD2) as a model system. PHD2 is a 2OG oxygenase involved in human oxygen sensing as part of the response to hypoxia [80, 88]. Under normal oxygen levels, PHD2 initiates the oxygen dependent degradation of the α-subunit of the hypoxia inducible factor (HIF-1α). The PHD2.Fe(II) complex can bind 2OG and its protein substrate, HIF-1α, forming a ternary enzyme-substrate complex [78].

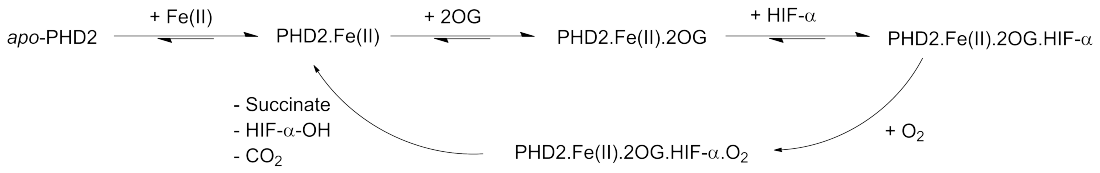

Figure 4.10: *Outline reaction scheme for PHD2 catalysis as described in [78].*

Use of the natural metal cofactor, Fe(II), was avoided in order to avoid 2OG turnover. Previous work on PHD2 [57] shows that Fe(II) from the active site can be replaced by other metal ions, including Zn(II). Consequently, Zn(II) was used as a substitute in displacement experiments. A strong competitive [89] bicyclic inhibitor (Figure 4.11) of 2OG oxygenases [90], that binds in the 2OG site was selected as a negative control (Figure 4.12C). Commercially available 1,2,3,4-^{13}C -2OG was used as the labelled substrate.

A coupled 1D HSQC spectrum selecting for the [3-^{13}C]-2OG protons at δ^{13}C = 30.5 ppm was acquired for a sample containing 50 μM ^{13}C-2OG and displayed signals at δ^{1}H = 2.35 ppm and δ^{1}H = 2.35 ppm.

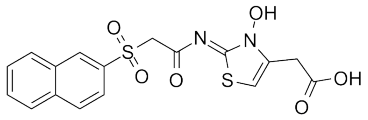

Figure 4.11: *The bicyclic inhibitor used as a negative control in the PHD2 displacement experiments.*

Performing the same experiment on a sample containing ^{13}C-2OG and the PHD2.Zn(II) complex leads to the broadening of the signals observed previously. By running the experiment again on the same mixture with the addition of an equimolar amount of inhibitor, a spectrum displaying the signals observed initially is obtained.

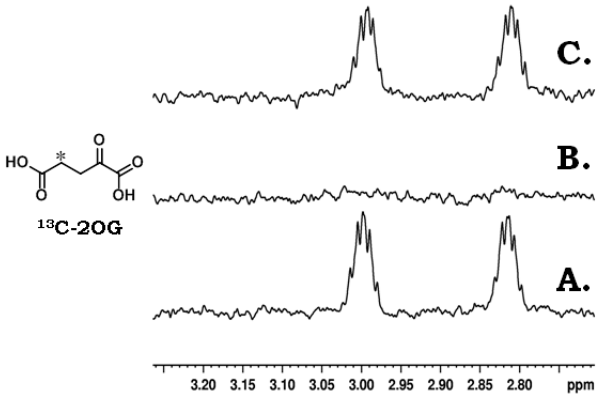

Figure 4.12: *Development of the ligand displacement method using PHD2. Spectra correspond to the following samples: (A) just ^{13}C-2OG, (B) ^{13}C-2OG+ PHD2.Zn(II), (C) negative control: inhibitor + PHD2.Zn(II).^{13}C-2OG. To simplify the figure, only the ^{13}C-2OG doublet at δ^1H = 2.35 ppm is displayed.*

The fact that the signals characteristic to ^{13}C-2OG (Figure 4.12(A)) are broadened in the presence of the PHD2.Zn(II) complex is indicative of ^{13}C-2OG binding (Figure 4.12(B)). The addition of the bicyclic inhibitor in the sample causes the signals of ^{13}C-2OG to reappear (Figure 4.12(C)), indicating that the labelled ligand is no longer bound to PHD2.

The information obtained from interpreting the spectra (Figure 4.12) is in agreement with existing literature data [78], thus validating selective 1D HSQC displacement experiments as an approach to the study of ligand binding by NMR.

4.2.3 DAOCS substrate displacement experiments

In the case of DAOCS, ESI-MS experiments confirmed that Fe(II) can be replaced by Zn(II). A two-fold excess of Zn(II) is required to obtain a saturated DAOCS.Zn(II) complex (Section 3.2.2.2). Due to the acidity of Zn(II), a concentration above 200 μM is not recommended as it causes DAOCS to precipitate. The conditions chosen for the binding studies were thus 50 μM DAOCS and 100 μM Zn(II), in order to reach a compromise between enzyme stability and complex formation. Apart from the commerically available ^{13}C -labelled 2OG, in house synthesised ^{13}C -NOG and ^{13}C -PenG were used in this set of

experiments. A bicyclic inhibitor [91] (Figure 4.13) was again used as a negative control. The bicyclic inhibitor was shown to bind by non-denaturing ESI-MS (Figure S1). Unfortunately, a ^{13}C -labelled version of the natural substrate, PenN, could not be synthesized so unlabelled PenN was used as a negative control in the ^{13}C -PenG experiments.

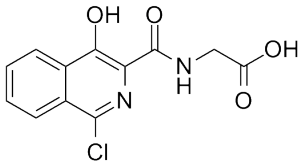

Figure 4.13: *The inhibitor used as a negative control in the DAOCS displacement experiments.*

4.2.3.1 Displacement using ^{13}C-2OG

Similarly to PHD2, when an equimolar mixture of DAOCS.Zn(II) complex and ^{13}C-2OG (50 μM ^{13}C-2OG) was analysed by 1D HSQC, no ligand peaks were visible due to exchange broadening (Figure 4.14B). ^{13}C-2OG was observed at δ^1H = 2.35 ppm by irradiating δ^{13}C = 30.5 ppm

As native ESI-MS experiments have shown that the 2OG oxygenase inhibitor binds to DAOCS (Section S1), it was used as a control molecule in the ^{13}C-2OG displacement experiments. As expected, by analysis of a 1D HSQC spectrum of a mixture of the DAOCS.Zn(II) and both ^{13}C-2OG (50 μM) and inhibitor (200 μM), the peaks of ^{13}C-2OG reappear. This indicates ^{13}C-2OG is no longer bound to the enzyme-metal complex, likely because it has been displaced by the inhibitor (Figure 4.14C).

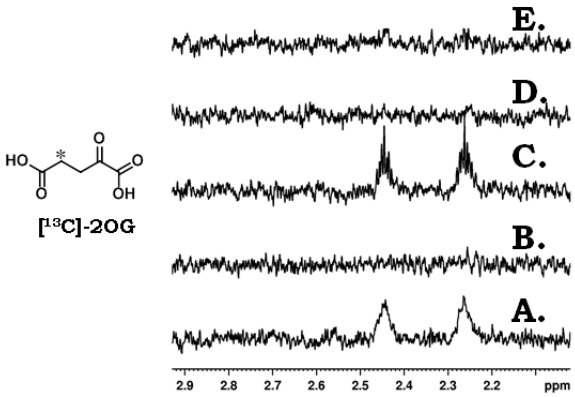

Figure 4.14: *Displacement experiments carried out by 1D HSQC at $\delta^{13}C$ = 30.5 ppm using 1,2,3,4-^{13}C labelled 2OG.Spectra correspond to the following samples: (A) just ^{13}C-2OG, (B) ^{13}C-2OG+ DAOCS.Zn(II), (C) negative control: inhibitor + DAOCS.Zn(II).^{13}C-2OG, (D) PenG + DAOCS.Zn(II).^{13}C-2OG, (E) and PenN + DAOCS.Zn(II).^{13}C-2OG. To simplify the figure, only the ^{13}C-2OG doublet at δ^1H = 2.90 ppm is displayed.*

If samples containing the DAOCS.Zn(II).^{13}C-2OG complex are mixed with a saturating amount of PenG (50 mM) or PenN (10 mM), the spectra displayed in Figure 4.14 D and E are obtained. Both spectra are the same as Figure 4.14B, meaning that ^{13}C-2OG remains bound to the DAOCS.Zn(II) complex, without being displaced by the large excess of penicillin substrate present.

4.2.3.2 Displacement using ^{13}C-PenG

Analogous experiments to the ^{13}C-2OG ones were performed using ^{13}C-PenG. ^{13}C-PenG was synthesised such that it contained a ^{13}C -methylene group in its side chain (synthesis was performed by Luc Henry). ^{13}C -labelled PenN could not be synthesised due to high cost/unavailability of ^{13}C -labelled precursors. The signals for ^{13}C-PenG were observed at δ^1H = 3.62 ppm by irradiating δ^{13}C = 41.8 ppm.

Upon mixing 50 μM ^{13}C-PenG with an equimolar amount of DAOCS.Zn(II) complex, the characteristic ^{13}C-PenG signals do not disappear completely (Figure 4.15 B). A certain degree of peak broadening can be observed which can be interpreted as weak binding of PenG to the DAOCS.Zn(II) complex. This weak binding is consistent with the information obtained from non-denaturing ESI-MS experiments (Section 3.2.2.4). Upon adding 200 μM bicyclic inhibitor to the mixture, there is no significant change in the spectrum (compare Figure 4.15 B and C). This indicates that binding of the inhibitor in the 2OG site does not seem to significantly affect the binding of ^{13}C-PenG.

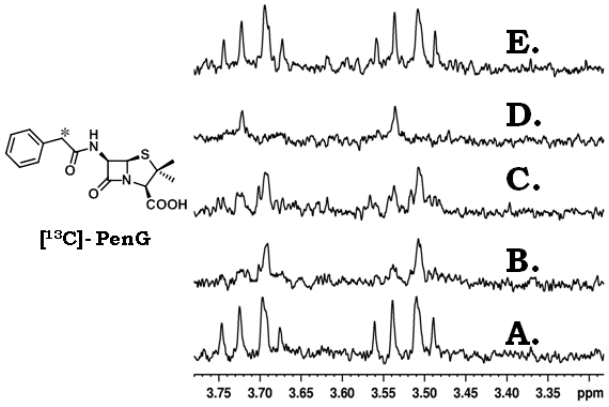

Figure 4.15: *Displacement experiments carried out by 1D HSQC at $\delta^{13}C$ = 41.8 ppm using methylene-^{13}C -labelled PenG.Spectra correspond to the following samples: (A) just ^{13}C-PenG, (B) ^{13}C-PenG+ DAOCS.Zn(II), (C) negative control: inhibitor + DAOCS.Zn(II) + ^{13}C-PenG, (D) 2OG + DAOCS.Zn(II) + ^{13}C-PenG, (E) and PenN + DAOCS.Zn(II) + ^{13}C-PenG. The signals that remain in spectrum D belong to labelled impurities from synthesis.*

However, if 2OG is added to the mixture instead of the inhibitor, the ^{13}C-PenG signals disappear, indicating binding of ^{13}C-PenG (Figure 4.15 D). Moreover, if PenN (10 mM) is added to the mixture containing the DAOCS.Zn(II) complex and ^{13}C-PenG, the ^{13}C-PenG signals reappear completely (Figure 4.15E). This result suggests that PenN disrupts the weak interaction between ^{13}C-PenG and DAOCS.Zn(II) complex. The disruption may occur either due to PenN being hydrolysed by Zn(II)[46] or due to PenN and PenG binding at the same or overlapping sites.

4.2.3.3 Displacement using ^{13}C-NOG

Experiments similar to the ones carried out with ^{13}C-2OG, were performed using ^{13}C-NOG (synthesised by Luc Henry). In this context, because ^{13}C-NOG is an unreactive 2OG analogue, the natural ferrous co-

factor can be used. However, addition of Asc is necessary to prevent Fe(II) oxidation to the paramagnetic trivalent species that would cause peak broadening thus giving false positives. ^{13}C-NOG was observed at δ^1H = 3.74 ppm by irradiating δ^{13}C = 43.2 ppm. Results obtained with this system are similar to the ones obtained using Zn(II) and ^{13}C-2OG. The signal obtained in Figure 4.16D is is a result of PenG having a signal in the carbon spectrum close to the frequency that is being selectively irradiated in this experiment and it is a result of cancellation error due to a spectrometer artefact.

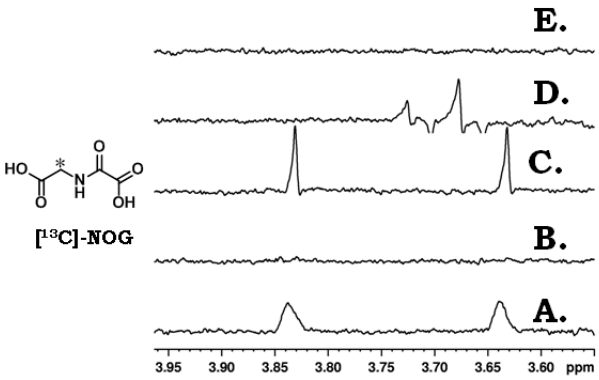

Figure 4.16: *Displacement experiments carried out by 1D HSQC at $\delta^{13}C$ = 43.2 ppm using ^{13}C -labelled NOG. Spectra correspond to the following samples: (A) just ^{13}C-NOG, (B) ^{13}C-NOG+ DAOCS.Zn(II), (C) negative control: inhibitor + DAOCS.Zn(II) + ^{13}C-NOG, (D) PenG + DAOCS.Zn(II) + ^{13}C-NOG, (E) PenN + DAOCS.Zn(II) + ^{13}C-NOG. The signals observed in spectrum (D) are a result of cancellation error due to a spectrometer artefact.*

4.2.4 Discussion

The results of the ligand-observe displacement experiments support the results obtained by mass spectrometry and water relaxation analyses.

Binding of 2OG to the DAOCS.Zn(II) complex is not prevented by the presence of an excess of PenG or PenN. Moreover, the presence of 2OG in a mixture of DAOCS.Zn(II) and PenG/PenN facilitates the binding of the latter. These two pieces of evidence are in agreement with the conclusions drawn from the water relaxation experiments, namely that only weak binding of PenG and no binding of PenN occurs in the absence of 2OG. These results further support the proposal for a conformational change in the active site induced by the binding of 2OG, that would allow the subsequent binding of the penicillin substrate.

An interesting aspect to be discussed is the binding of PenG to DAOCS. Simple observation of binding effects in 1D NMR experiments without any sort of competition is not recommended as binding effects are highly dependent on the nature of the ligand, particularly in terms of lipophilicity [48]. Such an assay set-up would run the risk of simply measuring non-specific interactions. ESI-MS experiments have shown weak binding of PenG to both apo-DAOCS and DAOCS.Fe(II) (Section 3.2.2.4). Water relaxation experiments showed lack of binding of PenG and PenN to DAOCS.Mn(II) in the absence of 2OG and

time-dependent displacement of water molecules from the active site only in the presence of 2OG. This result seems to indicate that PenG binding in the absence of 2OG is not related to the presence of a metal in the active site or does not occur with displacement of water molecules from the active site. It could be that PenG binding in the absence of 2OG occurs due to hydrophobic interactions established with hydrophobic amino acid residues.

PenG binding in the presence of 2OG was observed to occur with weak and time dependent displacement of water molecules from the active site. PenN on the other hand, was observed to bind in the presence of 2OG with an affinity comparable to the affinity of 2OG for the DAOCS.Mn(II) complex. The noticeably different affinities of PenG and PenN, the natural substrate, for the DAOCS.Mn(II).2OG complex could be explained by PenG binding not always occurring in the catalytically active conformation/site; this would lead to unproductive binding that would in turn, cause the substrate inhibition by PenG observed by Valegård *et al.*[1].

4.2.5 Conclusions

The displacement experiments carried out by 1D HSQC support the hypothesis that a conformational change in the active site is induced by the binding of 2OG. This conformational change is proposed to allow the binding of the penicillin substrate.

The fact that PenG is seen to bind, albeit weakly, in the absence of 2OG by mass spectrometry (Section 3.2.2.4) and 1D HSQC (Section 4.2.3.2) but not by T_1 relaxation measurements (Section 4.1.4.2.3) or UV-Vis (Section 4.3.2), suggests that PenG is not binding close to the metal centre. This could mean that the binding that is detected occurs non-specifically, via hydrophobic interactions.

4.3 Enzyme substrate complex detection by UV-Vis

4.3.1 UV-Vis studies on 2OG oxygenases

As previously discussed (Section 1.2.2), Fe(II) and 2OG dependent dioxygenases have been proposed to employ a common mechanism. Taurine dioxygenase is viewed as a model enzyme in the study of intemediates of the 2OG oxygenase catalytic cycle by means of UV-Vis spectroscopy. Studies on TauD [92] performed under anaerobic conditions have shown that the formation of a TauD.Fe(II).2OG complex results in the formation of a broad absorption feature centred at 530 nm. This feature was attributed to metal chelation by the substrate C-1 carboxylate and C-2 carbonyl groups. A combination of UV/visible absorption, circular dichroism, and magnetic circular dichroism spectroscopies and computational studies by Solomon *et al.* [93, 94, 95] have revealed that the iron centre in the enzyme.Fe(II).2OG complex is six-coordinate and in the high-spin configuration. Hausinger and co-workers have shown that subsequent

addition of substrate causes a shift in the absorption maximum to 520 nm, with formation of distinct shoulders at 480 and 570 nm. Substrate binding occurs in the vicinity of but not directly to the Fe (II) centre, which causes the iron site to become five-coordinate square pyramidal. This spectral change is characteristic to taurine (the natural substrate of TauD) and it was not observed to occur with substrate analogues.

UV-Vis studies have also been performed on other members of the 2OG oxygenase family. In the case of the human 2OG oxygenase PHD2, absorption spectra of the enzyme-substrate complexes revealed features that are consistent with the data obtained for TauD [16, 44].

4.3.2 Anaerobic enzyme-substrate complexes detected for DAOCS

The formation of an anaerobic DAOCS.Fe(II).2OG complex was observed in the UV-Vis absorption spectrum through the formation of a broad absorption feature with a maximum at 520 nm. The sample became light purple, a colour previously reported for 2OG oxygenase-substrate complexes. A final concentration of 200 μM DAOCS was used with a five-fold excess of Fe(II) in order to ensure complete formation of the DAOCS.Fe(II) complex, as previously shown by ESI-MS (Section 3). With higher enzyme concentrations, addition of Fe(II) caused heavy precipitation of the enzyme. The amount of 2OG used was 1 mM, an overall five fold excess relative to DAOCS. This ratio is again, a compromise between complex formation and DAOCS precipitation at higher 2OG concentrations.

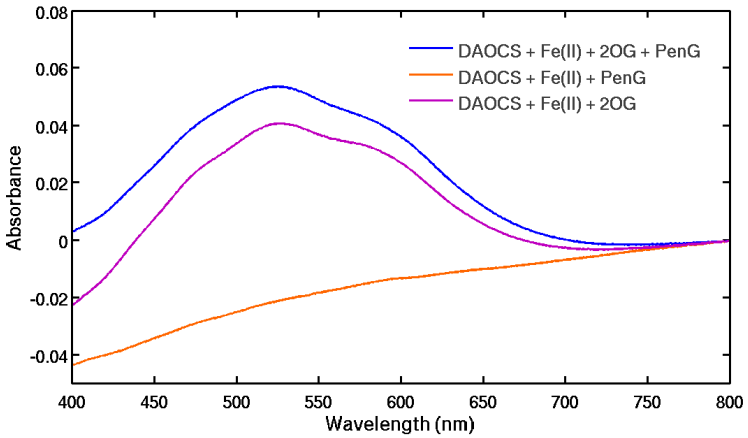

Figure 4.17: *Difference absorption spectra of DAOCS.Fe(II) in the presence of 2OG (purple) and PenG (dark purple). The anaerobic DAOCS+Fe(II)+2OG sample contained 200 μM DAOCS, 1 mM Fe(II) and 1 mM 2OG. In an attempt to obtain a spectrum for the DAOCS.Fe(II).2OG.PenG complex, 2 mM PenG was added. Addition of 2 mM PenG to a mixture conaining just DAOCS and Fe(II) did tot yield any absorption features in this region (orange). To highlight the spectral features, the spectrum of DAOCS.Fe(II) was subtracted from the raw spectra, as described by Ryle et al. [92].*

The possibility to form a DAOCS.Fe(II).PenG complex was also investigated. A ten-fold excess of PenG (relative to DAOCS) was added to the sample but the UV-Vis absorption spectrum did not display any features in the 400-800 nm region (Figure 4.17, brown trace).

Ternary enzyme-substrate complex formation was then studied using PenG. The addition of penicillin G to the mixture containing DAOCS, Fe(II) and 2OG did not cause a noticeable shift in the position of the absorption maximum (Figure 4.17, dark purple trace).

Oxygen leaks into the anaerobic mixture can cause disruptions to the absorption spectrum profile most likely due to Fe(II) oxidation. The spectrum will be distorted in that the absorption peaks are broadened and the absorption maxima are also altered (Figure S8).

However, the addition of the natural substrate, penicillin N, to a mixture containing DAOCS, Fe(II) and 2OG caused a bathochromic shift of the absorption maximum from 520 nm to 528 nm (Figure 4.18 dark red trace).

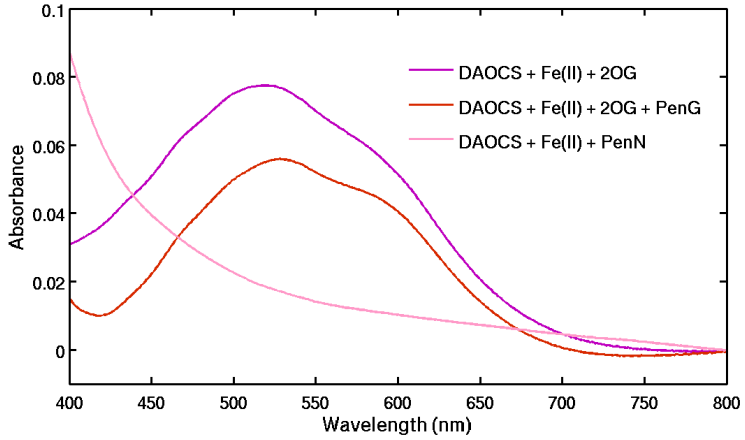

Figure 4.18: *Difference UV-Vis absorption spectra of DAOCS.Fe(II) in the presence of 2OG (purple), PenN (pink) and both 2OG and PenN (dark red). The spectrum for the mixture containing DAOCS, Fe(II) and 2OG has an absorption maximum at 520 nm. Upon addition of PenN in the mixture, the absorption maximum shifts to 528 nm. A mixture containing only DAOCS, Fe(II) and PenN (no 2OG) does not display any absorption features in this region. The concentrations used were 400 μM DAOCS, 2 mM Fe(II), 2 mM 2OG and 4 mM PenN. To highlight the spectral features, the spectrum of DAOCS.Fe(II) was subtracted from the raw spectra, as described by Ryle et al. [92].*

Equivalent experiments were performed using NOG instead of 2OG. However, in this case no absorption features were observed in the 400-800 nm region, both with and without PenN (Figure S9).

4.3.3 Discussion and Conclusions

A broad absorption peak with its maximum at 520 nm was found to be characteristic to the formation of the DAOCS.Fe(II).2OG complex. This is unusual within the 2OG oxygenase family since experimental data obtained so far on TauD and PHD2 show the absorption maximum characteristic for enzyme.Fe(II).2OG complex formation at 530 nm.

Ternary enzyme-substrate complex formation was investigated using both the natural substrate, penicillin N, as well as penicillin G. A shift in the absorption maximum was only observed for penicillin N. The

absorption maximum for the DAOCS.Fe(II).2OG.PenN complex was found to be located at 528 nm. This bathochromic shift observed upon prime substrate binding is opposite from what was reported for TauD[16] and PHD2[44].

These results should be regarded as a preliminary study that can serve as a starting point for future experiments including stopped-flow kinetics and Mössbauer spectroscopy on the reaction mechanism.

The preliminary studies have been carried out by UV-Vis under anaerobic conditions in order to observe enzyme-substrate complex formation. The formation of a DAOCS.Fe(II).2OG complex was associated with the formation of a broad absorption feature with a maximum at 520 nm. Subsequent addition of PenN led to a shift of the absorption maximum to 528 nm. This shift may be associated with the formation of a DAOCS.Fe(II).2OG.PenN complex. The striking characteristic of these two complexes is the fact that their absorption maximums are different from those reported in literature for other 2OG oxygenases [23, 16, 19].

Moreover, the fact that the presence of PenG in the mixture does not alter the absorption spectrum can be interpreted as PenG binding occurring in a conformation that is different from the natural substrate, PenN.

Chapter 5

Conclusions

The binding interactions between DAOCS and its substrates was investigated from both a qualitative and quantitative point of view, using a combination of protein-observe and ligand-observe methods. Penicillin G, the substrate used by Valegård *et al.* in their studies, as well as penicillin N, the natural substrate of DAOCS were used in these studies.

Non-denaturing mass spectrometry results suggest that it is possible to have both 2OG and the penicillin substrate bound to DAOCS simultaneously (Section 3.2.3). The binding of the two substrates appears to be ordered, with 2OG binding before the penicillin.

Dissociation constants for Mn(II), 2OG and the 2OG analogue, NOG, as well as penicillin N were determined using solvent water relaxation rate measurement (Table 4.1). In these experiments as well, penicillin N was only observed to bind in the presence of 2OG or NOG, which supports the result obtained by non-denaturing ESI-MS. A dissociation constant for penicillin G could not be measured using this method, probably because penicillin G binds too weakly.

1D-HSQC experiments showed that the 2OG and the penicillin substrate do not displace each other from their respecive binding sites (Section 4.2.4). These results do not support the overlapping binding sites for penicillin and 2OG hypothesis as proposed by Valegård *et al.* [1].

The preliminary studies carried out by UV-Vis under anaerobic conditions showed characteristic spectral features for each of the DAOCS.Fe(II).2OG and the DAOCS.Fe(II).2OG.PenN complexes in the 520-530 nm region (Section 4.3.3). The fact that the presence of PenG instead of PenN in the mixture does not alter the absorption spectrum can be interpreted as PenG binding occurring in a conformation that is different from the natural substrate, PenN.

The NMR-based activity assay offered additional insight into the coupling between 2OG decarboxylation and penicillin ring expansion under different conditions (Section 2.4); it also became apparent that substrate inhibition is probably not the reason why, as noted by Valegård *et al.*, turnover rate decreased

when the concentration of one of the substrates was increased [1]. By using only unnatural substrates in their studies and also by monitoring the concentration of only the ring expansion product, Valegård *et al.* had a biased interpretation of the results.

Overall, the results described in this thesis support the consensus 2OG oxygenase mechanism which implies the formation of a ternary complex between DAOCS, 2OG and the penicillin substrate, most probably through a sequential ordered mechanism.

Chapter 6

Materials and Methods

6.1 Materials and Reagents

Materials were obtained from the following suppliers:

Material	**Supplier**
Agarose	Bioline
SDS-PAGE reagents	Bio-Rad and Sigma
Bacto Agar	Difco
Molecular weight markers for SDS-PAGE gels (SeeBlue™ Plus 2)	Invitrogen
IPTG and kanamycin	Melford Laboratories
Bacto tryptone and yeast extract	Merck Chemicals
DNAseI and Complete™ protease inhibitor cocktail	Roche Diagnostics
DTT	Thermo Fisher Scientific

All other chemicals were obtained from the Sigma-Aldrich Chemical Company or Fisher Ltd, unless otherwise stated. All chemicals were obtained in the highest available quality where a choice existed. Purified (Milli-Q) water was obtained from a Millipore Elix® Reverse Osmosis system which was further purified by a Millipore Milli-Q® Synthesis system with a 0.22 mm filter on the outlet.

6.1.1 Reagents for molecular biology

6.1.1.1 Competent Cells used for Transformation

BL21(DE3) – F^- ompT gal dcm lon $hsdS_B(r_B^- m_B^-)$ λ(DE3 [lacI lacUV5-T7 gene 1 ind1 sam7 nin5])

XL10 (Gold) – Tet^r Δ(mcrA)183 Δ(mcrCB-hsdSMR-mrr)173 endA1 supE44 thi-1 recA1 gyrA96 relA1 lac The [F proAB lacIqZΔM15 Tn10 (Tet^r) Amy Cam^r] (U.S. Patent Nos. 5,512,468 and 5,707,841,

6,706,525)

6.1.2 Growth Media

All growth media were autoclaved (*Thermo Live Sciences* MAT 490 LEI) at 121 ℃ for 20 min before use.

6.1.2.1 Miller Luria Broth (LB) Medium

Reagents required per litre:

Reagent	Amount(g)
Bacto tryptone	10.0
Yeast extract	5.0
NaCl	10.0

15 g of agar was added prior to autoclaving for solid media (*i.e.* for LB Agar plates).

6.1.2.2 2 x Tryptone-Yeast (2TY) Extract

Reagents required per litre:

Reagent	Amount(g)
Bacto tryptone	16.0
Yeast extract	10.0
NaCl	5.0

6.1.2.3 Antibiotics

Final concentrations of antibiotics unless indicated otherwise were: Ampicillin, 100 μg/ml; Kanamycin 30 μg/ml.

6.1.3 Sodium dodecyl sulphate polyacrylamide gel electrophoresis (SDS-PAGE) materials [96]

6.1.3.1 SDS-PAGE Gels

Quantities for one gel:

Reagent	**Separating gel**	**Stacking gel**
Tris-HCl 1.5 M pH 8.8	1.25 mL	0.63 mL
MilliQ water	1.57 mL	1.57 mL
30% (w/v) acrylamide stock	2.08 mL	0.25 mL
SDS (10% w/v)	50 μL	25 μL
APS (10% w/v)	50 μL	25 μL
TEMED	4 μL	2.5 μL

The N, N, N', N'-tetramethylethylene diamine (TEMED) and freshly prepared ammonium persulphate (APS) were added just prior to pouring the gels. The acrylamide/bis-acrylamide ratio was 37:1.

6.1.3.2 10 x SDS-PAGE Running Buffer

Reagents required per 100 mL:

Reagent	Amount(g)
Tris-HCl	30
Glycine	144
SDS	10

6.1.3.3 SDS-PAGE Gel Stain

Reagent	Amount(g)
Acetic acid	10% (v/v)
Methanol	30% (v/v)
Coomassie® brilliant blue R	0.25% (w/v)

The SDS-PAGE gel destain contains the same quantities of reagents except there is no Coomassie® Brilliant Blue R present.

6.1.3.4 10 x SDS-PAGE Sample Loading Buffer

Reagents required per 100 mL:

Reagent	Amount(g)
Tris-HCl, 0.5 M, pH 6.8	10 mL
Bromophenol blue (0.2% w/v)	0.2 g
SDS (10% w/v)	20 mL
Glycerol	12 mL
β-mercaptoethanol	5.0 mL
MilliQ water	53 mL

6.2 Molecular Biology

6.2.1 Plasmid DNA purification

Plasmid DNA was purified from 3 mL cultures of *E. coli* XL10-Gold® (Stratagene) using the QUIAGEN™ purification system (Promega), following manufacturers protocol (Technical bulletin number 117).

6.2.2 DNA Quantification

DNA concentration was estimated by measuring the absorbance at 260 nm using a Nanodrop® ND-1000 spectrophotometer (NanoDrop® Technologies, Inc.). DNA concentrations were then determined using the program module 'DNA-50' according to the manufacturers instructions (ND-1000 users manual, page 5-1).

6.2.3 DNA Sequencing

DNA sequencing was performed by the Geneservice DNA Sequencing facility in the Department of Biochemistry at Oxford University.

6.3 Microbiological Techiniques

Standard sterile techniques were employed throughout. All instruments and pipette tips were sterilised in a TouchClave® II autoclave (LTE Scientific) at 121 ℃ for 20 min.

6.3.1 Incubations

Bacterial plate cultures were grown overnight at 37 ℃ in a Heraeus® TypB 6030 incubator (Thermo Fisher Scientific). Liquid cultures were incubated in a New Brunswick Scientific G25 environmental shaker and shaken at 250 rpm at the temperatures specified.

6.3.2 Competent Cell Transformations

Competent cells (Stratagene) were thawed on ice before 1 μL of plasmid DNA was added to 25 μL of the competent cells in pre-chilled 50 mL Falcon tubes. The tubes were left on ice for 30 minutes before placement into a water bath at 42℃ ('heat shocked') for the amount of time stated in the suppliers protocol. The tubes were then returned to ice for 2 min. Super Optimal Broth, Catabolite Repressing (SOC) medium (500 μL) was added to each tube which were then incubated at 37℃ for 1 hour before 100 μL of the transformation mixture was plated on agar plates containing the appropriate antibiotic. After the plates were dry, they were inverted and incubated at 37 C overnight. All agar plates were poured and streaked in a laminar flow hood (HeraSafe® Model KS12 Class II Biosafety Cabinet (Thermo Fisher Scientific) using sterile media and equipment.

6.3.3 Small Scale Growths for Starter Cultures

Either 5 ml (in 50 ml polypropylene tubes, Greiner Bio-One) or 100 mL (in 500 ml Duran flasks, Schott U.K.) of the relevant media containing the appropriate antibiotic was inoculated from a single colony on an agar plate or from a glycerol freeze, and grown at 37℃ overnight.

6.3.4 Production of BL21 (DE3) Cells Containing pET-24 Constructs

The pET-24 constructs (obtained from The CJS Laboratory Archive, Chemistry Research Laboratory, Oxford) were used to generate the protein. The construct was initially transformed into *E. coli* XL10-Gold cells (Stratagene) and streaked onto LB agar plates containing 30 μg/mL of kanamycin. A 5 mL culture was then grown in 2TY media, the constructs purified from these cells (Wizard™ Plus Minipreps DNA purification system, Promega) and transformed into *E. coli* BL21 (DE3) cells (Stratagene).

6.3.5 Glycerol Stocks

Samples of un-induced cells from growths were preserved by gently mixing 750 μL of culture with 250 μL of 100% sterile glycerol (sterilised by autoclaving at 121℃), flash freezing in liquid nitrogen and storage at –80℃.

6.3.6 Optical Density Measurements

Optical density readings were taken in 1.6 ml cuvettes with 5 x dilution in Milli-Q water against a reference sample of the growth media at zero time. The absorbance was measured at 600 nm using a Novaspec® II spectrophotometer (Pharmacia).

6.3.7 Large Scale Cell Growths

A 100 ml culture of *E. coli* BL21 (DE3), transformed with the appropriate expression plasmid in the appropriate media, was produced to act as a starter culture for large scale cell growths. Large scale recombinant protein expression was performed using 2000 ml PYREX® narrow-mouth graduated Erlenmeyer flasks containing either 500 or 600 mL of 2-TY medium containing the appropriate antibiotic. Additionally, 2,500 mL Tunair® polypropylene flasks (Sigma-Aldrich) containing 1000 ml of medium were used. Flasks containing growth medium were inoculated with 1% of the bacterial starter culture and grown at 37℃ until they reached an OD_{600} of approx. 0.6. At this point, the cultures were induced with 1 mM IPTG final concentration, and further incubated at 28℃ for 4 hours. After this time, the cultures were centrifuged and the resulting bacterial pellet frozen in a sealable plastic bag at –80℃.

6.3.8 Cell Lysate Preparation

Between 40 g to 45 g of cells, stored at –80℃, were re-suspended in approximately 3 times their mass (w/v ratio) of 50 mM Tris-HCl pH 7.5 (Lysis buffer, Table 6.1). Approximately 0.1 μg/mL of DNAse I was added to the suspension. The cells were lysed by sonication (5 x 30 second bursts with 40 seconds rest between) using a Vibra Cell VCX 500 with a 13 mm probe, on ice. Cell debris was removed by centrifugation at 14,000 r.p.m. for 20 minutes at 4℃ with the supernatant (the cell lysate) being decanted from the resulting pellet. The supernatant was then filtered using a 0.4 μm Omnipore™ filter (Millipore U.K.).

A similar procedure as above was followed for cell lysates prepared with a smaller mass of cells, except that the quantities of reagents and amounts of sonication were scaled down accordingly.

6.4 Protein Purification

Recombinant DAOCS was obtained as reported by Lloyd *et al.* [29], using the modified procedure detailed below. The composition of the buffers used in the purification procedures is described in Table 6.1.

Table 6.1: *Protein purification buffers*

Buffer	Composition
Lysis	50 mM Tris-HCl (pH 7.5), 0.1 μg/mL DNase I
Wash	50 mM Tris-HCl, 5 mM EDTA (pH 7.5)
Elution	50 mM Tris-HCl, 5 mM EDTA, 500 mM NaCl(pH 7.5)
Gel filtration	50 mM Tris-HCl (pH 7.5)

6.4.1 Fast Protein Liquid Chromatography (FPLC)

FPLC for protein purification was carried out using Äkta™ FPLC systems (GE Healthcare) at 4℃. Buffers were prepared in Milli-Q water. Samples up to 10 mL were loaded using a Superloop™ (GE Healthcare) with larger samples being loaded using the FPLC pump. Purification procedures were followed by monitoring absorbance at 280 nm with a UPC-900 monitor on the FPLC and by SDS-PAGE. Sample fractions were collected using a Frac-920 fraction collector. All columns were cleaned after each use according to the manufacturers instructions. Columns were stored in 20% (v/v) ethanol.

6.4.2 Ion Exchange Protein Purification

The first step of DAOCS purification was carried out using a 50 mL (settled bed volume) ion exchange column of QSepharose FF or QSepharose HP® resin (GE Healthcare). The column was equilibrated at 5 mL/min with 2 column volumes of wash buffer (Table 6.1).

The cell lysate was loaded onto the column at 2 mL/min. 12 column volumes of wash buffer (Table 6.1) at a flowrate of 4 mL/min were used in the wash step. Elution was carried out using a gradient of 0% to 50% elution buffer (Table 6.1), corresponding to a NaCl gradient of 0 mM to 250 mM over 5 column volumes at 4 mL/min. Fractions of 5 mL were collected during the elution step. DAOCS starts eluting at approximately 10% elution buffer (50 mM NaCl). Fractions of satisfactory purity (as judged by SDS-PAGE) were pooled and concentrated to a volume of 3-5 mL (Figure 6.7.5).

6.4.3 Preparative Size Exclusion Chromatography

Size exclusion chromatography was performed after ion exchange chromatography using a 300 ml Superdex™75 size exclusion chromatography column (GE Healthcare). The column was equilibrated at 2 mL/min with 1 column volume of Gel filtration buffer (Table 6.1) and the concentrated pooled fractions from the ion exchange step were injected using the Superloop™. The protein was eluted over 1 column volume of buffer at 0.75 ml/min and 5 ml fractions were collected. An A280 trace along with SDS-PAGE was used to determine which of the fractions contained the purified protein.

At this point, it was decided, as judged by SDS-PAGE and non-denaturing mass spectrometry, that the protein obtained was of above 95% purity and therefore suitable to be used in further experiments with no additional purification steps (Figure 6.7.5). The last ion exchange step described in the protocol of Lloyd *et al.* [29] was hence omitted.

The fractions of pure protein were combined and concentrated to an appropriate volume corresponding to the type of experiment the protein was intended for (Sections 6.5.1, 6.6.1, 6.6.2, 6.6.3).

6.5 Non-denaturing Mass Spectrometry

6.5.1 ESI-MS experiments

Samples containing 10-15 μM enzyme, cofactors and substrates were prepared using concentrated stock solutions and then incubated on ice for the corresponding amount of time. The enzyme was buffer exchanged into 15 mM ammonium acetate (AA) pH 7.5 buffer and diluted to 100 μM just before the experiment. The other stock solutions were prepared by dissolving the corresponding amounts into AA buffer (except for the Fe(II) salt that was initially dissolved in 20 mM HCl). All stock solutions were freshly prepared. For time-course experiments, larger volume solutions of the same concentrations were made up in wells of a 96-well plate. Aliquots were removed at intervals and delivered to the mass spectrometer by the NanoMate device.

6.6 NMR

6.6.1 T1 relaxation measurements

Apo-DAOCS was used in all experiments. Solutions were buffered using Tris-D11 (pH 7.5) dissolved in 12.5% H_2O and 87.5% D_2O. A stock solution of 320 μM Mn(II) was used throughout, and diluted to 40 μM or 80 μM final concentrations. Stock solutions of ligand molecules were made up freshly to concentrations between 1.6 mM to 8 mM. 1 μL or 2 μL samples were titrated into NMR tubes.

6.6.2 1D selective HSQC

1D-selective HSQC experiments were conducted at 700 MHz using a Bruker Avance III spectrometer equipped with an inverse TCI cryoprobe optimized for ^{1}H observation and 3 mm diameter Bruker MATCH micro tubes (Hilgenberg) containing 160 μL final sample volume. Solutions were buffered using Tris-D11 (pH 7.5) dissolved 100% D_2O or 95% H_2O and 5% D_2O. Pulse tip-angle calibration using the single-pulse nutation method was undertaken for each assay sample.Assays were conducted at 298 K in solutions typically containing 50 μL apo-DAOCS, 400 μL Zn(II), 50 μL 1,2,3,4-^{13}C-2OG and excess PenG or bicyclic inhibitor. Selective irradiation was applied at 35 ppm.

6.6.3 NMR activity assays

Reaction components – apo-DAOCS, $(NH_4)_2Fe(SO_4)_2$, penicillin substrate, 2OG, and ascorbate – were prepared as concentrated stock solutions in deuterated Tris buffer (pH 7.5, 50 mM in 10% D_2O). The

reaction mixture was obtained by diluting the stock solutions to the concentration required by the experiment (DAOCS concentration was maintained at 5 μM and $(NH_4)_2Fe(SO_4)_2$ concentration at 50 μM throughout, unless otherwise stated). The reaction was carried out at room temperature in a 5 mm diameter NMR tube, and initiated by the addition of DAOCS. ^{1}H-NMR spectra were recorded using a Bruker AVII 500 machine (running Topspin software; Bruker, Ettlingen, Germany) and reported in p.p.m. relative to H_2O (δ^1H 4.72). Spectra were obtained at 93 s intervals (8 scans per spectrum) and integrated using peak area scaling to monitor changes in the area of signals of interest.

6.7 Other Procedures

6.7.1 Concentration of Protein Solutions

Protein solutions were concentrated using Amicon® Ultra-4 or Ultra-15 Ultracel® PL ultrafiltration devices (Millipore U.K.) with 5,000, 10,000 or 30,000 Da nominal molecular weight limit membranes in an Allegra™ 21R centrifuge (Beckman Coulter; S4180 rotor, 3500 rpm, 4℃).

6.7.2 Protein Concentration Determination

Concentrations of purified proteins were determined by measuring the A280 using an ND-1000 spectrophotometer (NanoDrop® Technologies) and the program module 'Protein A280' using 'Other protein (E & MW)' sample type according to the manufacturers instructions. A sample of the buffer solution was used for the baseline reading. All molecular weights and extinction coefficients (ϵ) of the proteins of interest were calculated using the ProtParam tool (http://web.expasy.org/protparam/).

6.7.3 Sodium Dodecyl Sulphate Polyacrylamide Gel Electrophoresis (SDS-PAGE) [96]

Protein purity and expression levels were analysed by SDS-PAGE following the method of Laemmli [96]. 15 μL protein samples, containing up to 10 μg of protein, were mixed with 15 μL of 2 x SDS PAGE sample loading buffer and then boiled at 95℃ for 5 minutes. Gels were run on a Bio-Rad Mini Protean II system, at a constant potential of 200 V. Once complete, gels were stained in a solution of Coomassie® Brilliant Blue R for 5 minutes then subsequently de-stained for 15 minutes.

6.7.4 Centrifugation

Samples of volume less than 1.5 ml were centrifuged at room temperature using an accuSpin™ Micro benchtop centrifuge (Thermo Fisher Scientific) at 13,000 rpm. Samples of volume up to 50 mL, 50 mL to 150 mL and 150 mL to 400 mL were centrifuged at 4℃ in a Avanti™ J-25 centrifuge (Beckman Coulter)

using a JA-25.50, JLA-16.250 and JA-10 rotor, with compatible bottles, at 23,000, 14,000 and 9,000 rpm respectively. Protein concentrators were centrifuged at 4℃ in an Allegra® 21R centrifuge (Beckman Coulter) using an S-4180 rotor at 3,500 pm.

6.7.5 pH Measurement

Determination of pH was carried out using a Jenway 3305 pH meter with an Aldrich® polymer bodied combination pH electrode (Calomel reference, product code Z266213). Electrodes were calibrated to pH 7.0 and either pH 4.0 or 10.0 before use.

Supplementary Figures

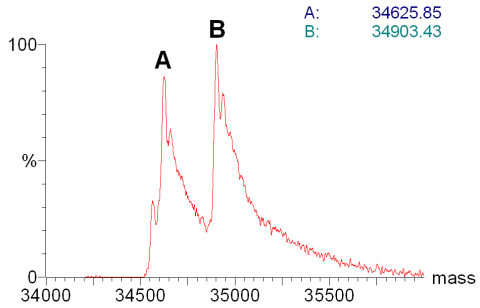

Figure S1: *The bicyclic inhibitor was shown to bind to the DAOCS.Zn(II) complex by non-denaturing ESI-MS. Complex A corresponds to the DAOCS.Zn(II) complex while B represents the DAOCS.Zn(II).inhibitor complex.*

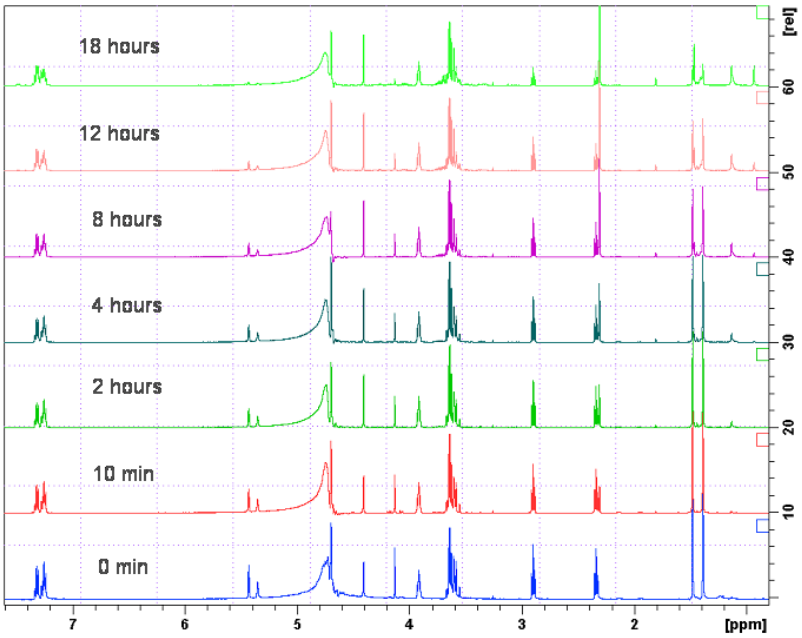

Figure S2: *Long NMR time course analysis of the DAOCS reaction system.*

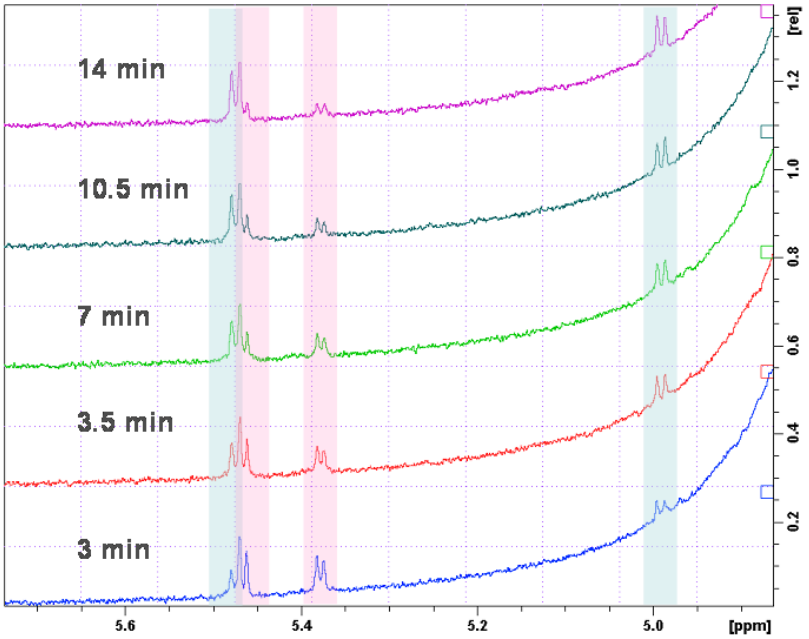

Figure S3: *Control experiments show no signs of β-lactam hydrolysis during the typical time-course experiments. The formation of the cephalosporin β-lactam proton signals (blue) can be seen appearing as the reaction proceeds. The penicillin (yellow) β-lactam proton signals (pink) disappear almost completely after 14 minutes.*

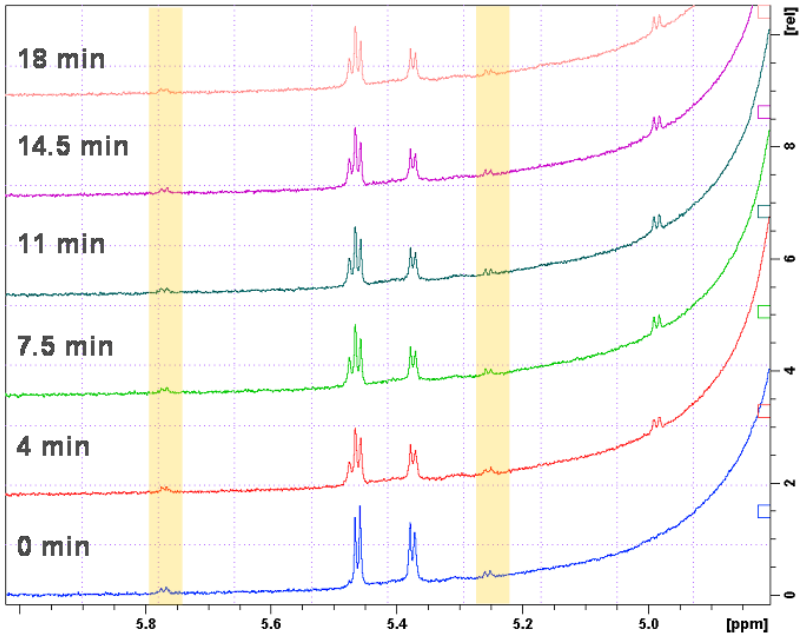

Figure S4: *Signals denoting the presence of hydrolysed β-lactam rings (orange).*

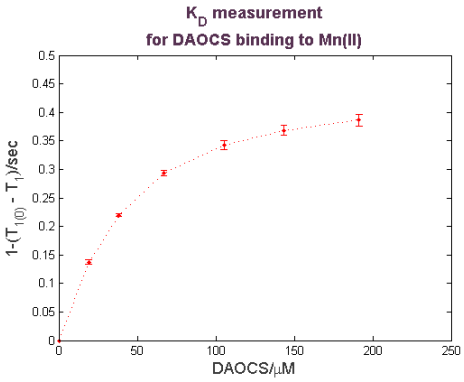

(a) Plot of relative T_1 variation for DAOCS titration

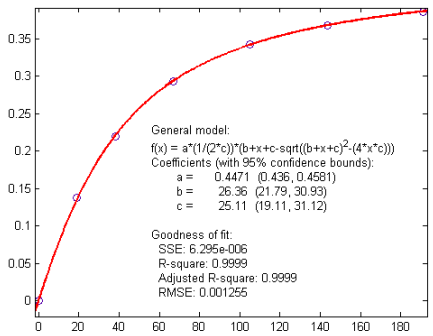

(b) Fitting for DAOCS K_d determination.

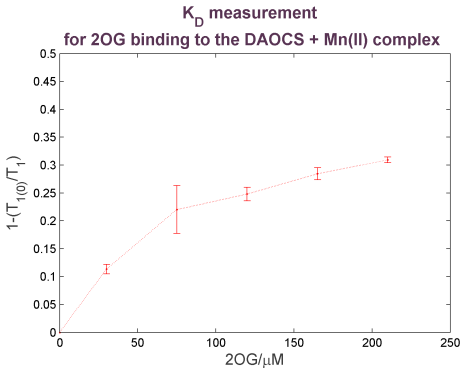

(c) Plot of relative T_1 variation for 2OG titration

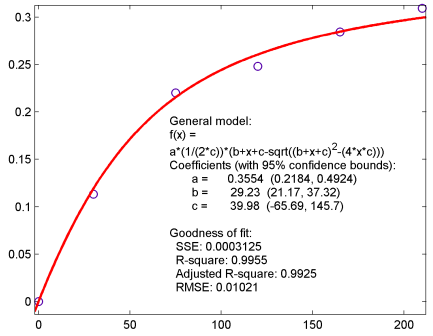

(d) Fitting for 2OG K_d determination.

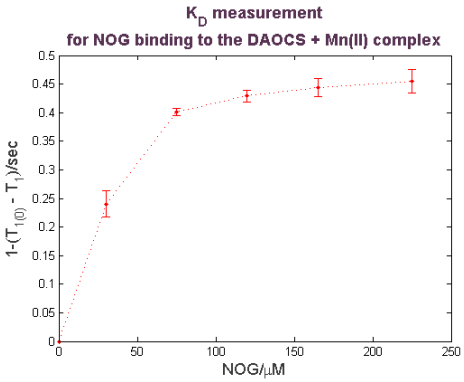

(e) Plot of relative T_1 variation for NOG titration

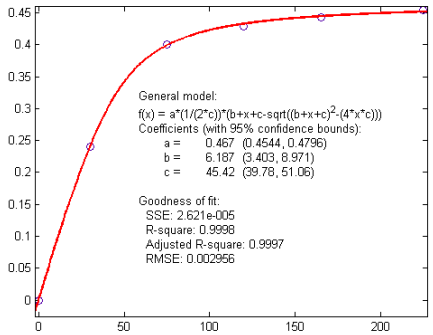

(f) Fitting for NOG K_d determination.

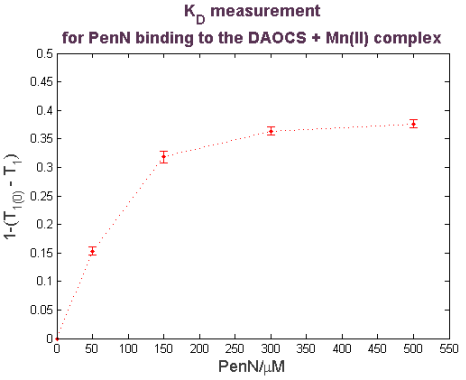

(g) Plot of relative T_1 variation for PenN titration

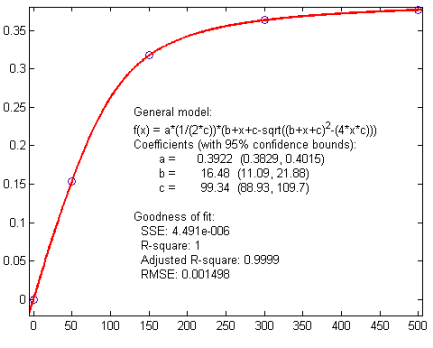

(h) Fitting for PenN K_d determination.

Figure S5: Figures of relative T_1 variation and fitting for K_d determination.

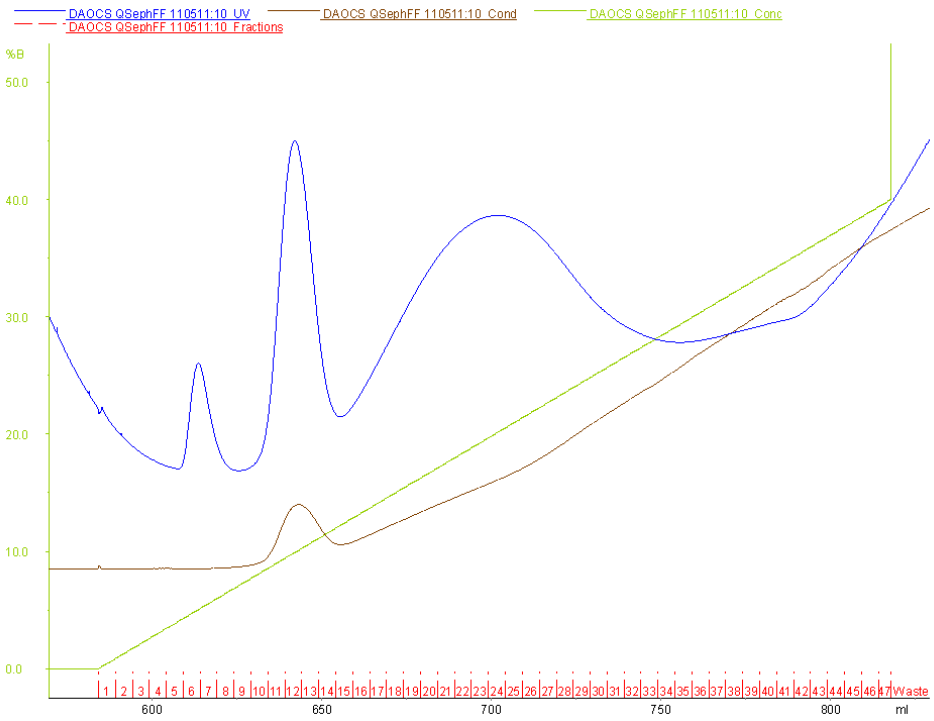

(a) QSepharoseFF elution profile for DAOCS.

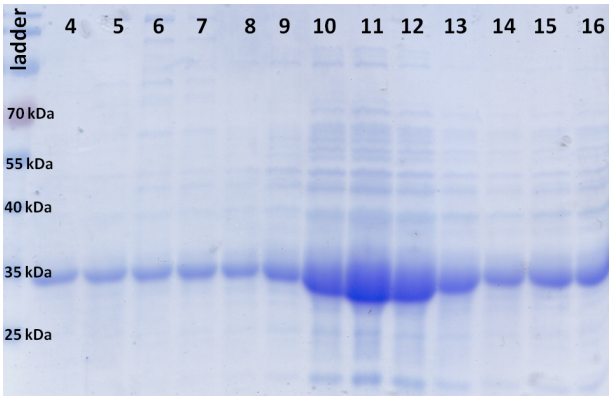

(b) SDS-PAGE gel of fractions 4 to 16 from subfigure (a)

Figure S6: Chromatograms and corresponding SDS-PAGE gels for DAOCS ion exchange purification. The protocol is described in Section 6.4.2. Fractions 10 to 15 were typically pooled and concentrated.

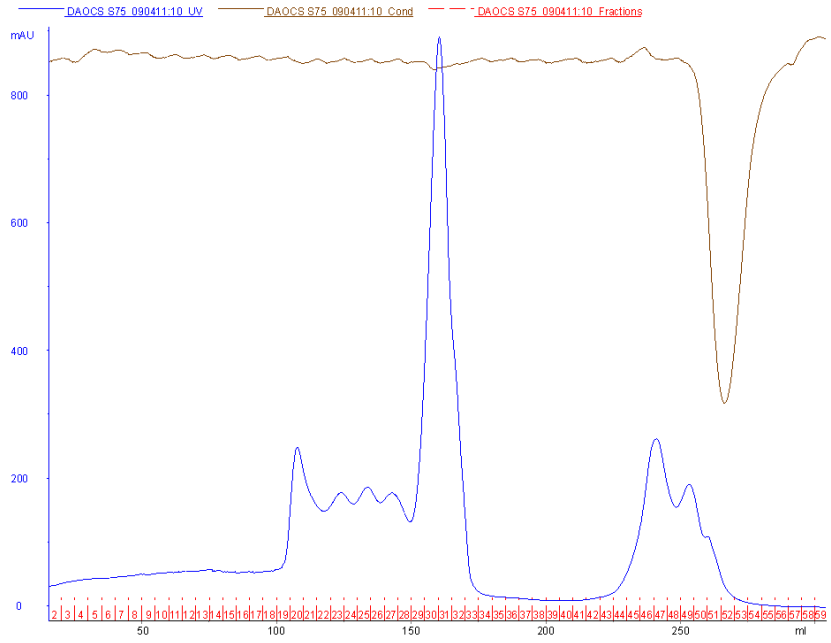

(a) Superdex 75 elution profile for DAOCS.

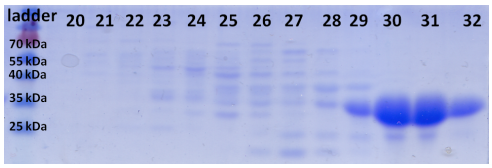

(b) SDS-PAGE gel of fractions 20 to 32 from sub-figure (a)

Figure S7: Chromatograms and corresponding SDS-PAGE gels for DAOCS size exclusion purification. The protocol is described in Section 6.4.3. Fractions 30 to 32 were typically pooled and concentrated.

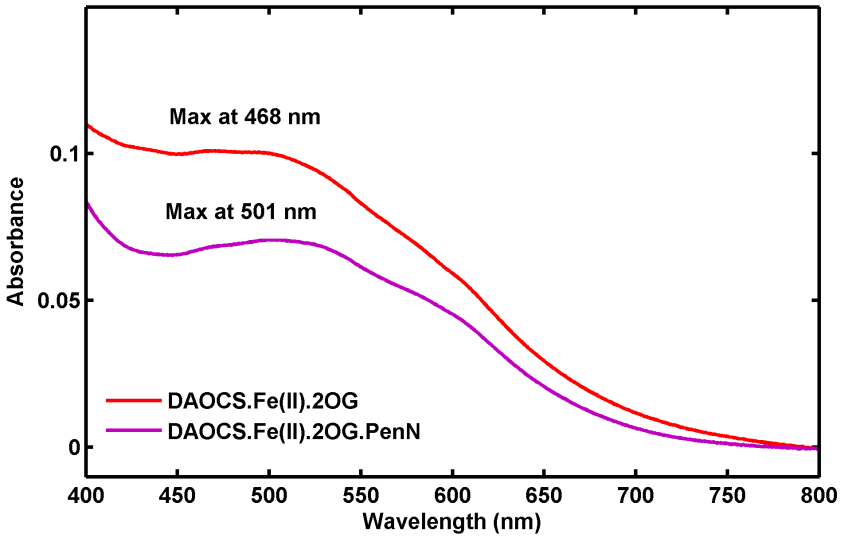

Figure S8: *UV-Vis spectrum of a sample that was not perfectly sealed. Small amounts of oxygen are present in the sample thereby initiating the catalytic process. Given the five-fold excess of Fe(II) and the lack of ascorbate in the system, it is likely that a certain amount of Fe(III) is also formed.*

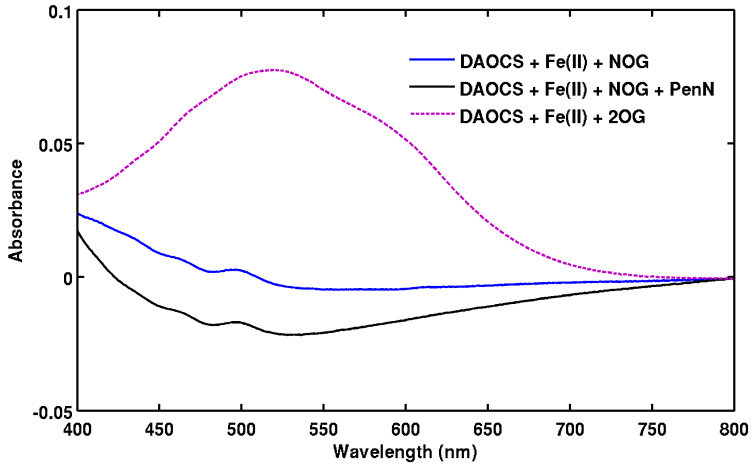

Figure S9: *Difference UV-Vis absorption spectra of DAOCS.Fe(II) in the presence of NOG (blue) and both NOG and PenN (black). The absorption spectrum for DAOCS.Fe(II) in the presence of 2OG (purple dashes) was introduced for reference.*

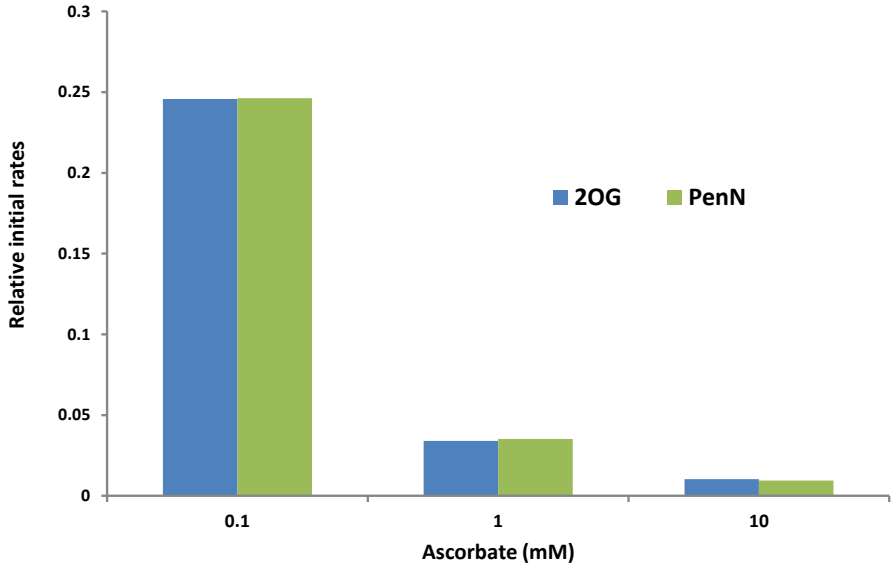

Figure S10: *The influence of ascorbate on penicillin N turnover and coupling. As with penicillin G, high concentrations of ascorbate have an overall inhibitory influence on DAOCS acitvity. 2OG decarboxylation (blue) remanins coupled to penicillin N ring expansion (green) in a 1:1 ratio at all ascorbate concentrations.*

References

[1] Karin Valegård, Anke C. van Scheltinga, Alain Dubus, Graziella Ranghino, Linda M. Oster, Janos Hajdu, and Inger Andersson. The structural basis of cephalosporin formation in a mononuclear ferrous enzyme. *Nature Structural & Molecular Biology*, 11(1):95–101, December 2003.

[2] Christopher J. Schofield and Zhihong Zhang. Structural and mechanistic studies on 2-oxoglutarate-dependent oxygenases and related enzymes. *Current Opinion in Structural Biology*, 9(6):722–731, December 1999.

[3] Matthew E. C. Caines, Mark C. Sleeman, and Christopher J. Schofield. The enzymology of clavam and carbapenem biosynthesis. *Chemical Communications*, (34):4251–4263, 2005.

[4] Kari I. Kivirikko and Johanna Myllyharju. Prolyl 4-hydroxylases and their protein disulfide isomerase subunit. *Matrix Biology*, 16(7):357–368, February 1998.

[5] Andrew C. R. Epstein, Jonathan M. Gleadle, Luke A. McNeill, Kirsty S. Hewitson, John O'Rourke, David R. Mole, Mridul Mukherji, Eric Metzen, Michael I. Wilson, Anu Dhanda, Ya-Min Tian, Norma Masson, Donald L. Hamilton, Panu Jaakkola, Robert Barstead, Jonathan Hodgkin, Patrick H. Maxwell, Christopher W. Pugh, Christopher J. Schofield, and Peter J. Ratcliffe. *C. elegans* egl-9 and mammalian homologs define a family of dioxygenases that regulate hif by prolyl hydroxylation. *Cell*, 107(1):43–54, October 2001.

[6] Tod Duncan, Sarah C. Trewick, Pertti Koivisto, Paul A. Bates, Tomas Lindahl, and Barbara Sedgwick. Reversal of DNA alkylation damage by two human dioxygenases. *Proceedings of the National Academy of Sciences*, 99(26):16660–16665, December 2002.

[7] Pål O. Falnes, Rune F. Johansen, and Erling Seeberg. Alkb-mediated oxidative demethylation reverses DNA damage in *Escherichia coli*. *Nature*, 419(6903):178–182, September 2002.

[8] Yu-ichi Tsukada, Jia Fang, Hediye Erdjument-Bromage, Maria E. Warren, Christoph H. Borchers, Paul Tempst, and Yi Zhang. Histone demethylation by a family of JmjC domain-containing proteins. *Nature*, 439(7078):811–816, December 2005.

[9] Ian J. Clifton, Michael A. McDonough, Dominic Ehrismann, Nadia J. Kershaw, Nicolas Granatino, and Christopher J. Schofield. Structural studies on 2-oxoglutarate oxygenases and related double-stranded β-helix fold proteins. *Journal of Inorganic Biochemistry*, 100(4):644–669, April 2006.

[10] J. E. Baldwin, R. M. Adlington, J. B. Coates, M. J. Crabbe, N. P. Crouch, J. W. Keeping, G. C. Knight, C. J. Schofield, H. H. Ting, and C. A. Vallejo. Purification and initial characterization of an enzyme with deacetoxycephalosporin C synthetase and hydroxylase activities. *The Biochemical Journal*, 245(3):831–841, August 1987.

[11] S. E. Jensen, D. W. Westlake, and S. Wolfe. Deacetoxycephalosporin C synthase and deacetoxycephalosporin C hydroxylase are two separate enzymes in *Streptomyces clavuligerus*. *The Journal of Antibiotics*, 38(2):263–265, February 1985.

[12] J. F. Martín, S. Gutiérrez, F. J. Fernández, J. Velasco, F. Fierro, A. T. Marcos, and K. Kosalkova. Expression of genes and processing of enzymes for the biosynthesis of penicillins and cephalosporins. *Antonie van Leeuwenhoek*, 65(3):227–243, 1994.

[13] P. L. Roach, I. J. Clifton, C. M. Hensgens, N. Shibata, C. J. Schofield, J. Hajdu, and J. E. Baldwin. Structure of isopenicillin N synthase complexed with substrate and the mechanism of penicillin formation. *Nature*, 387(6635):827–830, June 1997.

[14] K. S. Hewitson, N. Granatino, R. W. Welford, M. A. McDonough, and C. J. Schofield. Oxidation by 2-oxoglutarate oxygenases: non-haem iron systems in catalysis and signalling. *Philosophical Transactions Series A: Mathematical, Physical, and Engineering Sciences*, 363(1829):807–828, April 2005.

[15] Peter L. Roach, Ian J. Clifton, Vilmos Fulop, Karl Harlos, Geoffrey J. Barton, Janos Hajdu, Inger Andersson, Christopher J. Schofield, and Jack E. Baldwin. Crystal structure of isopenicillin N synthase is the first from a new structural family of enzymes. *Nature*, 375(6533):700–704, June 1995.

[16] John C. Price, Eric W. Barr, Lee M. Hoffart, Carsten Krebs, and Martin M. Bollinger. Kinetic dissection of the catalytic mechanism of taurine:alpha-ketoglutarate dioxygenase (taud) from *Escherichia coli*. *Biochemistry*, 44(22):8138–8147, June 2005.

[17] John C. Price, Eric W. Barr, Bhramara Tirupati, Martin M. Bollinger, and Carsten Krebs. The first direct characterization of a high-valent iron intermediate in the reaction of an alpha-ketoglutarate-dependent dioxygenase: a high-spin fe(iv) complex in taurine/alpha-ketoglutarate dioxygenase (taud) from *Escherichia coli*. *Biochemistry*, 42(24):7497–7508, June 2003.

[18] Michael A. McDonough, Christoph Loenarz, Rasheduzzaman Chowdhury, Ian J. Clifton, and Christopher J. Schofield. Structural studies on human 2-oxoglutarate dependent oxygenases. *Current Opinion in Structural Biology*, 20(6):659–672, December 2010.

[19] Jing Zhou, Wendy L. Kelly, Brian O. Bachmann, Michele Gunsior, Craig A. Townsend, and Edward I. Solomon. Spectroscopic studies of substrate interactions with clavaminate synthase 2, a multifunctional α-KG-dependent non-heme iron enzyme: Correlation with mechanisms and reactivities. *Journal of the American Chemical Society*, 123(30):7388–7398, August 2001.

[20] H. M. Hanauske-Abel and V. Günzler. A stereochemical concept for the catalytic mechanism of prolylhydroxylase. *Journal of Theoretical Biology*, 94(2):421–455, January 1982.

[21] Piotr K. Grzyska, Evan H. Appelman, Robert P. Hausinger, and Denis A. Proshlyakov. Insight into the mechanism of an iron dioxygenase by resolution of steps following the Fe(IV)=O species. *Proceedings of the National Academy of Sciences of the United States of America*, 107(9):3982–3987, March 2010.

[22] P. Hedden. 2-Oxoglutarate-dependent dioxygenases in plants: mechanism and function. *Biochemical Society Transactions*, 20(2):373–377, May 1992.

[23] Carsten Krebs, Danica Galonić Fujimori, Christopher T. Walsh, and J. Martin Bollinger. Non-heme Fe(IV)oxo intermediates. *Accounts of Chemical Research*, 40(7):484–492, July 2007.

[24] Wonwoo Nam. High-valent iron(IV)oxo complexes of heme and non-heme ligands in oxygenation reactions. *Accounts of Chemical Research*, 40(7):522–531, May 2007.

[25] J. Myllyharju and K. I. Kivirikko. Characterization of the iron- and 2-oxoglutarate-binding sites of human prolyl 4-hydroxylase. *The EMBO Journal*, 16(6):1173–1180, March 1997.

[26] Monica Mantri, Zhihong Zhang, Michael A. McDonough, and Christopher J. Schofield. Autocatalysed oxidative modifications to 2-oxoglutarate dependent oxygenases. *FEBS Journal*, 279(9):1563–1575, 2012.

[27] Emily Flashman, Sarah L. Davies, Kar Kheng, and Christopher J. Schofield. Investigating the dependence of the hypoxia-inducible factor hydroxylases (factor inhibiting HIF and prolyl hydroxylase domain 2) on ascorbate and other reducing agents. *The Biochemical Journal*, 427(1):135–142, April 2010.

[28] G. R. Buettner and B. A. Jurkiewicz. Catalytic metals, ascorbate and free radicals: combinations to avoid. *Radiation Research*, 145(5):532–541, May 1996.

[29] H. J. Lloyd, M. D. and, K. Harlos, Z. H. Zhang, J. E. Baldwin, C. J. Schofield, J. M. Charnock, C. D. Garner, T. Hara, A. C. Terwisscha van Scheltinga, K. Valegard, J. A. Viklund, J. Hajdu, I. Andersson, A. Danielsson, and R. Bhikhabhai. Studies on the active site of deacetoxycephalosporin C synthase. *Journal of Molecular Biology*, 287(5):943–960, April 1999.

[30] J. E. Baldwin and Sir E. P. Abraham. The biosynthesis of penicillins and cephalosporins. *Natural Product Reports*, 5(2):129–145, 1988.

[31] S. Kovacevic, B. J. Weigel, M. B. Tobin, T. D. Ingolia, and J. R. Miller. Cloning, characterization, and expression in *Escherichia coli* of the *Streptomyces clavuligerus* gene encoding deacetoxycephalosporin c synthetase. *Journal of Bacteriology*, 171(2):754–760, February 1989.

[32] Norio Shibata, Matthew D. Lloyd, Jack E. Baldwin, and Christopher J. Schofield. Adipoyl-6-aminopenicillanic acid is a substrate for deacetoxycephalosporin C synthase (DAOCS). *Bioorganic & Medicinal Chemistry Letters*, 6(13):1579–1584, July 1996.

[33] J. E. Dotzlaf and W. K. Yeh. Copurification and characterization of deacetoxycephalosporin C synthetase/hydroxylase from Cephalosporium acremonium. *Journal of Bacteriology*, 169(4):1611–1618, April 1987.

[34] A. Scheidegger, M. T. Küenzi, and J. Nüesch. Partial purification and catalytic properties of a bifunctional enzyme in the biosynthetic pathway of β-lactams in *Cephalosporium acremonium*. *The Journal of Antibiotics*, 37(5):522–531, May 1984.

[35] Karin Valegård, Anke C. van Scheltinga, Matthew D. Lloyd, Takane Hara, S. Ramaswamy, Anastassis Perrakis, Andy Thompson, Hwei-Jen Lee, Jack E. Baldwin, Christopher J. Schofield, Janos Hajdu, and Inger Andersson. Structure of a cephalosporin synthase. *Nature*, 394(6695):805–809, August 1998.

[36] Hwei-Jen Lee, Matthew D. Lloyd, Karl Harlos, Ian J. Clifton, Jack E. Baldwin, and Christopher J. Schofield. Kinetic and crystallographic studies on deacetoxycephalosporin C synthase (DAOCS). *Journal of Molecular Biology*, 308(5):937–948, May 2001.

[37] Matthew D. Lloyd, Sarah J. Lipscomb, Kirsty S. Hewitson, Charles M. H. Hensgens, Jack E. Baldwin, and Christopher J. Schofield. Controlling the Substrate Selectivity of Deacetoxycephalosporin/deacetylcephalosporin C Synthase. *Journal of Biological Chemistry*, 279(15):15420–15426, April 2004.

[38] A. Dubus, M. D. Lloyd, H. J. Lee, C. J. Schofield, J. E. Baldwin, and J. M. Frere. Probing the penicillin sidechain selectivity of recombinant deacetoxycephalosporin C synthase. *Cellular and Molecular Life Sciences*, 58(5-6):835–843, May 2001.

[39] Hwei-Jen Lee, Matthew D. Lloyd, Ian J. Clifton, Karl Harlos, Alain Dubus, Jack E. Baldwin, Jean-Marie Frere, and Christopher J. Schofield. Alteration of the co-substrate selectivity of deacetoxycephalosporin C synthase. *Journal of Biological Chemistry*, 276(21):18290–18295, May 2001.

[40] Hwei-Jen Lee, Young-Fung Dai, Chia-Yang Shiau, Christopher J. Schofield, and Matthew D. Lloyd. The kinetic properties of various R258 mutants of deacetoxycephalosporin C synthase. *European Journal of Biochemistry*, 270(6):1301–1307, 2003.

[41] Nathan R. Rose, Michael A. McDonough, Oliver N. F. King, Akane Kawamura, and Christopher J. Schofield. Inhibition of 2-oxoglutarate dependent oxygenases. *Chemical Society Reviews*, 40(8):4364–4397, 2011.

[42] J. E. Baldwin and M. J. Crabbe. A spectrophotometric assay for deacetoxycephalosporin C synthase. *FEBS Letters*, 214(2):357–361, April 1987.

[43] Hwei-Jen Lee, Matthew D. Lloyd, Karl Harlos, and Christopher J. Schofield. The effect of cysteine mutations on recombinant deacetoxycephalosporin c synthase from *S. clavuligerus*. *Biochemical and Biophysical Research Communications*, 267(1):445–448, January 2000.

[44] Emily Flashman, Lee M. Hoffart, Refaat B. Hamed, Martin M. Bollinger, Carsten Krebs, and Christopher J. Schofield. Evidence for the slow reaction of hypoxia-inducible factor prolyl hydroxylase 2 with oxygen. *FEBS Journal*, 277(19):4089–4099, October 2010.

[45] Richard J. Hopkinson, Refaat B. Hamed, Nathan R. Rose, Timothy D. W. Claridge, and Christopher J. Schofield. Monitoring the Activity of 2-Oxoglutarate Dependent Histone Demethylases by NMR Spectroscopy: Direct Observation of Formaldehyde. *ChemBioChem*, 11(4):506–510, March 2010.

[46] P. G. Navarro, I. H. Blázquez, B. Q. Osso, P. J. Martínez de las Parras, M. I. Puentedura, and A. A. García. Penicillin degradation catalysed by Zn(II) ions in methanol. *International Journal of Biological Macromolecules*, 33(4-5):159–166, December 2003.

[47] A. Márquez García, P. Gutiérrez Navarro, and P. J. Martínez de Las Parras. Degradation of ampicillin in the presence of cadmium (II) ions. *Talanta*, 46(1):101–109, May 1998.

[48] Geoff A. Holdgate, Malcolm Anderson, Fredrik Edfeldt, and Stefan Geschwindner. Affinity-based, biophysical methods to detect and analyze ligand binding to recombinant proteins: Matching high information content with high throughput. *Journal of Structural Biology*, 172(1):142–157, October 2010.

[49] Alison E. Ashcroft. Recent developments in electrospray ionisation mass spectrometry: noncovalently bound protein complexes. *Natural Product Reports*, 22(4):452–464, 2005.

[50] Mark A. Tito, Kaspar Tars, Karin Valegård, János Hajdu, and Carol V. Robinson. Electrospray time-of-flight mass spectrometry of the intact MS2 virus capsid. *Journal of the American Chemical Society*, 122(14):3550–3551, March 2000.

[51] Jürg M. Daniel, Sebastian D. Friess, Sudha Rajagopalan, Silke Wendt, and Renato Zenobi. Quantitative determination of noncovalent binding interactions using soft ionization mass spectrometry. *International Journal of Mass Spectrometry*, 216(1):1–27, April 2002.

[52] Albert J. R. Heck. Native mass spectrometry: a bridge between interactomics and structural biology. *Nature Methods*, 5(11):927–933, October 2008.

[53] H. Wollnik. Time-of-flight mass analyzers. *Mass Spectrometry Reviews*, 12(2):89–114, 1993.

[54] Sarah Sanglier, Cédric Atmanene, Guillaume Chevreux, and Alain Van. *Nondenaturing mass spectrometry to study noncovalent protein/protein and protein/ligand complexes: technical aspects and application to the determination of binding stoichiometries.*, volume 484 of *Methods in Molecular Biology*, chapter 15, pages 217–243. Humana Press, Totowa, NJ, 2008.

[55] Benoît M. R. Liénard, Nathalie Selevsek, Neil J Oldham, and Christopher J Schofield. Combined Mass Spectrometry and Dynamic Chemistry Approach to Identify Metalloenzyme Inhibitors. *ChemMedChem*, 2(2):175–179, 2007.

[56] Benoît M. R. Liénard, Rebekka Hüting, Patricia Lassaux, Moreno Galleni, Jean-Marie Frère, and Christopher J. Schofield. Dynamic Combinatorial Mass Spectrometry Leads to Metallo--lactamase Inhibitors. *Journal of Medicinal Chemistry*, 51(3):684–688, February 2008.

[57] Jasmin Mecinović, Rasheduzzaman Chowdhury, Benoît M. R. Liénard, Emily Flashman, Matthew R Buck, Neil J Oldham, and Christopher J Schofield. ESI-MS studies on prolyl hydroxylase domain 2 reveal a new metal binding site. *ChemMedChem*, 3(4):569–572, 2008.

[58] Robert J. Klose, Eric M. Kallin, and Yi Zhang. JmjC-domain-containing proteins and histone demethylation. *Nature Reviews Genetics*, 7(9):715–727, September 2006.

[59] Jasmin Mecinović, Christoph Loenarz, Rasheduzzaman Chowdhury, and Christopher J. Schofield. 2-Oxoglutarate analogue inhibitors of prolyl hydroxylase domain 2. *Bioorganic & Medicinal Chemistry Letters*, 19(21):6192–6195, November 2009.

[60] Sally-Ann Poulsen. Direct screening of a dynamic combinatorial library using mass spectrometry. *Journal of The American Society for Mass Spectrometry*, 17(8):1074–1080, August 2006.

[61] Nathan R. Rose, Stanley S. Ng, Jasmin Mecinović, Benoît M. R. Liénard, Simon H. Bello, Zhe Sun, Michael A. McDonough, Udo Oppermann, and Christopher J. Schofield. Inhibitor Scaffolds for 2-Oxoglutarate-Dependent Histone Lysine Demethylases. *Journal of Medicinal Chemistry*, 51(22):7053–7056, November 2008.

[62] Nathan R. Rose, Esther C. Woon, Guy L. Kingham, Oliver N. King, Jasmin Mecinović, Ian J. Clifton, Stanley S. Ng, Jobina Talib-Hardy, Udo Oppermann, Michael A. McDonough, and Christopher J. Schofield. Selective inhibitors of the JMJD2 histone demethylases: combined nondenaturing mass spectrometric screening and crystallographic approaches. *Journal of Medicinal Chemistry*, 53(4):1810–1818, February 2010.

[63] Jasmin Mecinović, Rasheduzzaman Chowdhury, Emily Flashman, and Christopher J. Schofield. Use of mass spectrometry to probe the nucleophilicity of cysteinyl residues of prolyl hydroxylase domain 2. *Analytical Biochemistry*, 393(2):215–221, October 2009.

[64] Christoph Loenarz, Mathew L. Coleman, Anna Boleininger, Bernd Schierwater, Peter W. H. Holland, Peter J. Ratcliffe, and Christopher J. Schofield. The hypoxia-inducible transcription factor pathway regulates oxygen sensing in the simplest animal, *Trichoplax adhaerens*. *EMBO Reports*, 12(1):63–70, November 2010.

[65] V. Alekseev, E. Shcherbakova, Yu Yakubovich, N. Vorob'ev, S. Larin, and O. Shigina. Interaction of ampicillin with Mn(II), Co(II), and Ni(II) ions. *Russian Journal of General Chemistry*, 76(2):321–324, February 2006.

[66] Fei Gao, Pin Yang, Jun Xie, and Hongfei Wang. Synthesis, characterization and antibacterial activity of novel Fe(III), Co(II), and Zn(II) complexes with norfloxacin. *Journal of Inorganic Biochemistry*, 60(1):61–67, October 1995.

[67] Barbara Becattini and Maurizio Pellecchia. SAR by ILOEs: An NMR-Based Approach to Reverse Chemical Genetics. *ChemInform*, 37(28):no, 2006.

[68] Ivano Bertini, Marco Fragai, Claudio Luchinat, and Eleonora Talluri. Water-Based Ligand Screening for Paramagnetic Metalloproteins. *Angewandte Chemie International Edition*, 47(24):4533–4537, 2008.

[69] C. Dalvit, G. Fogliatto, A. Stewart, M. Veronesi, and B. Stockman. WaterLOGSY as a method for primary NMR screening: practical aspects and range of applicability. *Journal of Biomolecular NMR*, 21(4):349–359, December 2001.

[70] Dawei Li, Eugene F. DeRose, and Robert E. London. The inter-ligand Overhauser effect: A powerful new NMR approach for mapping structural relationships of macromolecular ligands. *Journal of Biomolecular NMR*, 15(1):71–76, September 1999.

[71] Maurizio Pellecchia, Ivano Bertini, David Cowburn, Claudio Dalvit, Ernest Giralt, Wolfgang Jahnke, Thomas L. James, Steve W. Homans, Horst Kessler, Claudio Luchinat, Bernd Meyer, Hartmut Oschkinat, Jeff Peng, Harald Schwalbe, and Gregg Siegal. Perspectives on NMR in drug discovery: a technique comes of age. *Nature Reviews Drug Discovery*, 7(9):738–745, September 2008.

[72] Lee Fielding. NMR methods for the determination of protein-ligand dissociation constants. *Current Topics in Medicinal Chemistry*, 3(1):39–53, 2003.

[73] Bernd Meyer and Thomas Peters. NMR Spectroscopy Techniques for Screening and Identifying Ligand Binding to Protein Receptors. *Angewandte Chemie International Edition*, 42(8):864–890, February 2003.

[74] J. Martin Bollinger and Carsten Krebs. Stalking intermediates in oxygen activation by iron enzymes: Motivation and method. *Journal of Inorganic Biochemistry*, 100(4):586–605, April 2006.

[75] Lee Fielding. Determination of association constants (K_a) from solution NMR data. *Tetrahedron*, 56(34):6151–6170, August 2000.

[76] Timothy D. W. Claridge. *High-resolution NMR techniques in organic chemistry*. Elsevier Science Ltd, 2009.

[77] Edwin D. Becker, James A. Ferretti, Raj K. Gupta, and George H. Weiss. The choice of optimal parameters for measurement of spin-lattice relaxation times. II. Comparison of saturation recovery, inversion recovery, and fast inversion recovery experiments. *Journal of Magnetic Resonance (1969)*, 37(3):381–394, February 1980.

[78] Ivanhoe K. Leung, Emily Flashman, Kar Kheng K. Yeoh, Christopher J. Schofield, and Timothy D. Claridge. Using NMR solvent water relaxation to investigate metalloenzyme-ligand binding interactions. *Journal of medicinal chemistry*, 53(2):867–875, January 2010.

[79] A. E. Smith. A study of the variation with pH of the solubility and stability of some metal ions at low concentrations in aqueous solution. Part I. *Analyst*, 98(1162):65–68, 1973.

[80] Rasheduzzaman Chowdhury, Adam Hardy, and Christopher J. Schofield. The human oxygen sensing machinery and its manipulation. *Chemical Society Reviews*, 37(7):1308–1319, July 2008.

[81] Rasheduzzaman Chowdhury, Michael A. McDonough, Jasmin Mecinović, Christoph Loenarz, Emily Flashman, Kirsty S. Hewitson, Carmen Domene, and Christopher J. Schofield. Structural basis for binding of hypoxia-inducible factor to the oxygen-sensing prolyl hydroxylases. *Structure*, 17(7):981–989, July 2009.

[82] Sarah J. Lipscomb, Hwei-Jen Lee, Mridul Mukherji, Jack E. Baldwin, Christopher J. Schofield, and Matthew D. Lloyd. The role of arginine residues in substrate binding and catalysis by deacetoxycephalosporin C synthase. *European Journal of Biochemistry*, 269(11):2735–2739, 2002.

[83] Juan R. Anacona and Patricia Alvarez. Synthesis and antibacterial activity of metal complexes of cefazolin. *Transition Metal Chemistry*, 27(8):856–860, November 2002.

[84] G. Fazakerley and G. E. Jackson. Metal ion coordination by some penicillin and cephalosporin antibiotics. *Journal of Inorganic and Nuclear Chemistry*, 37(11):2371–2375, November 1975.

[85] J. R. Anacona and Gladys D. Silva. Synthesis and antibacterial activity of cefotaxime metal complexes. *Journal of the Chilean Chemical Society*, 50(2), June 2005.

[86] Claudio Dalvit, Maria Flocco, Stefan Knapp, Marina Mostardini, Rita Perego, Brian J. Stockman, Marina Veronesi, and Mario Varasi. High-Throughput NMR-Based Screening with Competition Binding Experiments. *Journal of the American Chemical Society*, 124(26):7702–7709, June 2002.

[87] Wolfgang Jahnke, Philipp Floersheim, Christian Ostermeier, Xiaolu Zhang, Rene Hemmig, Konstanze Hurth, and Doncho P. Uzunov. NMR Reporter Screening for the Detection of High-Affinity Ligands. *Angewandte Chemie International Edition*, 41(18):3420–3423, 2002.

[88] Gregg L. Semenza. Hypoxia-Inducible Factor 1 (HIF-1) pathway. *Sci. STKE*, 2007(407):cm8+, October 2007.

[89] Jennifer H. Dao, Robert J. M. Kurzeja, Jose M. Morachis, Henrike Veith, Jeffery Lewis, Violeta Yu, Christopher M. Tegley, and Philip Tagari. Kinetic characterization and identification of a novel inhibitor of hypoxia-inducible factor prolyl hydroxylase 2 using a time-resolved fluorescence resonance energy transfer-based assay technology. *Analytical Biochemistry*, 384(2):213–223, January 2009.

[90] Christopher M. Tegley, Vellarkad N. Viswanadhan, Kaustav Biswas, Michael J. Frohn, Tanya A. N. Peterkin, Catherine Chang, Roland W. Bürli, Jennifer H. Dao, Henrike Veith, Norma Rogers, Sean C. Yoder, Gloria Biddlecome, Philip Tagari, Jennifer R. Allen, and Randall W. Hungate. Discovery of novel hydroxy-thiazoles as HIF-α prolyl hydroxylase inhibitors: SAR, synthesis, and modeling evaluation. *Bioorganic & Medicinal Chemistry Letters*, 18(14):3925–3928, July 2008.

[91] Namal C. Warshakoon, Shengde Wu, Angelique Boyer, Richard Kawamoto, Justin Sheville, Sean Renock, Kevin Xu, Matthew Pokross, Artem G. Evdokimov, Richard Walter, and Marlene Mekel. A novel series of imidazo[1,2-a]pyridine derivatives as hif-1α prolyl hydroxylase inhibitors. *Bioorganic & Medicinal Chemistry Letters*, 16(21):5598–5601, November 2006.

[92] Matthew J. Ryle, Raghavakaimal Padmakumar, and Robert P. Hausinger. Stopped-flow kinetic analysis of *Escherichia coli* taurine/α-ketoglutarate dioxygenase: interactions with α-ketoglutarate, taurine, and oxygen. *Biochemistry*, 38(46):15278–15286, November 1999.

[93] Edward I. Solomon, Thomas C. Brunold, Mindy I. Davis, Jyllian N. Kemsley, Sang-Kyu Lee, Nicolai Lehnert, Frank Neese, Andrew J. Skulan, Yi-Shan Yang, and Jing Zhou. Geometric and electronic structure/function correlations in non-heme iron enzymes. *Chemical Reviews*, 100(1):235–350, December 1999.

[94] Andrea Decker and Edward I. Solomon. Dioxygen activation by copper, heme and non-heme iron enzymes: comparison of electronic structures and reactivities. *Current Opinion in Chemical Biology*, 9(2):152–163, April 2005.

[95] Andrea Decker, Michael D. Clay, and Edward I. Solomon. Spectroscopy and electronic structures of mono- and binuclear high-valent non-heme ironoxo systems. *Journal of Inorganic Biochemistry*, 100(4):697–706, April 2006.

[96] U. K. Laemmli. Cleavage of structural proteins during the assembly of the head of bacteriophage T4. *Nature*, 227(5259):680–685, August 1970.